HYDRO-MORPHODYNAMIC RESPONSES OF DETACHED BREAKWATER IN MANGROVE REHABILITATION PROJECT

ARNIZA FITRI

DEPARTMENT OF CIVIL ENGINEERING
FACULTY OF ENGINEERING
UNIVERSITY OF MALAYA
KUALA LUMPUR

2018

HYDRO-MORPHODYNAMIC RESPONSES OF DETACHED BREAKWATER IN MANGROVE REHABILITATION PROJECT

ARNIZA FITRI

THESIS SUBMITTED IN FULFILMENT OF THE REQUIREMENTS FOR THE DEGREE OF DOCTOR OF PHILOSOPHY

DEPARTMENT OF CIVIL ENGINEERING
FACULTY OF ENGINEERING
UNIVERSITY OF MALAYA
KUALA LUMPUR

2018

<div align="center">

UNIVERSITY OF MALAYA

ORIGINAL LITERARY WORK DECLARATION

</div>

Name of Candidate**:   ARNIZA FITRI**

Registration/Matric No: **KHA130040**

Name of Degree: **DOCTOR OF PHILOSOPHY**

Title of Project Paper/Research Report/Dissertation/Thesis ("this Work"):

**HYDRO-MORPHODYNAMIC   RESPONSES   OF   DETACHED
BREAKWATER IN MANGROVE REHABILITATION PROJECT**

Field of Study:

WATER RESOURCES MANAGEMENTS AND COASTAL ENGINEERING

 I do solemnly and sincerely declare that:

(1)   I am the sole author/writer of this Work;
(2)   This Work is original;
(3)   Any use of any work in which copyright exists was done by way of fair dealing and for permitted purposes and any excerpt or extract from, or reference to or reproduction of any copyright work has been disclosed expressly and sufficiently and the title of the Work and its authorship have been acknowledged in this Work;
(4)   I do not have any actual knowledge nor do I ought reasonably to know that the making of this work constitutes an infringement of any copyright work;
(5)   I hereby assign all and every rights in the copyright to this Work to the University of Malaya ("UM"), who henceforth shall be owner of the copyright in this Work and that any reproduction or use in any form or by any means whatsoever is prohibited without the written consent of UM having been first had and obtained;
(6)   I am fully aware that if in the course of making this Work I have infringed any copyright whether intentionally or otherwise, I may be subject to legal action or any other action as may be determined by UM.

Candidate"s Signature: Date: 30th August 2018

Subscribed and solemnly declared before,

 Witness"s Signature   Date:

Name:

Designation:

HYDRO-MORPHODYNAMIC RESPONSES OF DETACHED BREAKWATER IN MANGROVE REHABILITATION PROJECT

ABSTRACT

The coastal hydro-morphodynamic to detached breakwater are site specific that vary widely among different cases. This study attempts to investigate the coastal hydro-morphodynamic changes due to the presence of an existing design of detached breakwater at a representative cohesive intertidal area of Carey Island, Malaysia. In addition, the seabed level in the mangrove degradation area due to changes of the various configurations of geometry and position of the detached breakwater in the study site were also investigated. Regarding the morphodynamic changes in the mangrove degradation area, bed profiling activities in the vicinity of the breakwater were done after three to six years of construction of the breakwater. Bed profiling data in the vicinity of breakwater before and one year after breakwater''s installation were obtained from a previous study. For evaluating the changes of coastal hydrodynamic characteristics including nearshore currents, nearshore waves and sediment transport patterns, a coastal hydraulic study using *MIKE 21 2D* numerical model was carried out at the site. To verify the accuracy of simulation results, the values of root-mean square error (RMSE), coefficient of determination (R^2) and Theil''s coefficients were calculated. Further, the calibrated *MIKE 21* model was used to simulate the bed level changes in the degraded mangrove area after changing the design parameters of existing detached breakwater. Based on the values of RMSE (e.g. $0.07 - 0.09$ m/s), R^2 (e.g. 0.82 to 0.94) and Theil''s coefficients (e.g. $0.06 - 0.18$), it is evident that the models were well calibrated and validated against field conditions. The simulation results show that the presence of detached breakwater at intertidal area of Carey Island has reduced the current speeds and significant wave heights approximately up to 0.14 m/s and 0.9 m, respectively in protected area behind its structure. The reduction of current speeds and

significant wave heights behind the structure created more calm hydrodynamic conditions in the mangrove degradation area and increased the settling velocities of sediments due to flock formation. Thus, it helped in settling down suspended sediments. In addition, field monitoring showed that the presence of detached breakwater has trapped sediment accumulations in the vicinity of its structure and increased the seabed elevations in the mangrove degradation area. However, average increase of seabed elevations during six years period of breakwater installation with existing design is not significant for mangrove rehabilitation project. Based on results from numerical model, by increasing the height and length of the detached breakwater approximately by 1 m and 50 m, respectively, detached breakwater in the study site can increase the seabed elevations in the mangrove degradation area approximately by 0.73 m during six years of breakwater installation. It means that the presence of detached breakwater with higher and longer dimensions can optimize the increase of the bed level elevations in mangrove degradation area and thus, it would support the success of mangrove rehabilitation project in the site.

Keyword: coastal hydro-morphodynamic, detached breakwater, MIKE 21, erosion-accretion pattern, sediment

MAKLUM BALAS DARIPADA HIDRO-MORPODINAMIK PANTAI TERHADAP PEMECAH OMBAK DI KAWASAN PROJEK PEMULIHAN BAKAU

ABSTRAK

Hidro-morpodinamik pantai terhadap pemecah ombak adalah suatu aspek yang mengalami perubahan secara meluas pada kes-kes yang berbeza. Kajian ini bertujuan untuk menyiasat perubahan hidro-morpodinamik pantai terhadap kehadiran pemecah ombak yang sedia ada di kawasan pasang surut di pesisir pantai berlumpur Pulau Carey, Malaysia. Di samping itu, perubahan ketinggian dasar laut di kawasan kemusnahan bakau yang berlaku disebabkan oleh perubahan daripada pelbagai konfigurasi geometri dan kedudukan pemecah ombak di kawasan kajian juga disiasat. Berdasarkan perubahan morpodinamik di kawasan kemusnahan bakau, didapati aktiviti profil dasar laut di sekitar pemecah ombak telah dijalankan selepas tiga hingga enam tahun selepas pembinaan pemecah ombak. Data profil dasar laut di kawasan persekitaran pemecah ombak pada sebelum dan satu tahun selepas pemasangan pemecah ombak diperolehi daripada kajian sebelumnya. Bagi membuat penilaian perubahan hidrodinamik pantai termasuk arus, gelombang dan corak pengangkutan sedimen, kajian hidraulik pantai menggunakan *MIKE 21 2D* model numerik telah dijalankan di kawasan kajian. Bagi mengesahkan ketepatan keputusan simulasi, nilai-nilai RMSE, R^2 dan Theil"s koefisien telah dikira. Seterusnya, model MIKE 21 yang telah dikalibrasi terlebih dahulu telah digunakan untuk mensimulasikan perubahan ketinggian dasar laut di kawasan kemusnahan bakau setelah mengubah parameter rekabentuk pemecah ombak yang sedia ada. Berdasarkan nilai-nilai RMSE (sebagai contoh 0.07-0.09 m/s), R^2 (sebagai contoh 0.82-0.94) dan Theil"s koefisien (sebagai contoh 0.06-0.18), ini telah membuktikan bahawa model yang digunakan telah dikalibrasi dan divalidasi dengan baik bersesuaian dengan keadaan lapangan. Keputusan simulasi menunjukkan bahawa kehadiran

pemecah ombak sedia ada di kawasan pasang surut Pulau Carey telah mengurangkan kelajuan arus dan ketinggian gelombang kira-kira sehingga 0.14 m/s dan 0.9 m, masing-masing di kawasan terlindung di belakang struktur pemecah ombak. Pengurangan kelajuan arus dan ketinggian gelombang di belakang struktur telah mencipta keadaan hidrodinamik yang lebih tenang di kawasan kemusnahan bakau dan meningkatkan halaju mendapan sedimen akibat pembentukan kawanan. Selanjutnya, ia membantu dalam memendapkan sedimen yang terampai. Selain itu, pengukuran di tapak kajian telah menunjukkan bahawa pemasangan pemecah ombak telah memerangkap sejumlah sedimen di kawasan sekitar strukturnya dan telah meningkatkan ketinggian dasar laut di kawasan kemusnahan bakau. Walau bagaimanapun, peningkatan purata ketinggian dasar laut selepas tempoh enam tahun pemasangan pemecah ombak ini adalah tidak signifikan. Berdasarkan keputusan daripada model numerik, dengan meningkatkan ketinggian dan panjang pemecah ombak sedia ada kira-kira 1 m and 50 m, masing-masing, ia digambarkan bahawa keberadaan pemecah ombak di kawasan tapak kajian boleh meningkatkan ketinggian dasar laut di kawasan kemusnahan bakau sehingga 0.73 m kedalaman purata selama tempoh enam tahun pemasangan pemecah ombak. Itu bererti bahawa kehadiran pemecah ombak dengan dimensi yang lebih tinggi dan panjang dapat mengoptimakan peningkatan ketinggian dasar laut dan seterusnya dapat menyokong kejayaan projek pemulihan bakau di tapak kajian.

Kata kunci: hidro-morpodinamik pantai, pemecah ombak, MIKE 21, corak hakisan-pertambahan, sedimen

ACKNOWLEDGEMENTS

TABLE OF CONTENTS

LIST OF FIGURES

LIST OF TABLES

LIST OF APPENDICES

CHAPTER 1: **INTRODUCTION**

1.1   Research Background

Coastal defense structures, such as detached breakwaters are a common feature in non-cohesive coastal landscapes at intertidal and shallow sub-tidal environment since the last few decades (Airoldi *et al.*, 2005). They are used worldwide as an alternative to reduce coastal erosion problems (Cáceres *et al.*, 2005; Fairley *et al.*, 2009; Munari *et al.*, 2011; Nam *et al.*, 2011b; Saied & Tsanis, 2008; Sierra *et al.*, 2010; Zyserman & Johnson, 2002).

Detached breakwaters are wave energy barrier designed to protect any landform area behind them from the direct attack of waves. It also reduces the sediment transport capacity and allows the sediment deposition on the shoreward side (Dean *et al.*, 1997; Van Rijn, 2011). However, the implementations of detached breakwaters are rarely found on the cohesive shores. It can be attributed to the understanding of the morphodynamic responses on cohesive shore due to complexity in the behavior of cohesive sediment (Baas *et al.*, 2013; Fan *et al.*, 2006; Holland *et al.*, 2009; Shi & Chen, 1996).

Despite the efficiency of the coastal defense structures, they can locally result in complex changes to the coastal hydro-morphology especially near their structures (Barbaro & Foti, 2013; Nam *et al.*, 2011a; Sierra *et al.*, 2010; Zyserman *et al.*, 2005). The coastal hydro-morphodynamics response to the coastal structures varies widely among different cases affected by differences in sediment type; location, dimension and design of the structures; and climate condition (Fairley *et al.*, 2009). Therefore, there is a need to carry out more research works addressing various responses towards coastal protection structures on cohesive shore.

Monitoring the shore responses to the specific coastal structures in the specific locations is required to evaluate the performance of the specific structures. Besides, the variability of the accretion and erosion locations and also the increase and reduction of beach volumes caused due to the presence of certain coastal structures need to be considered by coastal managers in strategizing specific coastal management aims. Such a step is expected to help in creating the proper environmental and suitable design of coastal defense structures on cohesive shore.

1.2   Problem Statement

Mangroves are the most important ecosystem in the tropical coasts that naturally protects the coastline from ocean impact. Over the past decades, rapid development has taken place in Malaysian coastal states. These development activities have disturbed the mangrove ecosystem though clear-cutting of some mangroves along the coastline (DID, 2006; FAO, 2007; Ghazali, 2006). It has made the coastal area exposed to tidal inundation and wave actions, causing erosion problems. Further, the erosion problems result in changing of tidal regime and disrupt remaining mangrove ecosystem. Moreover, it creates mangrove degradation issues similar to that observed at the coastline of Carey Island, west coast of Peninsular Malaysia. Figure 1.1 presents the mangrove degradation and erosion problems at the coastline of Carey Island.

The mangrove degradation and erosion problems faced at the Carey Island coastline, requires mangrove rehabilitation projects to be carried out for coastal protection. According to Lewis (2005), calm hydrodynamic conditions and normal tidal regime are the most important factors in mangrove rehabilitation projects. Therefore, in order to reduce the energy of nearshore hydrodynamics and increase the bed elevation for creating the suitable tidal regime for mangrove survival, additional studies are urgently required.

Figure 1.1: Mangroves degradation in the coastline of Carey Island, West Coast of Peninsular Malaysia

University of Malaya has been giving serious attention to this major issue of erosion on the bank of Carey Island coastline since 2009. The mangrove rehabilitation works were done by constructing 80 m long detached breakwater around the mangrove degradation area at intertidal area of cohesive shore of Carey Island. Detached breakwater is expected to reduce the current speeds and wave actions; and increase the sediment accumulation as well as seabed elevation at protected area behind its structure (in the mangrove degradation areas) and thus create a suitable tidal regime for mangrove survival.

At the end of year 2012, four years after implementation of detached breakwater at intertidal area of Carey Island, accretions and increment of seabed elevations observed in the mangrove degradation areas behind the breakwater. However, the increments of bed elevations recorded were not very significant. It probably was attributed to several reasons: 1) the local hydrodynamic conditions after construction of the detached breakwater were still not calm enough to settle down more sediment behind its structure, 2) lack of suspended sediment sources minimized the sediment to enter the

degradation area, 3) the design parameters of existing detached breakwater were not proper enough to allow more sediments entering the site area and then well trapped, etc.

Therefore, a coastal hydraulic study (including; the coastal hydrodynamics and sediment transports) and monitoring activities are needed to investigate the coastal hydro-morphodynamic changes before and after construction of the existing detached breakwater on cohesive shore of Carey Island. In addition, the better design parameters of detached breakwater are required to optimize the increases of seabed elevations in the mangrove degradation areas to support the successful of mangrove rehabilitation project at Carey Island coastline.

1.3   Research Objectives

The objectives of this research study are:

1)   To investigate the coastal hydrodynamic changes due to the presence of an detached breakwater.

2)   To identify the suspended sediment transports and general patterns of erosion and accretion around the existing detached breakwater.

3)   To evaluate the coastal morphodynamic changes in the vicinity of an existing detached breakwater.

4)   To investigate various configurations of geometry and position of the detached breakwater for the purpose of mangrove rehabilitation project at the Carey Island.

The mainly aim of this study is to investigate the coastal hydro-morphodynamic responses to an existing detached breakwater at intertidal area of cohesive shore of Carey Island. Besides, the better design parameter of the detached breakwater is also investigated in order to optimize the increases of seabed elevations in the mangrove degradation areas.

1.4   Scope of Work

The coastal hydro-morphodynamic responses to an existing detached breakwater at intertidal area of cohesive shore of Carey Island is carried out through field monitoring and numerical model simulations by using *MIKE 21 Flexible Mesh* package Model consist of *MIKE 21 Hydrodynamic*, *Mud Transport and Spectra Wave Models*. Besides, an effort in improving the performance of the existing detached breakwater was carried out by evaluating various configurations of geometry and position of detached breakwater that can optimize the increase of seabed elevations in the mangrove degradation areas. For this, simulation of bed level changes in the mangrove degradation areas (from few cases) was carried out by changing the position and dimension of existing detached breakwater at intertidal area of cohesive shore of Carey Island.

1.5   Research Methodology

This part describes the general method used in order to fulfill the research objectives mentioned in the previous section. Firstly, a comprehensive review of literature related to the characteristics of cohesive shore (tidal flat), coastal hydrodynamic, coastal morphodynamic, detached breakwater, coastal hydro-morphodynamic response to the detached breakwater and coastal numerical models were carried out and simultaneous site investigation and preparation were done. After obtaining adequate literatures, the required data were collected. Further, the coastal hydraulic study and profiling activities were prepared and accomplished. Schematically, this research study followed the flow chart as depicted in Figure 1.2.

In this research, a coastal hydraulic study and coastal profiles measurement were carried out to present the impacts of the existing detached breakwater on currents, wave, sediment transport pathways and morphodynamic changes at intertidal area of cohesive

shore of Carey Island. The coastal hydraulic study was done by simulating the hydraulic conditions (tides, nearshore currents, offshore and nearshore wave and sediment transport) around the Malacca Strait and study area by using a numerical model *MIKE 21 2014 Flexible Mesh* software package established by *Danish Hydraulic Institute* (DHI). In addition, the coastal profile measurement was carried out in the vicinity of the existing detached breakwater before and during six years (between years 2009 and 2014) of its installation by using total station.

Here, simulation of tides and nearshore currents were carried out using *MIKE 21 Hydrodynamic FM model,* while *MIKE 21 Spectra Wave FM model* and *MIKE 21 Mud Transport FM models* were used for simulation of wave and sediment transport patterns. To facilitate an accurate representation of the study area and provide a high level of confidence in the model outcomes, the simulation models were calibrated and validated against measured conditions. The calibrated and validated models were finally used to simulate the bed level changes in the mangrove degradation area after changing the existing parameters of detached breakwater in order to establish the better position and dimensions of the detached breakwater for supporting the successful implementation of mangrove rehabilitation project at Carey Island Coastline.
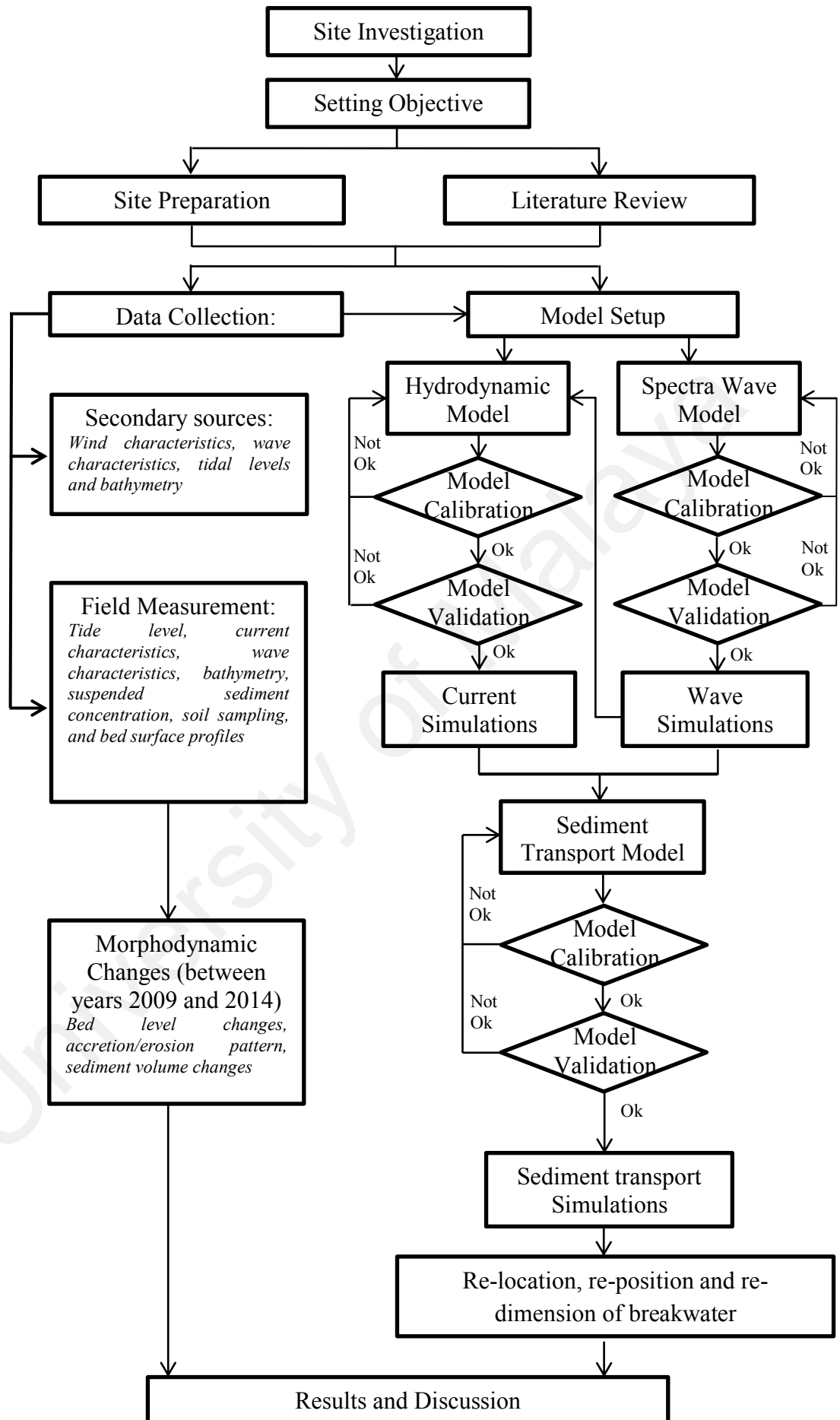
Figure 1.2: Schematic diagrams for research methodology

1.6   Research Significance

In the past few decades, there was little research available on the responses of coastal hydro-morphodynamics to detached breakwaters along the cohesive shore. Since the responses of the shore to coastal structures varied widely among different case studies, this study can contribute additional knowledge about the coastal responses to the detached breakwater on cohesive shore. Besides, it is necessary to evaluate the performance of detached breakwater in the specific locations and conditions before they are going to be popular in local coastal management aims.

In addition, the presence of mangroves in the coastline of tropical coasts can provide the natural protection for the coastline from the ocean impacts. Mangroves are also great sources of timber and wood, and they can support large population of bird and fishes. This study aims to strengthen the mangrove rehabilitation project and reduce the erosion problems at the Carey Island coast, and, therefore, it has a positive impact on economic and social in the local state of Carey Island.

1.7   Thesis Structure

In order to achieve the specific objectives listed in section 1.3 above, the dissertation is structured as follows:

Chapter 1: Introduction

> This chapter introduces briefly the research study, which includes research background, problem statement, research objectives, scope-of work, research significance and general methodology in completing the research study.

Chapter 2: Literature Review

> This chapter contains comprehensive review of literature relating to the characteristics of coastal dynamics, characteristics of cohesive shore (tidal

mudflat), coastal protection, detached breakwater, coastal hydro-morphodynamic response to the detached breakwater and coastal numerical models, especially MIKE 21 Numerical Model.

Chapter 3: Research Methodology

This chapter provides a description of the study area, explains the required data to fulfill the research objectives, and presents the detail methods used in data collection, data analyses, and obtaining the final results.

Chapter 4: Results and Discussion

This chapter presents and discusses the impact of existing detached breakwater on the coastal hydrodynamic condition: current and wave characteristics, suspended sediment transport and coastal morphodynamic condition, including bed level changes, pattern of accretion and erosion and deposition volumes in the intertidal area of cohesive shore of Carey Island, Peninsular Malaysia.

Chapter 5: Conclusions

This chapter gives the overview and conclusion of major findings obtained from simulation results and field measurements. Besides, this chapter also makes suggestion for future work.

CHAPTER 2: **LITERATURE REVIEW**

2.1   Coastal Areas

Coastal zones play a crucial role in the economic, social and politic development of most countries. They support various productive coastal ecosystems that provide valuable natural resources and services (Airoldi *et al.*, 2005).

Based on Shore Protection Manual (1984a), coastal zone is a dynamic area which covers land, shore and nearshore with valuable natural resources. Shore is the zone of unconsolidated material that extends landward from the low water line to the line of permanent vegetation that has effective limit of storm waves (Shamji, 2011). A shore can includes foreshore known as intertidal areas (located between tidemarks approximately above water at low tide and under water at high tide) and backshore (zone acted upon by water flows only during severe storms). Nearshore is the zone in the seaward of shore from approximately the step at the base of the surf zone.

In the tropical coast, intertidal zone is the most valuable and productive areas. This area is known as biological zones where coastal vegetation such as mangroves can grow healthily to support the large population of birds and provide nursery and feeding areas for fisheries (Awang, 2010; Barbier, 2015). Based on previous study, it is proved that there are positive correlation between the areas of mangrove and annual catch of prawn and fishes (Baran & Hambrey, 1999; Martosubroto & Naamin, 1977; Paw & Chua, 1991; Robertson & Blaber, 1993; Sasekumar *et al.*, 1992; Staples *et al.*, 1985). In addition, mangroves are great sources of commercial timber and fuel woods (Airoldi *et al.*, 2005). They also can function as natural coastal protection against tide, storms and ocean impact to the coastline (Barbier, 2015; Bosire *et al.*, 2008). Regarding the terminologies of shore and nearshore profiles in coastal area by Shore Protection Manual (1984a), the tropical coastal areas can be described in Figure 2.1.
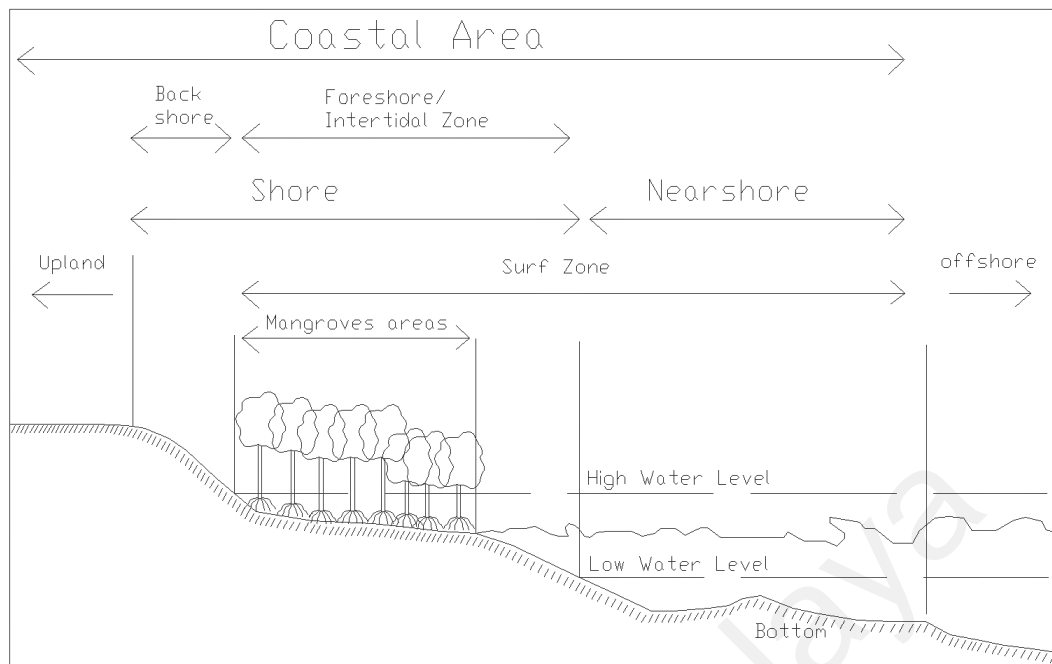
Figure 2.1: Description of a shore profile in tropical coastal areas (Modified Shore Protection Manual, 1984a)

2.2 Coastal Dynamics

The coastal dynamics involve the dynamic processes of coastal hydraulic (hydrodynamic) and coastal morphology (morphodynamic). In the coastal areas, these processes are very complex. As shown by Friedrichs & Aubrey (1996), the coastal hydrodynamics and morphodynamics are interrelated.

2.2.1 The Coastal Hydrodynamics

Coastal hydrodynamics are related to tidal, current, wave, and wave-current interactions (Chiang & Hsiao, 2011). They are important for many coastal engineering design and application. They allow the study of new engineering methods for coastal defense and plays an essential role in the calculation of sediment transport and morphological evolution (Nam *et al.*, 2011a, 2011b). More explanation about coastal hydrodynamics is summarized below.

2.2.1.1 Nearshore Currents

Current is water motion caused by differences in water elevation. When the total head in one area becomes higher than the total head in another area, water from the higher elevation flows towards the lower level, creating currents. In nearshore areas, currents are caused by local wind, wind generated wave, tidal and river discharges (SPM, 1984b). Wind creates currents as it blows over the water surface, producing a stress on surface water particles and starting the movement of the particles in the direction in which the wind is blowing. Wind-generated wave creates strong currents as they approach the shoreline at large angles (Goodfellow & Stephenson, 2005). At tidal cycles, tide forces water and generates currents as the tide rise (filling) and fall (emptying) at shoreline, while on the ebb tide period, the water from river discharges to the sea with introduction of currents into the nearshore zone.

Based on circulation system in the nearshore area, nearshore currents can consist of cross-shore current, long-shore current and rip current (Shamji, 2011). Cross shore current flows perpendicular toward shoreline while longshore current flows paralel to the shoreline. Moreover, when wind-generated waves approach the coast at an angle, they generate strong long-shore current. These current under certain condition may turn and flow seaward in what is know as a rip current (current flows seaward caused by water moving down slope). Rip currents are concentrated seaward through the breaker zone as a result of wave setup.

Near-shore currents play an important role in physical system and can decide the sediment distribution in nearshore areas. They are responsible for sediment/pollutant transport. Longshore current bring the sediment through offshores and cross-shore currents bring the sediment to the shoreline.

2.2.1.2 Offshore and Nearshore Waves

Waves are sources of input energy into the coastal zone (SPM, 1984b). They are generated locally and propagate into other areas. However, waves are complex and difficult to be described due to their nonlinearitiesm and random behavior. Waves in the ocean often have irregular shapes and variable propagation directions since they are under the influence of wind (Özger & Şen, 2008).

Generally, waves derive their energy from the wind. Because of the wind, the waves travel across the ocean until they reach land where their remaining energy is expended on the shore. Wind-generated waves are by far the largest contribution of energy from the sea to neashore system. The heights of wave are dependent on their fetch length, wind speed, time of wind blows and water depth. For a fixed fetch length, the wave height increases approximately linearly with wind speed and water depth. The wave height decreases as the wave moves towards the shoreline.

Waves are the major factor in determining the geometry and composition of beachs/shore and significantly influence the planning and desing of harbors, waterway, shore protection and coastal structures (Seif *et al.*, 2011). This is because wave affects the formation of beaches/shores, sorting of bottom sediment on the shoreface, and transporting bottom material onshore, offshore and alongshore for causing many of the forces to which coastal structures are subjected.

Design of coastal defence structures and shore protection measures are dependent on the ability to predict wave characteristics such as significant wave height and wave period. The wave effects on coastal and marine activities related to the ocean environment (such as the construction and maintenance of coastal structures and environmental protection) requires identifying the wave characteristics accurately (Mahjoobi *et al.*, 2008).

The important wave parameters in numerical modeling and coastal strcuture designs include (i) significant wave height (H_s), (ii) mean wave period (T_m), (iii) peak wave period (T_p) and (iv) mean wave direction (θ_m). These wave parameters are described in the next sections.

(a) *Significant wave height (Hs)*

Significant wave height is the mean of the highest third of the waves in a time-series of waves representing a certain sea state. This corresponds well with the average height of the highest waves in a wave group. H_s computed on the basis of a spectrum, which is referred to as H_{m0}.

(b) *Mean wave period (Tm)*

Mean wave period is the mean of all wave periods in a time-series representing a certain sea state. It represents the period taking for consecutive wave crests or wave troughs to pass a given point.

(c) *Peak wave period (Tp)*

Peak wave period is the wave period with the highest energy. This is the highest part of the wave above still water level. The analysis of the distribution of the wave energy as a function of wave frequency for a time-series of individual waves is referred to as a spectral analysis. The peak wave period is extracted from the spectra. As a rule of thumb, the relation can be expressed as $T_p \sim 5.3\,H_{m0}^{1/2}$.

(d) *Mean wave direction (θ_m)*

Mean wave direction is defined as the mean of all the individual wave directions in a time-series representing a certain sea state. Wave peak direction is the wave direction at the frequency at which a wave spectrum reaches its maximum.

In deep waters, the water particle motion of waves is confined to the vicinity of the surface and therefore water particle's velocities and pressure fluctuation are non-existent near the bottom. In shallow waters, the waves undergo transformation under the influence of the bottom area (Shamji, 2011; SPM, 1984b). The significant wave transformations in shallow waters involve wave shoaling, wave refracting, wave diffracting and wave breaking. The phenomena of wave transformation in shallow water can be described in Figure 2.2.

However, in the intertidal area, the wave height is smaller compare to tidal range and tidal forcing tends to dominate over wave forcing (Friend *et al.*, 2005; Liu *et al.*, 2011; Roberts *et al.*, 2000).
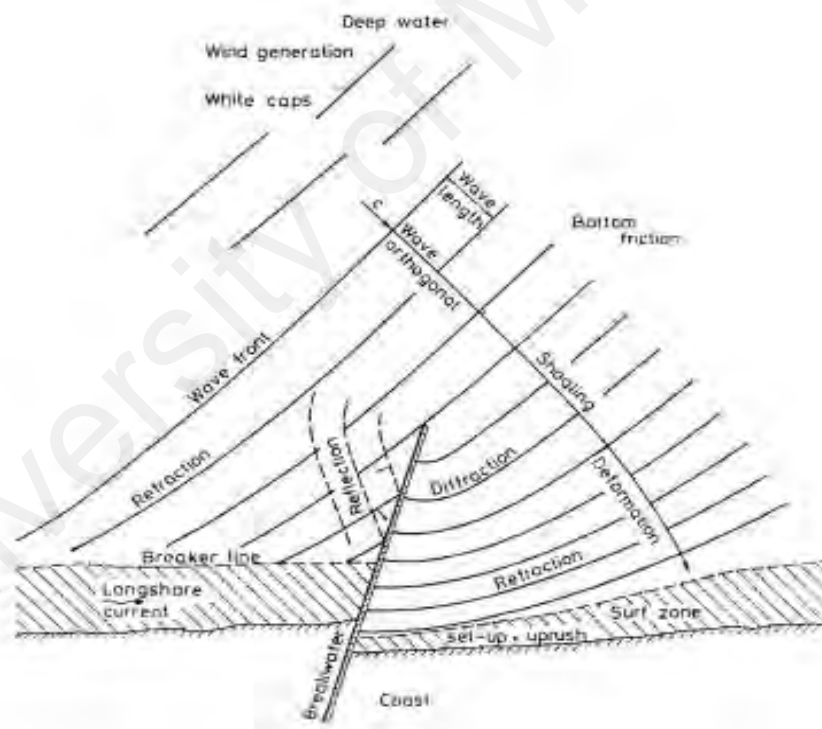
Figure 2.2: Wave transformation in shallow water
(Shore Protection Manual, 1984a)

Initially, as waves move into shallow water, the group velocity slightly increases and then decreases with decreasing water depth. Where group velocity increases, wave crest move further leading to a reduction in wave height. Decreasing group velocity occurs

15

for most of the nearshore region so that wave crests move and wave height increase. This process is called wave shoaling. If waves are incident normal to the beach/shore with almost straight and parallel bottom contours, change in the wave profile is solely due to the change in water depth.

Besides, a gradient in the wave celerity occurs along the crest of a wave moving at an angle to underwater contours because that part of the wave in deeper water moves faster than the part in shallow water. This variation causes the wave crest to bend toward alignment with the contours. Such a kinematic process of wave transformation is referred to as wave refraction, which depends on the relation of water depth to wave length. Refraction coupled with shoaling, determines the wave height in any particular water depth for a given set of incident deep water wave. The change of direction of waves results in convergence or divergence of wave energy. Refraction therefore has a significant effect on the distribution of wave height and wave energy along a coast. This variation of energy is responsible for the beach morphological changes along the coastline.

Wave shoaling can cause the process of wave breaking. Generally, wave breaking is caused by excessive energy input or the instability caused by the shoaling effects. Wave breaking is a very complicated hydrodynamic process in nearshore processes (Zhou, 2011). It can increase the rate of transfer of energy; generate significant loading on coastal engineering structures and dissipate the wave energy.

Apart of that, when wave meets an obstacle such as a breakwater or an offshore platform, waves can propagate into a sheltered basin, which bends around the obstacle and thus penetrate into the lee zone of the obstacle or they may be reflected backward. The phenomenon of diffusion or transverse flow of wave energy is called wave

diffraction, while the phenomenon of reflecting the wave energy is called wave reflection.

In diffraction, transfer of energy takes place laterally along a wave crest. The degree of diffraction depends on the ratio of the characteristic lateral dimension of the obstacle to the wavelength. In reflection, water waves may be either partially or totally reflected from both natural and manmade barriers. When a wave interferes with an impermeable vertical rigid surface-piercing wall, essentially all of the wave energy will reflect from the wall. On the other hand, when a wave propagates over a small bottom slope, only a very small portion of the energy will be reflected. Consideration of wave reflection may often be as important as diffraction in the design of coastal structures or harbor development.

2.2.1.3 Tidal Force

Tides are created by the gravitational force of the moon and to a lesser extent the sun. These forces of attraction and the fact that the sun, moon and earth are always in motion relative to each other cause water of ocean basin to be set in motion. These tidal motion of water masses are a form of very long period wave motion, resulting in a rise (floodtide) and fall (ebbtide) of water surface at a point.

Tides are commonly semi-diurnal (two high waters and two low waters each day/two tidal cycle per day), or diurnal (one tidal cycle per day) (Boothroyd, 1978). The two high waters on a given day are typically not the same height (the daily inequality); these are the higher high water and the lower high water in tide tables. Similarly, the two low waters each day are the higher low water and the lower low water. The daily inequality is not consistent and is generally small when the Moon is over the equator.

Tides constantly change the water surface level at which waves attack the beach/shore. Tides compound the dynamic beach response by constantly changing the

elevation at which the water intersect the shore and by providing tidal currents. Thus, the beach is always adjusting to changes in both wave energy and water level.

Speed of tidal currents tend to be stronger in the direction parallel to the coast rather than perpendicular to it (Le Hir *et al.*, 2000). The speed of the tidal currents can be increased by wind effect and become an important access for sediment transport to the shoreline. Based on Friend et al, (Friend *et al.*, 2005), tide currents and wave currents plays important role in sediment dynamics in intertidal systems.

In the coastal area approaches, characteristics of tidal forces can be distinguished as microtidal, macrotidal and mesotidal. Microtidal characteristics are applied to coastal areas in which the tidal range is less than 2 m. Wave action dominates the processes active in microtidal areas. Macrotidal characteristics are applied to coastal areas where the tidal range is in excess of 4 m. Tidal currents dominate the processes active in macrotidal areas. Mesotidal characteristics are applied to coastal areas where the tidal range is 2–4 m. Tidal action and wave activity both tend to be important in such areas (Boothroyd, 1978).

2.2.2   The Coastal Morphodynamics

As a multi-purposed area, the coastal zone is affected by all kinds of components, including both natural processes and human activities (Ding & Wang, 2008; Hashim *et al.,* 2010). Natural processes, such as geologic activities, wind, wave, tide and storm surge, are the initial forces that determine the characteristics of a coast. However, human activities, such as coastal sand mining, land reclamation, dredging and building coastal structures along the shoreline, play a more important role in shaping the coast area. More importantly, the natural processes and human interventions are always interactional and cause the morphological variations to the coastal zone; meanwhile, the morphological changes also react on the natural and human-induced processes.

Wind, tide, wave and storm surge influence the changes of beach/shore profiles indirectly by influencing the hydrodynamic processes. The strong winds drive the currents and waves, and significantly alter the tidal patterns in relatively shallow environment. Based on study carried by Franz *et al*., (2014), it is found that wind plays a secondary role in the Tagus estuary hydrodynamics, but it can be important for contaminant transport at the water surface.

Human activities in the coastal areas can also cause directly and indirectly shoreline changes. Man-made structures in the coastline alter/disturb the natural process through changes of hydrodynamic condition and sediment transport pattern.

To describe the coastal morphological change, the terminologies 'erosion' and 'accretion' are used over a period of time (Liu *et al*., 2011; SPM, 1984a). Whenever there is a build-up of material in a temporal frame, the beach is said to accrete. Alternatively, when there is loss of sediment from the beach, it is said to erode. Another method of describing beach morphological changes is in terms of the advance or retreat of shoreline. An advance of shoreline is indicative of accretion, while a retreat is indicative of erosion.

There are several method used to estimate the coastline morphological changes (Appendix A). The method are described in the next sections.

(a) *Shore profile measurements*

The most accurate method of estimating shoreline change is by measurement of beach/shore profiles by level and staff method. Beach profile measurement by level using the total station is an effective tool to measure surface elevations with an accuracy of $\pm$ 1 cm on large scales of high resolution coverage (Fairley, 2009). Moreover, a shoreline can be compiled by interpolating between a series of discrete shore-normal

beach profiles (Boak & Turner, 2005). Such beach profiling at regular time intervals can give accurate estimates of seasonal, annual and long-term shoreline change.

(b) *Aerial photography*

Shoreline can be extracted from aerial photographs, preferably of scale 1:15,000 or more. Aerial photography is an old method and it provides good spatial coverage of the coast (Komar, 1983). By definition, the „shoreline" obtained from aerial photography is based on a visual feature. However, this method has some weaknesses such as distortion. It includes both radial and relief distortions, which depend on pitch of the aircraft and scale variation caused by changes in altitude along a flight line (Anders & Byrnes, 1991). The rapid development of modern technique of photogrammetry allows a digitally scanned pair of aerial photos to be converted into a three-dimensional digital terrain model (Hapke & Richmond, 2000; Overton *et al.*, 1996).

Initially, only a few studies used digital imagery to reveal the coastal morphodynamic changes and to describe the temporal variation in the topography of the seabed (Hansen, 2004). However, with the development of digital imagery with high resolution, it has been a common technique recently for studying morphodynamic changes, especially to determine past shoreline positions.

(c) *Field survey using global positioning system (GPS)*

Nearshore morphology can be mapped using GPS (Global Positioning System). This is a more recent method used to map shoreline positions as well as nearshore characteristics (berm, vegetation, scarp, etc.). The GPS survey can be effectively used to map the shoreline poison at regular time interval. The short-term as well as long-term shoreline change can be easily derived from the GPS surveyed data. This method is more accurate than aerial photography (Pajak & Leatherman, 2002).

(d) *Satellite remote sensing*

Shoreline changes can be monitored using satellite images (Chen, 1998; Maiti & Bhattacharya, 2009). Images can be georeferenced from base maps using GIS software and shoreline map. The advent of high-resolution satellite sensors has increased the accuracy of this method in recent times. The advantage of this method is the high receptivity of the satellite data, which enable mapping of shoreline changes at a cheaper cost when compared to any other method.

(e) *Airborne detection and ranging technology (LIDAR)*

Airborne LIDAR surveys can be used for shoreline monitoring and it has the ability to cover hundreds of kilometers of coast in a relatively short period (Stockdonf *et al.*, 2002). This technique obtains highly accurate and detailed topographic measurements of the nearshore areas. LIDAR can provide data with vertical precision from 8 to 15 cm and data-point less than 1m. From these data, a shoreline may be extracted for use in shoreline change analyses (Gibeaut *et al.*, 2001). However, LIDAR data is generally limited in its temporal and spatial availability because of high cost. The main advantage of LIDAR data is that it can be used to obtain a large coverage within a short period of time.

(f) *Video imaging*

Continuous monitoring of shoreline can be carried out by installing a video camera at higher level overlooking the area of interest (Boak & Turner, 2005; Ranasinghe *et al.*, 2004). By connecting the installed camera to a computer, the images at programmed intervals can be captured. Further, the images of shoreline or any other littoral environmental parameter can be derived from appropriate image processing software. The advantage of this method is the facility to monitor shoreline changes in micro time scale.

2.3   Tidal Mudflats

The majority of shorelines on the west coast of Peninsular Malaysia are tidal mudflat (Figure 2.3). The sediments covering mudflats are mainly composed of mud and sand with the clay content sufficiently high that sediments exhibit cohesive properties (Dyer, 1986). Coastal mud deposits generally composed of clay and silt with varying amount of sand and organic materials (CEM, 2006) are found in variety of environments ranging from low energy coastal environments and particularly sheltered estuaries to exposed coast. These mud deposits might have been supplied by large rivers transported by wave and currents from deep sea to the coasts (Kamali, 2011). Example of such mud deposits have been reported at coastline of China, the mouth of most large Asian rivers such as Yellow River and Yangtze River, southwest of India, Brazil, USA, etc. Mudflats have constantly attracted research efforts, particularly on the interactions between mud and the hydrodynamic forcing, between mud and shoreline and between mud and mangroves (Anthony, 2004).
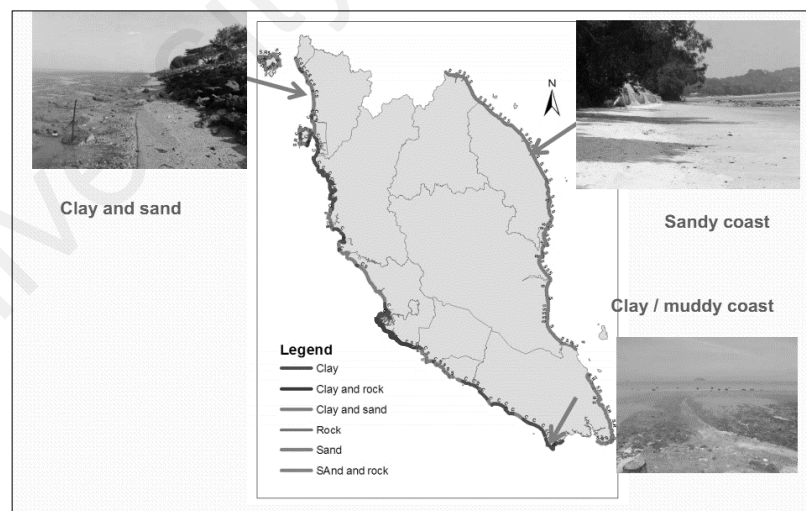
Figure 2.3: Geomorphology constituent in West Coast of Peninsular Malaysia (NAHRIM, 2010)

Morphodynamics of mudflats is not well understood compared to sandy coasts, partly, due to greater complexity of the behaviour of cohesive sediments (Kirby, 2002).

Mudflats show repeated erosion-accretion cycles over rough and calm seasons (Fan *et al.*, 2006). The processes of morphodynamics changes are often site specific and can be attributed to combination of hydrodynamic conditions, and sediment supply (Fan *et al.*, 2006).

Based on Huettel et al., (1996), suspended sediments concentrations in the water column or deposited on the seabed depending on combinations of hydrodynamic processes including baroclinic (density-driven/SSC) or barotropic (mainly tidal and wind driven) currents, and wave action (Ward et al., 1984; Huettel et al., 1996). Spatial and temporal variations in hydrodynamics, or interventions such as engineering structures which alter hydrodynamics, should therefore be a major determinant of turbidity.

Muddy bed reaction on waves compared to sandy beds is quite different because, after occurrence of fluid mud in the bed, the energy depreciates and wave height is reduced. It was commonly proved that the friction coefficient of wave-induced bed shear stress for muddy bottoms is greater than for sandy bottoms (Jain, 2007, Nikmanesh and Talebbeydokhti, 2013). In other words, soft mud interacts with waves, resulting in attenuation of wave height due to bottom friction, percolation losses and viscous damping within the sediment. These interactive modes are also manifested as changes in wave length, water particle motion, and the elevation of the interface between the fluid and bottom sediment (Jain, 2007). Wave breaking in near shore zones is the dominant phenomenon to cause long shore and on–off shore currents, which play a significant role in sediment transportation (Nikmanesh and Talebbeydokhti, 2013).

Rheology, defined as the science of fluid mud deformation, is an important field in the investigation of fluid mud behavior response to wave actions. The rheological property of the mud has been known to be rather complicated, which depends on many

factors, such as mud density, mineral constituents, grain composition of mud, and type and concentration of ions in the water, etc.

Erosion is one of the major factors in sediment re-suspension, sediment transport and beach deformation of cohesive shorelines. Erosion of cohesive sediments occurs when hydrodynamic erosive forces exceed gravitational, cohesive or frictional forces (surface erosion). The second condition occurs when flow-induced shear stress exceeds bed bulk shear stress which is called mass erosion (Nikmanesh and Talebbeydokhti, 2013).

Cohesive sediments tend to agglomerate together. This process is called flocculation and the resulting particle is called floc. Floc size is different, which complicates prediction of settling velocity (DHI, 2014, Nikmanesh and Talebbeydokhti, 2013). Settling of mud floc is one of the most important parameters in evaluating the concentration profile in marine environments. When the muddy bed thickness is higher, the wave breaker line is moved to the shoreline; on the other hand, if the mud bed is too thick, the water waves may not break, due to bottom friction (Nikmanesh and Talebbeydokhti, 2013). Maximum bed shear stress and erosion rate occur near the breaker line, as expected. For shear stress less than critical shear stress for surface erosion, the erosion rate is low and approximately constant, while, above it, the erosion rate increases rapidly with higher shear stress.

2.4   Protection of Coastal Areas

The most significant problem in the coastal areas at all over the world is erosion. Globally, coastal erosion represents serious threats along many coastlines in the world mainly driven by natural causes or human development activities which disturbed the dynamic equilibrium of the coastal region (Airoldi *et al.*, 2005; Rambabu & Mani, 2005; Van Rijn, 2011). Moreover, increased human interventions in coastal processes with poor coastal protection rules caused the more severe coastal erosion problems.

In the tropical coast, coastal protection against erosion can be naturally performed through ecosystem engineering species such as mangroves, which have the ability to modify the local physical environment (Awang, 2010; Borsje *et al.*, 2011). Based on previous study, there is proof that the mangroves could provide natural protection against tidal surge and storms mainly through their ability to attenuate waves (reducing the height of the storm surges) and reduce the current speeds (Barbier, 2015; Hashim *et al.*, 2010).

Over the past decades, the activities of clear-cutting of mangrove along the coastline for coastal development purposes have brought tropical coast such as Malaysian coast into critical conditions due to mangrove degradation and erosion problems (Affandi *et al.*, 2010; Awang, 2010; Blasco *et al.*, 1996; DID, 2006; FAO, 2007; Hashim *et al.*, 2010). Figure 2.4 presents the mangrove degradation and erosion problems at one of the coastal areas in west coast of Peninsular Malaysia.

Figure 2.4: Mangroves degradation in West Coast of Peninsular Malaysia

Regarding the erosion and mangrove degradation problems, coastal rehabilitation through mangrove restoration has received worldwide attention in the tropical coast (Hashim *et al.*, 2010). Coastal rehabilitation is an act of replacing structural or

functional characteristics of lost coastal ecosystems in the disturbed coastal area (Edwards, 1999). However, coastal rehabilitation activities are site specific and can act on limited spatial and temporal scales (Borsje *et al.*, 2011; Wolters *et al.*, 2005). Therefore, specific techniques, depending on specific conditions and greater efforts based on an engineering perspective, are required to be carried out. It can be done by applying or constructing various types of coastal defense structures (i.e. groynes and breakwaters) as a response to defend the coast and replace the natural condition for mangrove to survive (Borsje *et al.*, 2011; Hashim *et al.*, 2010).

2.5 Detached Breakwater

Detached breakwaters are an implementation of coastal protection against erosion that is widely used in coastal engineering practice during the past of few decades (Fairley *et al.*, 2009; Zyserman & Johnson, 2002). They were built in many parts of world, particularly in Japan and Europe. Detached breakwaters are barriers designed to protect the landward area from direct ocean impact. Recently, they have been increasingly popular for mangrove rehabilitation project (Hashim *et al.*, 2010). This was due to their low construction costs, effectiveness in reducing erosion problems, effective in trapping sediment accumulation behind its structures and imposing low environmental impacts (Bricio *et al.*, 2008; Burcharth *et al.*, 2006; Hashim *et al.*, 2010; Taveira Pinto & Valente Neves, 2004).

Generally, detached breakwaters are constructed parallel to the coastline. They are designed in trapezoidal shape as shown in Figure 2.5. They have a low crest elevation and homogeneous stone size (Scheffer, 1999). However, as rapid development of detached breakwater continues, there are many variant in the design of detached breakwater. They could be built with different stone size and variant crest elevation (emergent, submerged or partially submerged). Besides, they could be combined with

armor units which form their exterior layer. Armor layer help their structure to dissipate incident wave, keep the structure stable during water forcing flows (wave or currents) and protect inner layer from eroding.
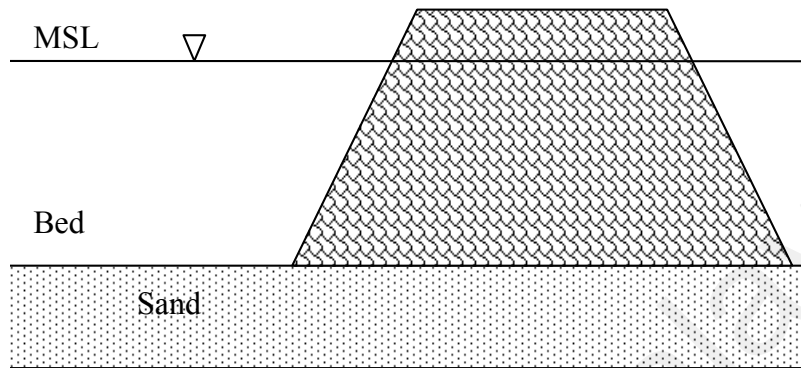
Figure 2.5: Detached breakwater (Scheffer, 1999)

2.6 Coastal Responses to Detached Breakwater

Regardless of the benefit of the coastal defense structures, they can cause complex changes to the coastal morphology (related to shore profile changes in term of accretion and erosion) in the vicinity of their structures (Barbaro & Foti, 2013; Nam *et al.*, 2011a; Sierra *et al.*, 2010; Zyserman *et al.*, 2005). Its coastal morphodynamics vary widely among different cases affected by differences in sediment type, location and design of the structure, and climate condition (Fairley *et al.*, 2009). The complexity of the morphodynamic response to coastal structures is suspected to be higher when the structures are located on intertidal area of cohesive shore with rapidly varying water depths both in time and space, and occupied by mangroves.

Earlier studies done on shoreline response to detached breakwaters have mostly focused on the sandy coast (Archetti & Zanuttigh, 2010; Lamberti & Zanuttigh, 2005; Martinelli *et al.*, 2006; Zanuttigh, 2007). Because the implementation of detached breakwater is rarely found on the cohesive shore, there is a poor understanding of the

morphodynamics on cohesive shores as a result of complexity in the behavior of cohesive sediment (Baas *et al.*, 2013; Fan *et al.*, 2006; Shi & Chen, 1996).

Theoretically, when the land (without breakwater) meets the ocean in a coastal area, the shore has natural defences against attack by wave, currents, and storm (Birben *et al.*, 2007; SPM, 1984b). The first of these defences is the sloping nearshore bottom that causes wave to break offshore, dissipating their energy over the surf zone. The process of breaking often creates an offshore bar in front of the shore that helps to trip following waves. The broken waves re-form to break again and may do this several times before finally rushing up the foreshore.

However, when breakwaters are constructed in the coastal area, the presence of the breakwater will be interacted with waves (Chang *et al.*, 2012). Further, a portion of the wave energy will be dissipated, a portion will be reflected and a portion of the energy may be transmitted past the structure (depending on the geometry of the structure) (De Jong, 1996). If the crest of the structure is submerged, the wave will simply transmit over the structure. If the crest of the structure is above the waterline, the wave may generate a flow of water over the structure, which, in turn, regenerates waves in the lee of the structure. Also, if the structure is sufficiently permeable, wave energy may transmit through the structure. Due to transmission at the breakwater, the wave spectrum is changed not only with respect to the total energy, but also with respect to the spectral shape. The loss of total energy results in the decrease of significant wave height, while the spectral shape change results in lower mean wave periods (Young, 2008).

At non-cohesive shore, the presence of breakwaters leads to a sand accretion in the lee of its structure and form sandbar (tombolo). The tombolo is grown from shore towards the structure. When the sand accretion is still not reaching the structure, the

sandform is known as salient. If a breakwater is built perpendicular to the shoreline, the longshore sediment transport is cut at the breakwater, thus significant morphological changes occur near the breakwater. As depicted Figure 2.6, there will be accretion on the updrift side while erosion on the downdrift side of the breakwater after the breakwater is built for two and four years, respectively (Birben *et al.*, 2007; Young, 2008).

At cohesive shore, it is still required more research work related to investigation of hydro-morphodynamic changes due to the presence of breakwater and provide the valuable information for coastal managers in helping them for creating the proper environmental management and coastal suitable design of coastal defense structures on cohesive shore.
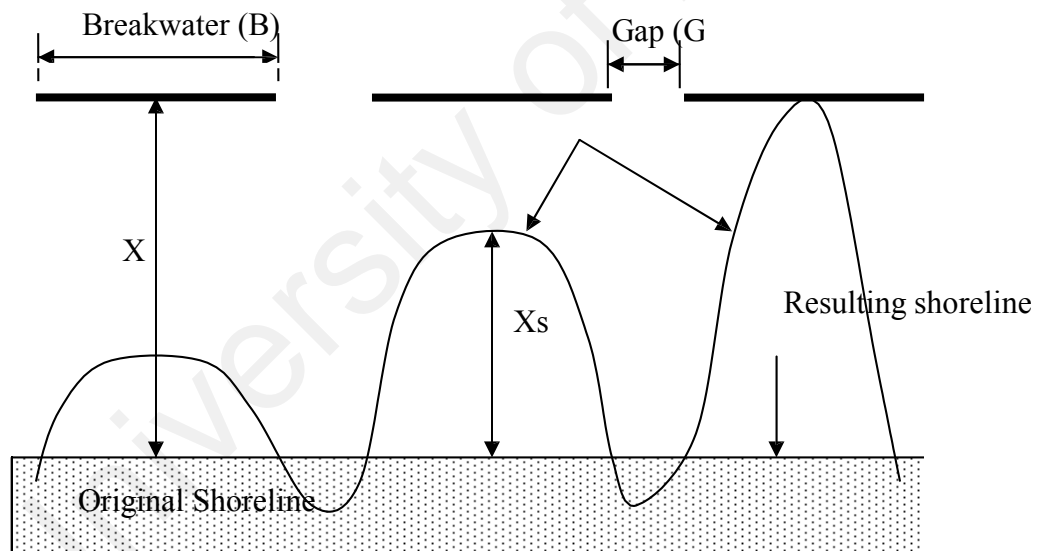
Figure 2.6: Shoreline responses to breakwater on non-cohesive shore (Birben *et al.*, 2007)

Where:

B   : breakwater length (m)

G   : breakwater gap (m)

X   : distance to shoreline (m)

Xs   : salient length (m)

2.7 Coastal Modelling

Basically, there are two types of models used to evaluate the coastal hydro-morphodynamic changes. They are physical models and numerical models. The physical models are advantageous in correctly reproducing physical behavior. However, they have certain limitations such as selecting the appropriate scale, high cost, randomness of natural phenomena, non-availability of complete understanding of coastal hydrodynamic behaviour and existence of outnumbered factors that influence behaviour of waves and tidal regime. Hence, the prediction of the coastal hydro-morphodynamic changes has largely relied on the numerical models supported by physical tests (Nam *et al.*, 2011b; Nicholson *et al.*, 1997; Shamji, 2011; Zanuttigh, 2007).

Numerical models are a powerful tool in understanding the coastal physical systems (Toorman, 2001). They facilitate study of the coastal hydraulic and coastal profile changes, particularly where both time and spatial scales are large. They provide an effective and efficient ways to solve equations that have been theoretically and empirically derived from previous studies (Black & de Lange, 1995 in Awang, 2010). The models are able to examine the complex systems of the multiple processes in the coastal areas that may occur simultaneously and generate an output for scientific analyses.

Due to the possibility of simulating a wide variety of conditions at limited cost, numerical models have become more popular in coastal engineering project and has been an indispensable tool in coastal hydro-morphological studies (Nam *et al.*, 2011b). These models have been under intensive development in the past 28 years with a concentration on two dimensions such as MIKE 21, ICEM, DELF2D (Archetti & Zanuttigh, 2010; Nam *et al.*, 2011b; Nicholson *et al.*, 1997; Saied & Tsanis, 2005; Saied

& Tsanis, 2008) and quasi three dimensions (Q3D) (Rakha, 1998), while the applications of 3D models need the validation against high-quality data sets, which are still limited (De Vriend *et al.*, 1993; Rakha, 1998).

Based on previous study, MIKE 21 model by Danish Hydraulic Institute (DHI) has proved the accurate prediction of hydrodynamic, spectra wave and mud transport characteristics (Eissa & Lebleb, 2015; Patra *et al.*, 2015; Sravanthi *et al.*, 2015). Jose & Stone (2006) and Jose *et al.* (2007) used MIKE 21 Spectra Wave model to investigate the spectral wave transformation in south-central Louisiana. Patra (2015) estimated and validated the offshore wave characteristics in Bay of Bengal, East Coast of India by using MIKE 21 Spectra Wave FM. Sravanthi *et al.* (2015) carried out the suspended sediment transport study along the cohesive shore of Central Kerala, west coast of India.

However, numerical models also have certain limitations. They need multiple inputs which widely varied among different sites. Most of the numerical models are based on large number of geological and oceanographic assumptions. Model assumptions should be examined collectively also in isolation. No numerical model can be an ideal representation of actual field conditions. There is a need for a theoretical re-examination of mathematical models used to predict any physical system (Roberts *et al.*, 2000). In addition, although some equations in a numerical model cannot be changed, some of the coefficients can be varied from site to site. Therefore, calibration and validation are needed in numerical simulations in order to match the predictions and the measured data (Black *et al.*, 2008).

2.8   Summary

Based on obtained literatures, it can be concluded that:

1) Detached breakwaters are an implementation of coastal protection against erosion that is widely used in coastal engineering practice during the past few decades

(Zyserman & Johnson, 2002; Fairley *et al.,* 2009). Recently, detached breakwaters are being used in mangrove rehabilitation projects (Hashim *et al*., 2010; Kamali, 2011).

2) Detached breakwaters have been used worldwide in non-cohesive coastal landscape (Zyserman & Johnson, 2002, Airoldi *et al*., 2005, Caceres, 2005; Saied and Tsanis, 2008; Fairley *et al.,* 2009, Sierra *et al*., 2010; Munari *et al.,* 2011; Nam *et al.,* 2011). Therefore, shoreline responses to detached breakwaters have mostly focused on the sandy coast (Lamberti & Zanuttigh, 2005, Martinelli *et al.,* 2006, Zanuttigh, 2007, Archetti & Zanuttigh, 2010).

3) Limited study has been done on the responses of coastal hydro-morphodynamics to detached breakwaters along the cohesive shore.

4) Numerical modelling is a powerful tool in understanding physical systems. It facilitates study of the coastal hydraulics, particularly, where both time and spatial scales are large. The models are able to examine the complex systems of the multiple processes in the coastal areas that may occur simultaneously.

5) Based on previous study, MIKE 21 model has provided the accurate prediction of hydrodynamic, spectra wave and mud transport characteristics (Patra *et al.,* 2015; Eissa & Lebleb, 2015; Sravanti *et al.,* 2015).

6) For the coastal morphodynamic studies, shore profile measurement using leveling equipment such as Total Station is the most accurate method used to estimate the coastal morphodynamic changes. Total Station is an effective tool to measure the surface elevations with an accuracy of $\pm$ 1 cm on large scales of high resolution coverage (Fairley, 2009).

CHAPTER 3: **RESEARCH METHODOLOGY**

This chapter describes the conditions of the study area, explains the required data to fulfill the research objectives and discusses detail methods used in data collection, data analyses and obtaining final results. The detail descriptions of items mentioned earlier are presented in the sections below:

3.1 Description of Study Area

This study was carried out at the coastline of Carey Island, west coast of Peninsular Malaysia with longitude $02^049"26"$ N to $02^049"29"$ N and latitude $101^020"22"$ E to $101^020"27"$ E. The coastline of Carey Island is located within the Strait of Malacca. Figures 3.1 and 3.2 present the plan view of the study area.

Figure 3.1: Location of the study area
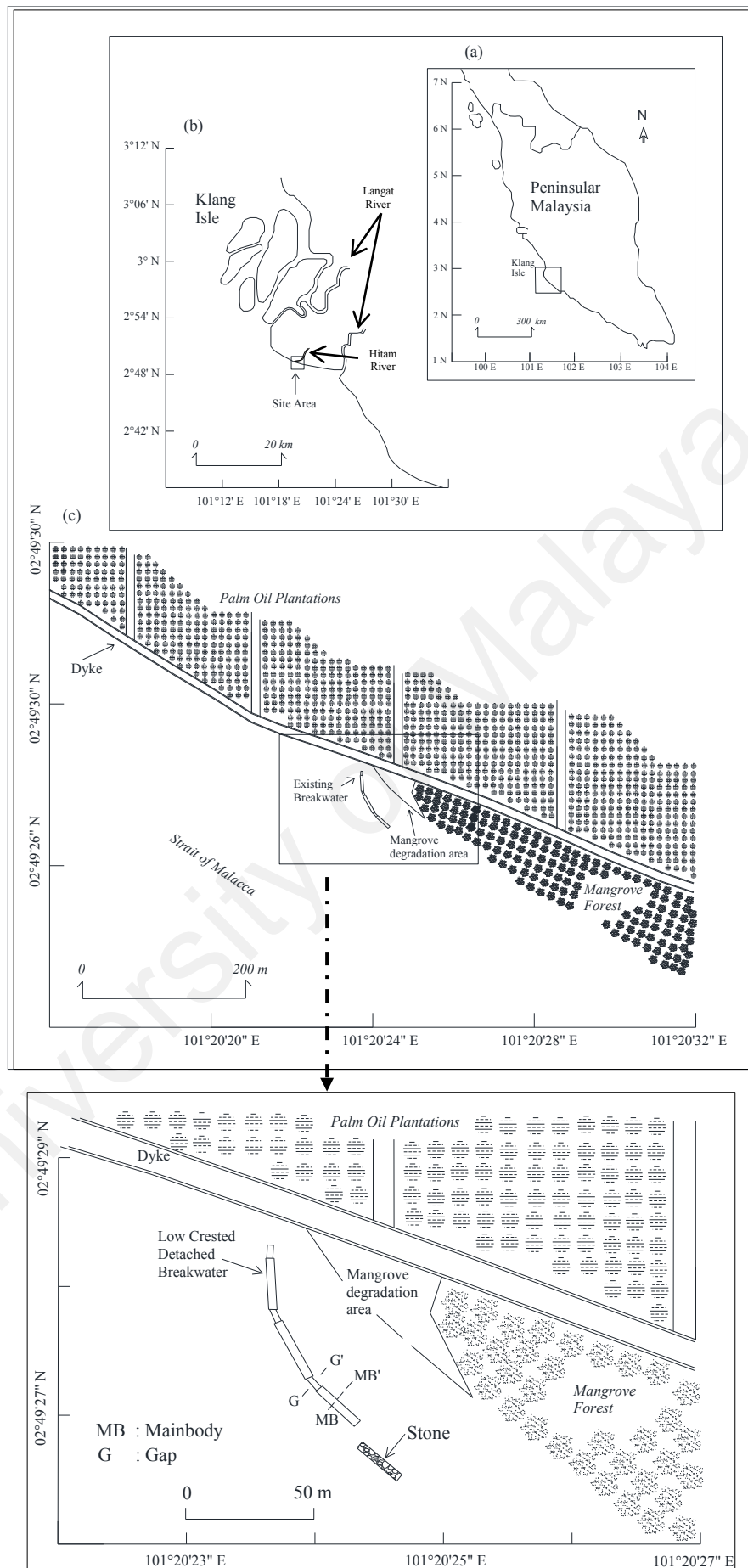
Figure 3.2: Plan view of the study site at Carey Island, (a) map scale 1:300000 m, (b) map scale 1: 20000 m, (c) map scale 1:200 m

3.1.1 Background

Klang Isle in Malaysia is a cluster island composed of 8 small islets. Carey Island is located within Klang Isle and it is the largest island separated from the mainland by the Langat River. Langat River meets the coastline some 8 km away from the site. Moreover, there is a small clogged river named Hitam River at the middle coastline of Carey Island approximately 1.5 km away from the site with 1.5 km length. This river is dead-end and the water flows are depended on tidal-induced currents.

The coastline of Carey Island is one of the mangrove forest reserves in the Strait of Malacca (Kamali, 2011; Motamedi *et al.*, 2014). Mangrove forest grows in the intertidal zone areas approximately 80 m width, with specific bed elevations, which result the specific tidal regime for mangrove survival. Based on field monitoring, the suitable bed elevations for local mangrove survival are approximately between 1.2 m above MSL and 2.2 m above MSL.

In 1995, an earth dyke was constructed along the coastline of the island by the *Department of Irrigation and Drainage (DID)* to protect landward against tidal inundation and prevent salt water intrusion during high tides (Kamali, 2011). Although the dyke was successful in protecting the land from tidal inundation, its construction has disturbed the mangrove forest areas due to clear-cutting of mangrove plantations during their construction stage. Therefore, the section of bare shoreline has undergone massive erosion. It also caused reduction of the bed elevations and changed the tidal regime (Hashim *et al.*, 2010; Kamali, 2011; Motamedi *et al.*, 2014).

Recently, the critical condition of Carey Island coastline in term of erosion and mangroves degradation problems attracted the attention of local decision-makers. It is because these problems bring more severe coastline threat. In this respect, a greater effort is needed in order to reduce erosion and rehabilitate the mangroves. As one of the

engineering approaches for achieving these purposes, an innovative design of an 80-m long detached breakwater was constructed on the intertidal zone of Carey Island coast (exactly at the front of mangrove degradation area) in 2009 by University of Malaya. It is expected to reduce the shoreline erosion at the site and increase the sediment deposition behind the structure for replacing the lost sediment in mangrove degradation areas.

3.1.2 Geographical Condition

The intertidal area of Carey Island coast is predominantly covered by cohesive sediment. The original elevations at the site (particularly near to the mangrove degradation areas) before the construction of the breakwater in year 2009 was 1.2 m above MSL near the shoreline and 0.5 m below MSL about 50 m seaward from the shoreline. The existing mangroves were recorded on elevations between 1.2 m and 2.2 m above MSL. Figure 3.3 shows the coastal profiles at the site before construction of the detached breakwater.
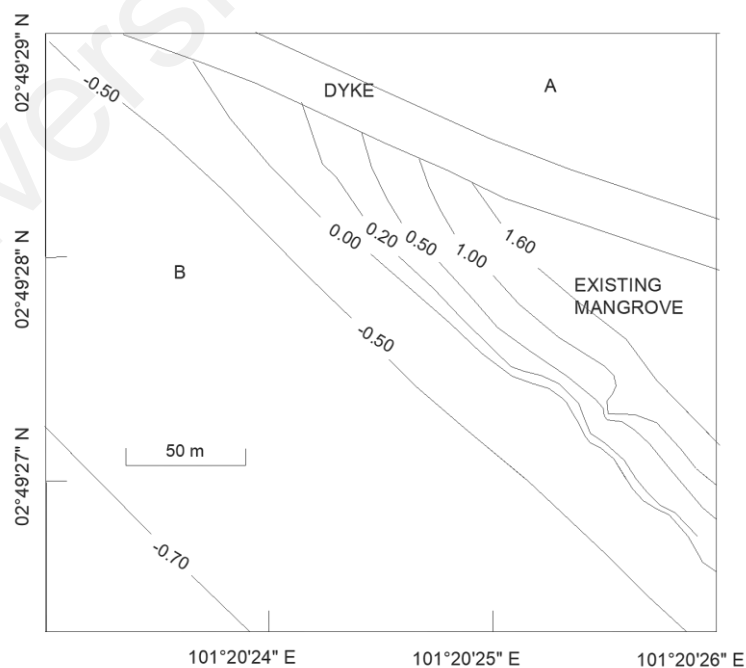
Figure 3.3: Topographical condition at the study site before construction of the breakwater, (A: landward, B: seaward).

3.1.3   Climate Conditions

The climate at Carey Island, Malaysia is mainly influenced by two monsoons during the year, the Southwest monsoon (May to September) and the Northeast monsoon (November to March). The period between both monsoons is a transition period (April and October). Carey Island coastline receives daily tidal inundation. It has a typical semi-diurnal tidal regime (two tidal cycle per day) and has characteristics as mesotidal with a maximum spring rise of 4.33 m above MSL and a maximum neap rise of 2.96 m above MSL (JUPEM, 2014). Therefore, tidal currents and wave energies both tend to be important at intertidal areas of Carey Island.

Rainfall data for the study area was obtained from the West Estate Office, Sime Darby Plantation Berhad, carey Island. In 2009, the total annual precipitation at the study area was 2220.51 mm while the maximum and minimum monthly rainfalls were 372.20 mm in August and 112.20 mm in June, respectively. From in situ measurements conducted monthly using an IQ Scientific Multiparameter Probe, with samples collected at depths of 10 and 20 cm, the soil water had a mean pH value of 7.13 ± 0.19, the salinity ranging from 24.3 to 29.2 and the temperatures averages from 22 to 33oC throughout the year.

3.1.4   Construction Records of Existing Detached Breakwater

The detached breakwater is located in a barren area at front of to the mangrove degradation area (02˚49"27" N to 02˚49"28.5" N latitude and 101˚20"23.5' E to 101˚20"24.5" E longitude) which has been previously occupied by fringing mangroves (Figure 3.2).

The breakwater is a homogenous rubble mound built with a combination of quarried rock/stone (D_{50} = 17 cm) and an innovative armoring unit termed as *L-Block* (Kamali, 2011). The stones were placed in gabion baskets along the shoreward slope to (a)

improve structural stability, (b) reduce the amount of required stones and (c) allow the existence of smaller stones.

The breakwater was designed such that it submerges at high tide (approximately when the tide level > 1 m above MSL) and emerges at low tide (approximately when tide level < 0.8 m above MSL). The first head of the breakwater was positioned nearly perpendicular to the shoreline and the last head was placed parallel to the shoreline approximately 40 m away from the shoreline.

The mainbody of the breakwater is 1.40 m high and 2.5 m wide giving it a crest level of 0.9 m above MSL. The mainbody was separated into three segments. The first and third segments are 20 m long and the second segment is 30 m long (Figure 3.2). In order to reduce the velocity of return flow/rip current and prevent erosion at the gap areas, the gap was not left empty but it was also constructed with a height which is approximately half the height of the mainbody, having a crest level of 0.3 m above MSL. The gap can also limit the wave energy passing through it, while ensuring water circulation, reducing wave diffraction and subsequently increasing the sediment accumulation in the lee of the breakwater (Hashim *et al.*, 2013). Figure 3.4 illustrates the details of the cross-section of mainbody and gap of the breakwater.
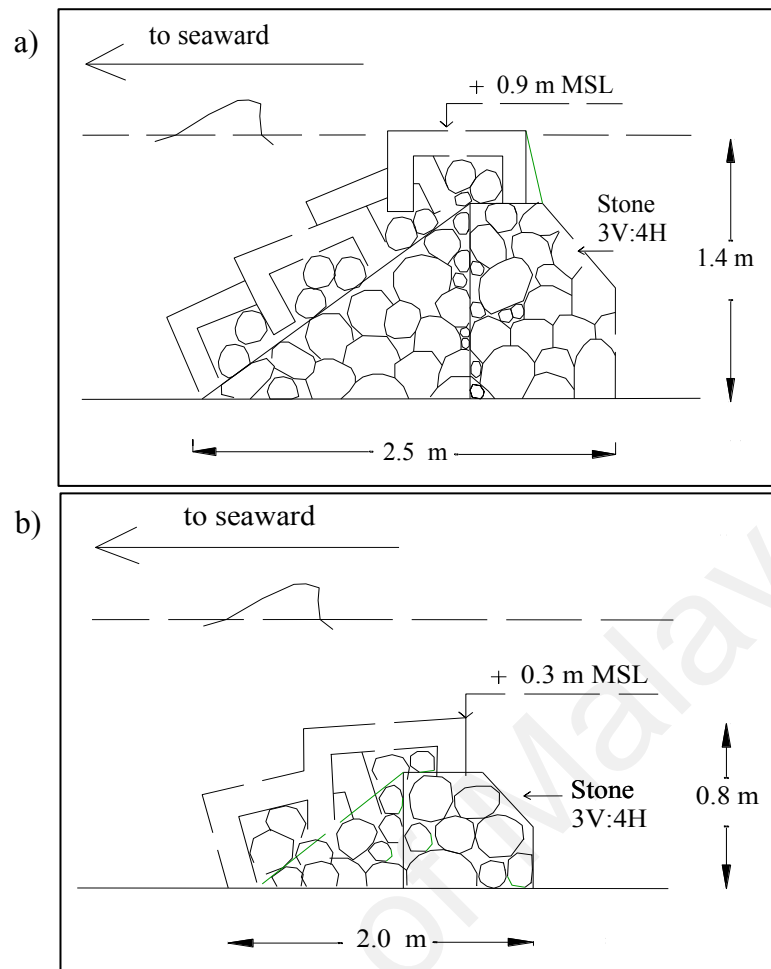
Figure 3.4: Cross sections of the breakwater (a) the mainbody (MB-MB') and (b) the gap (G-G')

3.2   Data Collection and Analyses

The data required for completing this research study consists of field-measured data and secondary data. Field-measured data include: the soil samplings along the coastline of Carey Island; fine resolution of the bathymetry data along Hitam River, Langat River and Carey Island coastline; measurement of currents, waves, water level, suspended sediment concentration (SSC) characteristics near the study site area; water samplings at the mouth of Langat River; and monitoring of coastal bed profiles in the vicinity of the breakwater.

Soil samplings were used to determine the coastal bottom characteristic along the coastline of Carey Island. For this, soil analyses tests were conducted in the laboratory.

Characteristics of currents, such as current speeds and current directions; characteristics of waves, such as wave heights, wave periods and wave directions; water level, suspended sediment concentrations measured near the study site area were used for the model calibration and validation purposes. Water samplings were used to obtain the amount of total suspended sediment (TSS) contributed from the Langat River to the Strait of Malacca. While, the coastal bed profiles were used to analyze the changes of morphodynamic around the mangrove degradation area due to the presence of detached breakwater.

The secondary data include the long-term period (approximately 10 years) of climate data consist of wind data and wave data; long-term period of tide at Lumut station, Belawan station, Tanjung Keling station and Dumai station; and bathymetry data for ocean region. The detail descriptions for data collection and analyses are presented in the next sections.

3.2.1 Field Works

The detail descriptions of the data collection in the field are given under different sub-heading in the following sections.

3.2.1.1 Soil Sampling

Ten bed samples were collected in the site area on 5th December 2014 (at front and behind of the detached breakwater) at depths 0~100 cm using a sediment core sampler. In addition, ten more bed samples were collected along the coastline of the Carey Island at depths 5~30 cm using grab sampler. It was carried out to characterize the particle size distributions of bottom sediments in the Carey Island coastline and to calculate the soil density around the study area. Figure 3.5 presents the locations of the soil bed samplings.
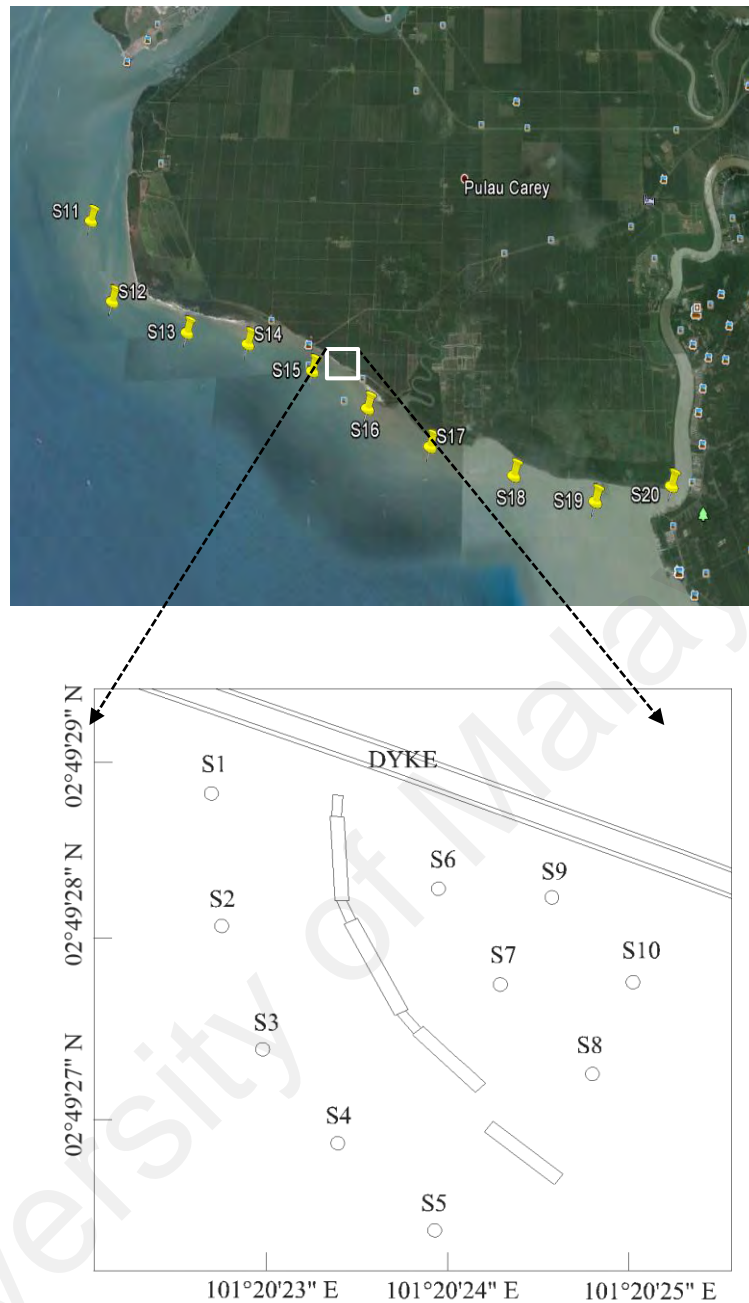
Figure 3.5: Location of the soil samplings

3.2.1.2 Bathymetry Measurements

Precise or accurate bathymetry measurements are essential to get the good and reliable results in hydrodynamic modeling (Mourre *et al.*, 2004). Lack of good bathymetry results in poor calibration and validation of the results. Therefore, collection of bathymetric data is one of the most important aspects in numerical hydrodynamic modeling.

A bathymetry survey with fine resolution was conducted around the coastline of Carey Island and Langat River covering an area of 17.5 km x 5 km with lines space at 20 – 500 m intervals. The survey activities were carried out during the spring tide on 8th to 12th December 2014. Figure 3.6 presents the locations of the bathymetry survey. In order to reduce the cost of the survey, lines space at 20 m intervals were conducted for the areas near the study site (approximately 1 km x 5 km). Subsequently, line spacing at 50 m intervals was conducted for 2 km at its right and left sides, and for the remaining area, the line spacing were are 100 m, 250 m and 500 m.

During the bathymetry survey, a tide gauge is necessary to record and produce tidal water levels. A tide gauge was installed near to study area during the survey for the purpose of correcting the water depths and establishing a sounding datum linked to a known datum. The tide gauge was secured in a 20 m length PVC pipe before lowering into the water column. The pipe was then tied to the jetty pillar to secure the tidal gauge sensor.
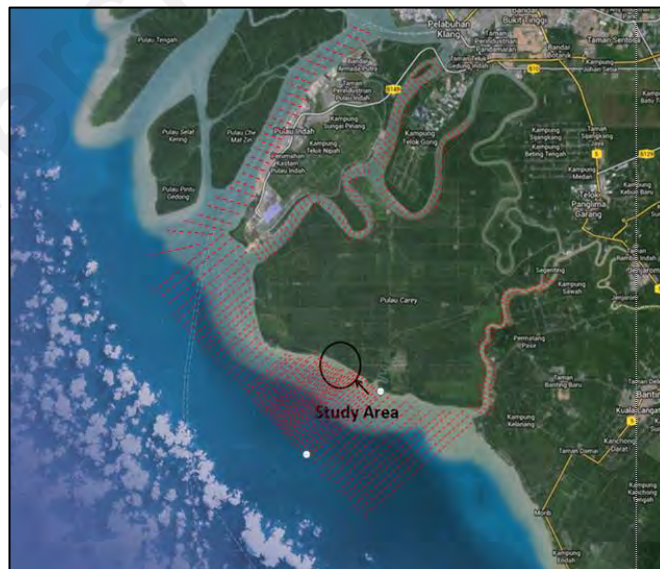
Figure 3.6: Bathymetry measurements at the coastline of Carey Island and Langat River on 8th to 12th December 2014

The bathymetry survey on 8th to 12th December 2014 was carried out using a boat. A portable single beam Reson-210 model of echo sounder unit was used to execute the bathymetry survey in that times (Figure 3.7(a)). Besides, a hummingbird differential global positioning system (DGPS) was used throughout the survey to get the coordinate positions of the bathymetry data. The positioning of system differential correction data was based on the respective reference station received via satellite. The horizontal accuracy of the DGPS was ± 0.5 m.

During the bathymetry survey operation, the HYPACKMax survey software (Figure 3.7 (c)) was interfaced with a Reson-210 survey echo sounder, as well as with the Humminbird DGPS (Figure 3.9(b)). The Reson-210, which used a narrow beam (3°) and was configured with a single frequency of 208 kHz transducer, produced a continous analog record of the bottom and transmitted approximately 5-10 digital depth values per second to HYPACKMax depending on the echo sounder settings. Within HYPACKMax, the time-tagged positions and depth data were merged to create depth records along the actual survey track. These records were viewed in real time to ensure adequate coverage of the survey area.
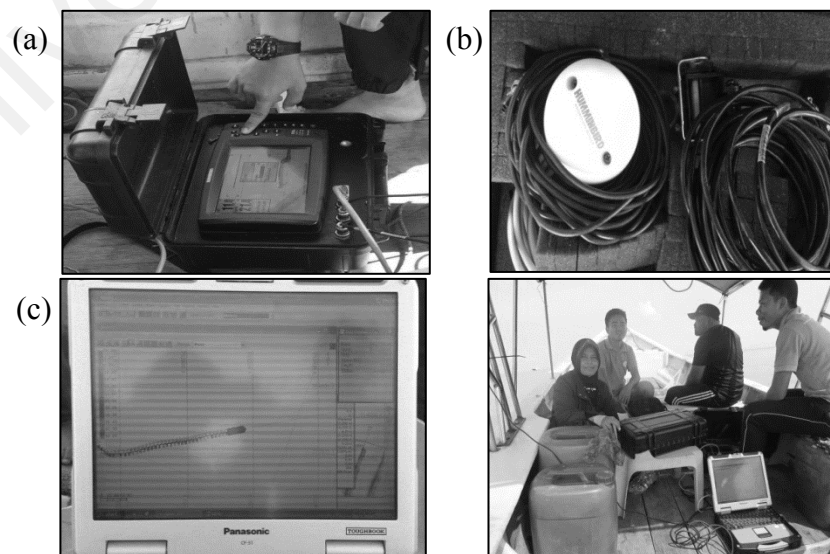
Figure 3.7: Bathymetry survey operation, (a) single beam echo sounder, (b) Humminbird DGPS, (c) HYPACMax software

3.2.1.3 Water Levels, Currents and Waves Measurements

Two units of *Acoustic Wave and Current Profiler* (AWAC) with 600 kHz frequency from Nortek were utilized to measure the water levels, currents and waves parameters from two locations in the field (approximately 5 km from the study area). These data are used to calibrate and validate the simulation results of hydrodynamic and spectra wave models. The measurements were performed from 23rd December 2014 to 7th January 2015 to cover neap tide and spring tide conditions. The water level, current speeds and current directions were recorded at 10 minutes interval, while wave parameters were recorded at 1 hour intervals. The locations of the AWAC are presented in Figure 3.8 and Table 3.1.

Figure 3.8 Locations of AWAC 1 and AWAC 2

Table 3.1: Co-ordinate locations of AWAC 1 and AWAC 2

Station	Longitude (x)	Latitude (y)	Depth (m)
AWAC 1	101˚ 20'' 11.18''E	02˚ 48'' 40.02''N	10.324
AWAC 2	101˚ 18'' 58.14''E	02˚ 49'' 26''N	12.557

3.2.1.4 Suspended Sediment Concentration (SSC) Measurements

Four units of optical backscatter sensors (OBS-3A) were installed at four locations, while two of them were installed together with AWAC equipments. These sensors were used to record the suspended sediment concentration (SSC) required as boundary conditions and calibration and validation purposes of the sediment transport model of *MIKE 21 Mud Transport FM*. The measurements were performed from 23rd December 2014 to 7th January 2015 to cover neap tide and spring tide conditions. The suspended sediment concentrations (SSC) were recorded at one hour interval. Table 3.2 describes the locations of OBS-3A sensors.

The OBS-3A is an optical backscatter (OBS) sensor used for measuring turbidity and suspended solids concentrations by detecting near infrared (NIR) radiation scattered from suspended particles (Campbell, 2008). It is supplied with a software programme „OBS for Windows (OFW)"which acts as an interface the OBS-3A and is used to turn the instrument ON and test the sensors; recording data directly with a PC or uploading stored data from the OBS-3A; exporting data to spreadsheet; plotting data and turning the OBS-3A off.

Table 3.2: Co-ordinate locations of OBS-3A sensors

Station	Longitude (x)	Latitude (y)	Depth (m)
OBS 1	101° 20" 11.18'E	02° 48" 40.02" N	10.324
OBS 2	101° 18" 58.14" E	02° 49" 26" N	12.557
OBS 3	101° 26' 10.06" E	02° 40' 7.91" N	15.221
OBS 4	101° 06' 44.34" E	03° 8' 36.81" N	10.483

3.2.1.5 Water Sampling

Langat River can contribute an amount of sediments to the study site areas through the Strait of Malacca. In this study, water samples were collected at mouth of Langat

river on 23rd December 2014 to 7th January 2015 (at Longitude 101°24'6.24" E and Latitude 2°48'2.72" N) to measure the total suspended sediment, which flows from Langat river to the coast (Strait of Malacca). The water samplings were carried out hourly using a boat and a Niskin water sampler (Model 1010).

3.2.1.6 Coastal Bed Profiling

Bed surface elevations in the vicinity of the detached breakwater at intertidal area of cohesive shore of Carey Island were monitored during the years 2009 to 2014 by using a bed profiler method. The instrument used in this study was a high end TOPCON total station. The total station is an effective tool to measure the surface elevations with an accuracy of $\pm$ 1 cm on large scales of high resolution coverage (Fairley, 2009).

In this study, the bed surface monitoring was mainly concentrated in the vicinity of the breakwater where the efficiency of the structure was expected to be more significant. The monitoring activities were commenced shortly before the construction of the structure in January 2009 and continued for a six years period with four months surveying interval. The bed surveying were conducted along 24 profile lines (CS1 to CS24), which were nearly perpendicular to the shoreline as illustrated in Figure 3.9. The bed surface profiles from the year 2009 to 2010 were obtained from the previous study done by Kamali (2011). Table 3.3 presents the detail monitoring schedules for bed profiling surveys at the Carey Island.

However, it is often difficult to conduct surveys on cohesive shores due to the limitation of accessibility. This is because any movement on the bed level can significantly disturb the sedimentary surface. In order to ease the monitoring process, at every 5 m distance of each profile line, we pushed the staff into the cohesive sediment in the vicinity of the breakwater (Figure 3.9). The measurements were then carried out

during low tide exposure referenced to the *Department of Survey and Mapping Malaysia (JUPEM)* datum (B 5345 and B 63083).
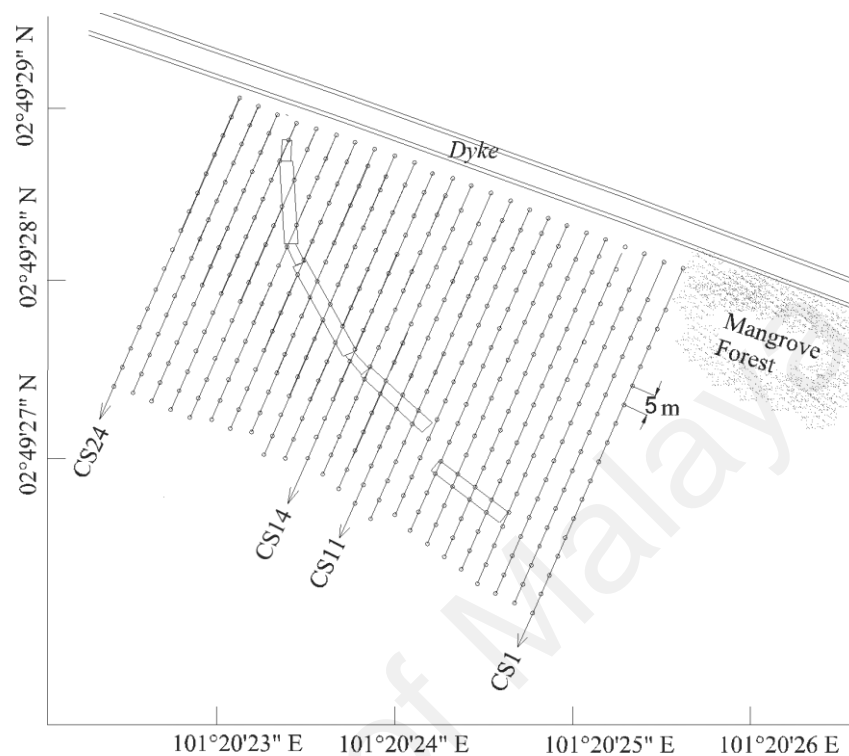
Figure 3.9: The profiling method in the site area

Table 3.3: Monitoring schedule of bed profiling

No Survey	Date at every Consecutive Survey	Surveying interval (period)
1	January 2009	0 (Before construction of the breakwater)
2	April 2009	4 months
3	August 2009	4 months
4	January 2010	4 month
5	16-17 December 2012	3 years
6	14-15 April 2013	4 months
7	20-21 August 2013	4 months
8	22-23 January 2014	4 months
9	16-17 April 2014	4 months
10	6-7 August 2014	4 months
11	8-9 December 2014	4 months

3.2.2 Laboratory Works

3.2.2.1 Soil Particle Analyses and Density Determination

Before conducting the soil particle analyses, the soil samples of sediment core and grab were dried. For the sediment core samples, the soil samples were divided for the first layer (0 to 40 cm depth) and the second layer (40 to 100 cm depth). Further, 500 g dried soil of each sample was sieved using 2 mm – 0.063 mm sieves. Subsequently, a hydrometer test was conducted for soil that passed through 0.063 sieves. In this study, the *British Standard (BS) 1377 part 2*, method 9.2 and 9.3 were used for dry sieving test, while method 9.5 was used for hydrometer test. For determining the density values of bed soils in the site area, standard test *ASTM D 2937* was followed. Soil samples with 5 cm diameter (each layer) were extruded from the tubes approximately 10 cm length. The mass and volume of the soil specimens were further measured and moisture contents of the soils were determined.

Based on the results of the soil particle analyses, the grain diameter (D_{50}) of the cohesive sediments at intertidal area of Carey Island at depth of 0 to 40 cm was about 0.015 – 0.022 mm. Furthermore, the subsoil condition at depths of 40 to 100 cm was found to be stiff clay. The bulk density values of the bed soils in the study site varied from 1.13 to 1.27 g/cm^3 at the top layer and 1.41 to 1.66 g/cm^3 at the bottom layer.

3.2.2.2 Total Suspended Sediment (TSS)

The water samples collected at mouth of the Langat River were subsequently brought to the laboratory for *total suspended sediment* (TSS) test analyses. For TSS test, 100 ml water of each water sample was filtered through a pre-weighed glass fiber filter. The filters were then dried at 105^0 C in a drying oven and weighted. The differences in mass between the post weight and pre weight of the filter are total suspended sediment in 100 ml water. In this study, TSS test analyses were performed in accordance to standard

method of APHA 2540D. The results of the TSS tests show that the Langat River gives a contribution of suspended sediments to the Strait of Malacca, which include the site area. The average of the total suspended sediments (TSS) that was conveyed from Langat River to the Strait of Malacca is approximately 0.15 kg/m^3.

3.2.3   Data from Secondary Sources

3.2.3.1   Climate Conditions

The daily climate data including wind speeds, wind directions, wave heights and wave periods at the range of latitude 2° N to 3°30" N and longitude 100° E to 102° E from years 2005 to 2015 were obtained from the *Department of Meteorology, Malaysia*. Based on these data, the monthly significant wave heights between year 2005 and 2015 were identified and depicted in Figure 3.10. Figure 3.11 depicts the wind rose generated during northeast monsoon, southwest monsoon and transition period between years 2005 and 2015.
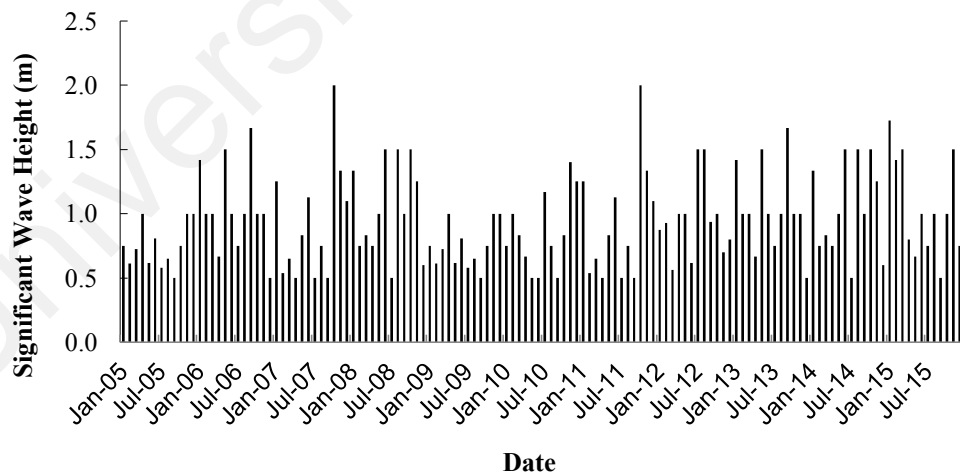
Figure 3.10: Monthly significant wave heights for the period of years between 2005 and 2015 at range of latitude 2° to 3°30"N and longitude 100° to 102° E

a)

b)

c)
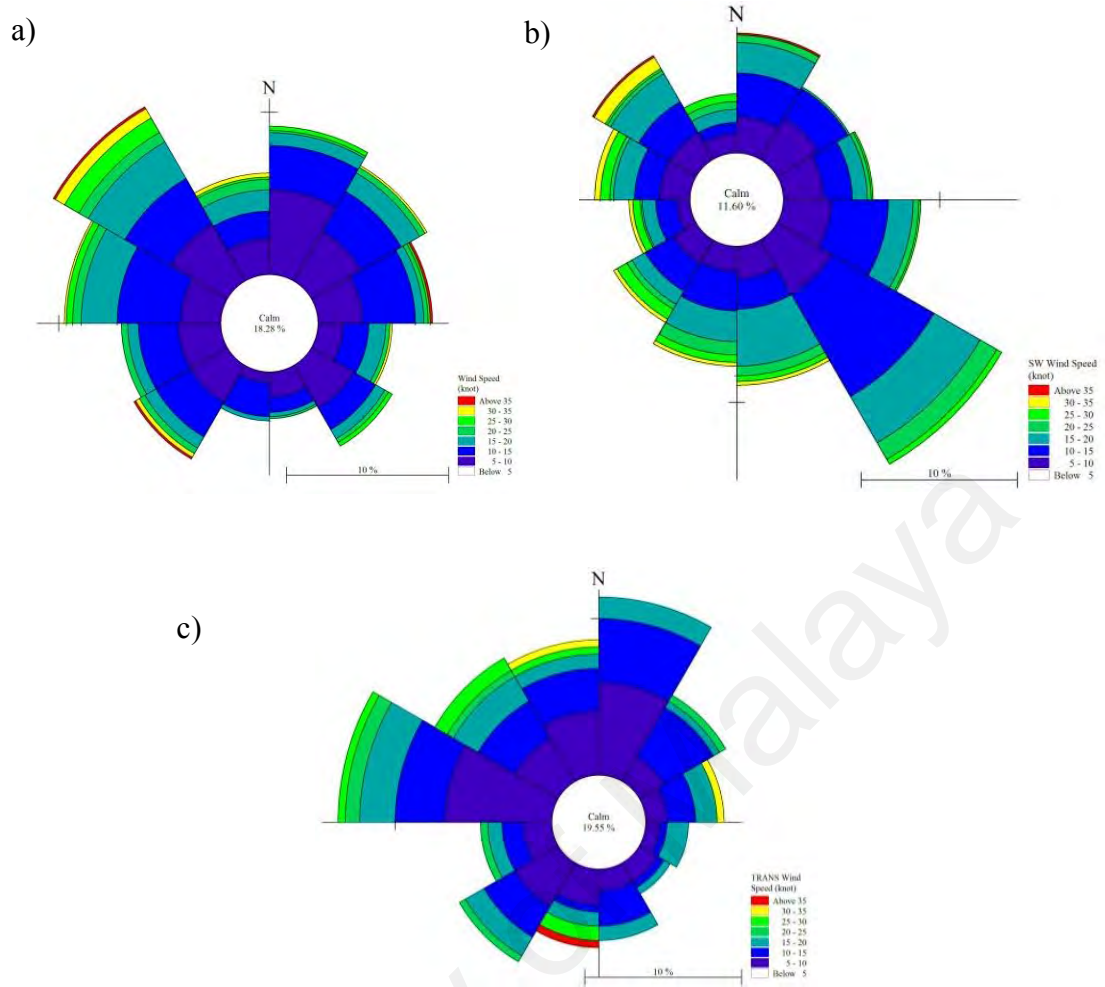
Figure 3.11: Wind rose for the period of years 2005 – 2015 at range of latitude 2° to 3°30"N and longitude 100° to 102° E, a) Northeast monsoon, b) Southwest monsoon, c) Transition period

Based on Figure 3.11, the dominant wind during the Northeast monsoon came from 300º to 330º (magnetic) with the speed of 2.5 to 17.5 m/s while the dominant wind during Southwest monsoon came from 120º to 150º (magnetic) with dominant speed of 2.5 to 15 m/s. In addition, the dominant wind during transition period came from 270º to 300º (magnetic) and from 0º to 30º (magnetic) with the speed of 2.5 to 10 m/s. Figure 3.11 also shows that the strongest wind speeds occured during northeast monsoon.

The wind climate conditions have locally affected the wave climate conditions. Based on Figure 3.10, it is apparent that the monthly highest significant waves are

approximately 1.2 m to 2.0 m in heights and occur between November and January (northeast monsoon). The monthly lowest significant waves are approximately 0.4 m to 1 m in height that are found between April and August (southwest monsoon and transition period).

Besides daily climate data, the 3-hour interval of wind speeds, wind directions, significant wave heights, mean wave periods and mean wave directions at the range of latitude 2° to 3^o30" N and longitude 100° to 102° E from December 2014 to January 2015 were also collected. These data were obtained from *European Centre for Medium-Range Weather Forecasts* (ECMWF) and were used as input in hydrodynamic and spectra wave models of MIKE 21 for model calibration and validation purposes.

3.2.3.2 Water Level Conditions (Tidal)

Water Level conditions (tidal) during the years 2005 to 2015 at Lumut station, Belawan station, Dumai station and Tanjung Keling station are required as northern and southern boundary conditions for the hydraulic study. Tidal data at Lumut station and Tanjung Kelling station were obtained from *Department of Survey and Mapping, Malaysia* while the tidal data at Belawan station and Dumai station were obtained from *Dinas Hidro-Oceanografi* (DISHIDROS), Indonesia.

3.2.3.3 Bathymetry Data

The bathymetric data of the year 2009 for near-shore and ocean regions with fine resolution were obtained from *National Hydrography Centre, Malaysia.* Besides, for the year 2014, the bathymetry data for ocean region was generated by using *C-MAP 2014* software. Figure 3.12 presents bathymetry data generated from *C-MAP 2014* software.
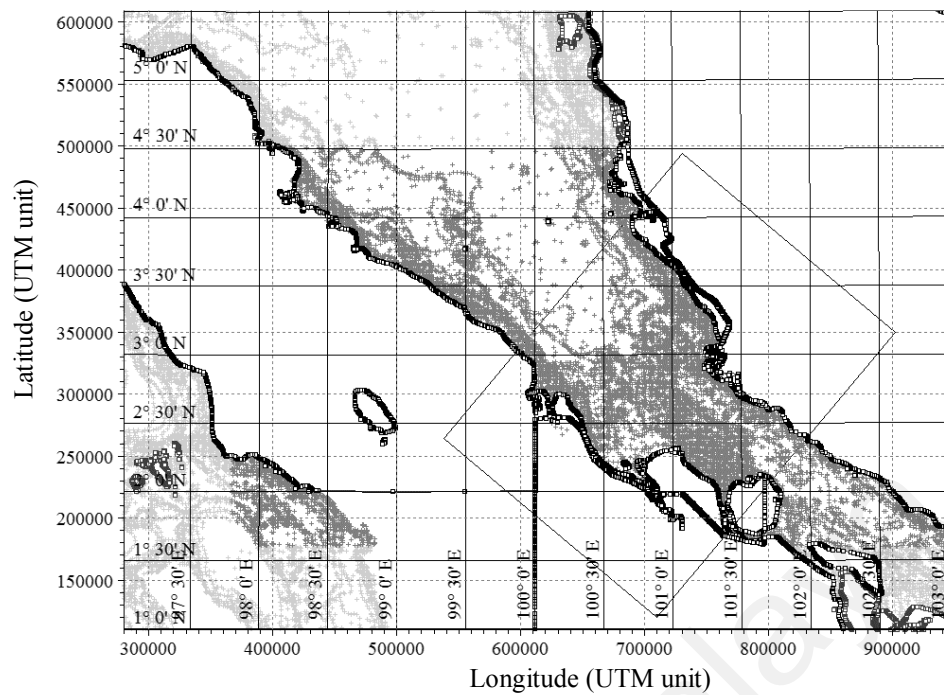
Figure 3.12 Bathymetry in the Strait of Malacca generated using *C-MAP 2014*

3.3 Numerical Modelling

In this study, *MIKE 21 2014 Flexible Mesh (FM) model* packages consisting of *MIKE 21 Hydrodynamic FM, MIKE 21 Spectra Wave FM and MIKE 21 Mud Transport FM* were used to simulate the changes of current, wave and sediment transport characteristic in the coastline of Carey Island due to the presence of detached breakwater. *MIKE 21 FM* is a complete coastal modelling suite, which is capable in designing the data assessment for coastal and offshore structures; and environmental impact assessment of marine infrastructures based on flexible mesh approach. This model was established by *Danish Hydraulic Institute* (DHI) Denmark. The detail descriptions of numerical modeling carried out in this study are given in the next sections.

3.3.1 MIKE 21 Hydrodynamic FM Model

MIKE 21 Hydrodynamic FM is the basic module of the *MIKE 21 FM* system for free surface flows based on flexible mesh approach. It simulates water level fluctuations and

flows in response to a variety of forcing functions in lakes, estuaries, bays and coastal areas. The water levels and flows are resolved following a two-dimensional shallow water equation which is the integration of horizontal momentum equations and the continuity equation.

The integration of horizontal momentum equations and the continuity equation following two-dimensional shallow water equation over depth $h=\eta+d$ are obtained:

$$\frac{\partial h}{\partial t} + \frac{\partial h\bar{u}}{\partial x} + \frac{\partial h\bar{v}}{\partial y} = hS \tag{3.1}$$

X direction of momentum:

$$\frac{\partial h\bar{u}}{\partial t} + \frac{\partial h\bar{u}^2}{\partial x} + \frac{\partial h\bar{v}\bar{u}}{\partial y} = f\bar{v}h - gh\frac{\partial \eta}{\partial x} - \frac{h}{\rho_o}\frac{\partial Pa}{\partial x} - \frac{gh^2}{2\rho_o}\frac{\partial \rho}{\partial x} + \frac{\tau_{sx}}{\rho_o} - \frac{\tau_{bx}}{\rho_o} - \frac{1}{\rho_o}\left[\frac{\partial S_{xx}}{\partial x} + \frac{\partial S_{xy}}{\partial y}\right] + $$

$$\frac{\partial}{\partial x}(hT_{xx}) + \frac{\partial}{\partial y}(hT_{xy}) + hu_s \tag{3.2}$$

Y direction of momentum:

$$\frac{\partial h\bar{v}}{\partial t} + \frac{\partial h\bar{u}\bar{v}}{\partial x} + \frac{\partial h\bar{v}^2}{\partial y} = f\bar{u}h - gh\frac{\partial \eta}{\partial x} - \frac{h}{\rho_o}\frac{\partial Pa}{\partial y} - \frac{gh^2}{2\rho_o}\frac{\partial \rho}{\partial y} + \frac{\tau_{sy}}{\rho_o} - \frac{\tau_{by}}{\rho_o} - \frac{1}{\rho_o}\left[\frac{\partial S_{yx}}{\partial x} + \frac{\partial S_{yy}}{\partial y}\right] + $$

$$\frac{\partial}{\partial x}(hT_{xy}) + \frac{\partial}{\partial y}(hT_{yy}) + hv_sS \tag{3.3}$$

$$\tau_b = \rho_o c_f |u_b|\bar{u}_b) \tag{3.4}$$

$$c_f = \frac{g}{(Mh^{1/6})^2}$$

$$\tau_s = \rho_a c_d |u_w|\bar{u}_w) \tag{3.5}$$

Where:

t   : time (s)

x,y   : cartesian co-ordinates

η   : surface elevation (m)

h   : total water depth (h=η+d) (m)

d   : still water depth (m)

u,v   : velocity components in x and y direction (m/s)

$\bar{u},\bar{v}$: depth average velocities (m/s)

$u_s, v_s,$: velocity by which water is discharged into the ambient water (m/s)

$\bar{u}_b = (u_b, v_b)$: flow velocity above the bottom (m/s)

$\bar{u}_w = (u_w, v_b)$: wind speed, 10 m above the sea surface (m/s)

g   : acceleration due to gravity (m/s^2)

f   : coriolis parameter, latitude dependent (s^{-1})

Pa : atmospheric pressure (kg/m^2)

ρ_o : reference density of water (kg/m^3)

ρ_a : density of air (kg/m^2)

S   : magnitude of the discharge due to point sources

$S_{xx}, S_{xy}, S_{yx}, S_{yy}$: components of radiation stress (N/m^2)

τ_{sx}, τ_{sy} : component of surface wind stress (N/m^2)

τ_{bx}, τ_{by} : component of bottom stress (N/m^2)

T_{xx}, T_{xy}, T_{yy} : frictions, including viscous friction, turbulent friction and differential advection (estimated using an eddy viscosity formulation based on of the depth average velocity gradients).

c_d, c_f : drag coefficient

M   : Manning number (m$^{1/3}$/s)

MIKE 21 Hydrodynamic FM model was used to investigate the changes of current speeds and current directions before and after the construction of the detached breakwater. The changes of the current characteristics were investigated for three

scenarios, which are during northeast monsoon, southwest monsoons and transition period. Besides, the changes of the hydrodynamic characteristics are also presented for different water level conditions as:

(1)   When water levels (WL) are lower than 0.4 m of MSL (crest of gap"s breakwater)

(2)   When water levels (WL) are higher than 0.4 m of MSL and lower than 0.9 m of MSL (crest of mainbody"s breakwater)

(3)   When water levels (WL) are higher than 0.9 m of MSL

During the northeast monsoon, dominant values of the wind speeds and directions between November and March from 10 years period data (section 3.2.3.1) were used. During southwest monsoon, the dominant values of wind speeds and directions between May and September from 10 years period data were used, while dominant values of wind speed and direction on April and October from 10 years period were used for the scenario during the transition period.

Initially, the model setup was prepared using the latest bathymetry measured on December 2014 and generated by *C-MAP software* (section 3.2.1.2 and section 3.2.3.3); and the climate condition (water level and wind) in December 2014 to January 2015 (section 3.2.3.1 and section 3.2.3.2). The wave radiation stresses obtained from spectra wave model were included in the model simulation. The model was further calibrated and validated against field measurement of current speed, current direction and water level measured in December 2014 to January 2015 (section 3.2.1.3).

The calibration parameters used were bed roughness and horizontal eddy viscosity. After obtaining the best model setup, the model was run using bathymetry condition of year 2009 (section 3.2.3.3) and dominant climate conditions (water level and wind) during northeast monsoon, southwest monsoons and transition period from 10 years

period (section 3.2.3.1 and section 3.2.3.2). The model was simulated for two cases that are with breakwater and without breakwater. Finally, the simulation results were compared and analyzed. The steps required for completing the hydrodynamic simulation are represented in the flow chart below in Figure 3.13.
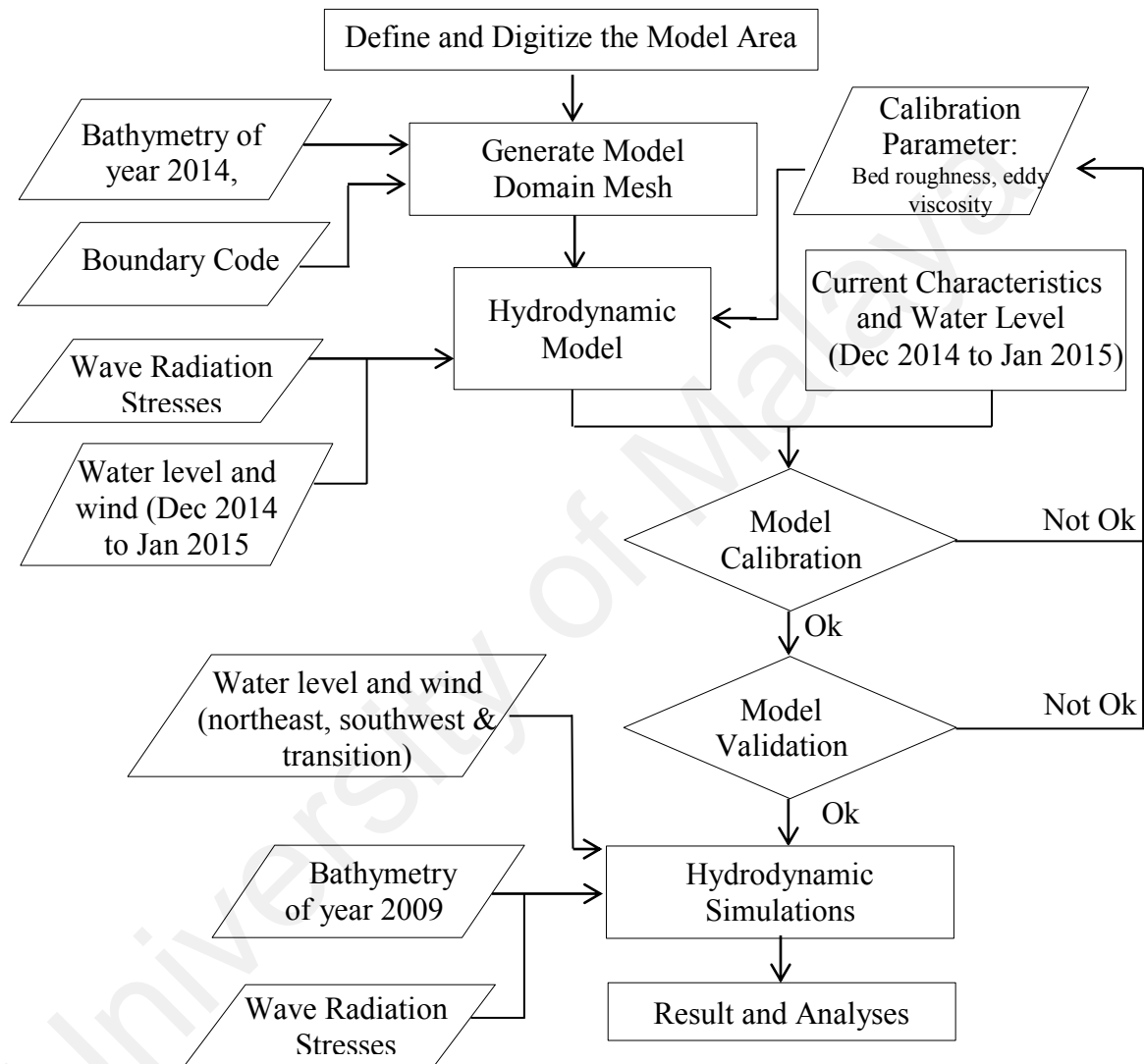
Figure 3.13: Flow chart of the Hydrodynamic Simulations

3.3.1.1 Model Computational Domain

Based on the guideline for coastal hydraulic study established by *Department of Irrigation and Drainage (DID), Malaysia* (2013), the model computational domain used in hydraulic simulations should be sufficiently far away from the study area. In this

study, the computational domain used in the hydrodynamic simulation was expanded to Lumut and Tanjung Keling areas, so that a wider area could be covered for simulation purposes. In this manner, the boundary condition would not affect the area of interest (the study area). Figure 3.14 shows the computational domain of the hydrodynamic model in this study.

The wider mesh along the Strait of Malacca covers an area of 160 km (long-shore) and on average 45 km (cross-shore) with 9241 elements, 4126 nodes and average length of 3 km to 500 m. The near-shore mesh around the Carey Island coast covers an area of 60 km (long-shore) and 30 km (cross-shore) with 14263 elements, 8027 nodes and average length of 300 m to 1 m from offshore to near the detached breakwater structures.

In the hydrodynamic simulations, two scenarios of computational domain were prepared. In the first scenario of computation domain, the bathymetry conditions of the year 2009 surveyed by *National Hydrography Centre, Malaysia* were used. In the second scenario, the bathymetry conditions surveyed in December 2014 compiled with bathymetry generated by using *C-MAP* software were used. The first scenario was used to simulate the hydrodynamic changes before and after construction of the breakwater. The second scenario was used to simulate the hydrodynamic conditions for the model calibration and validation purposes.
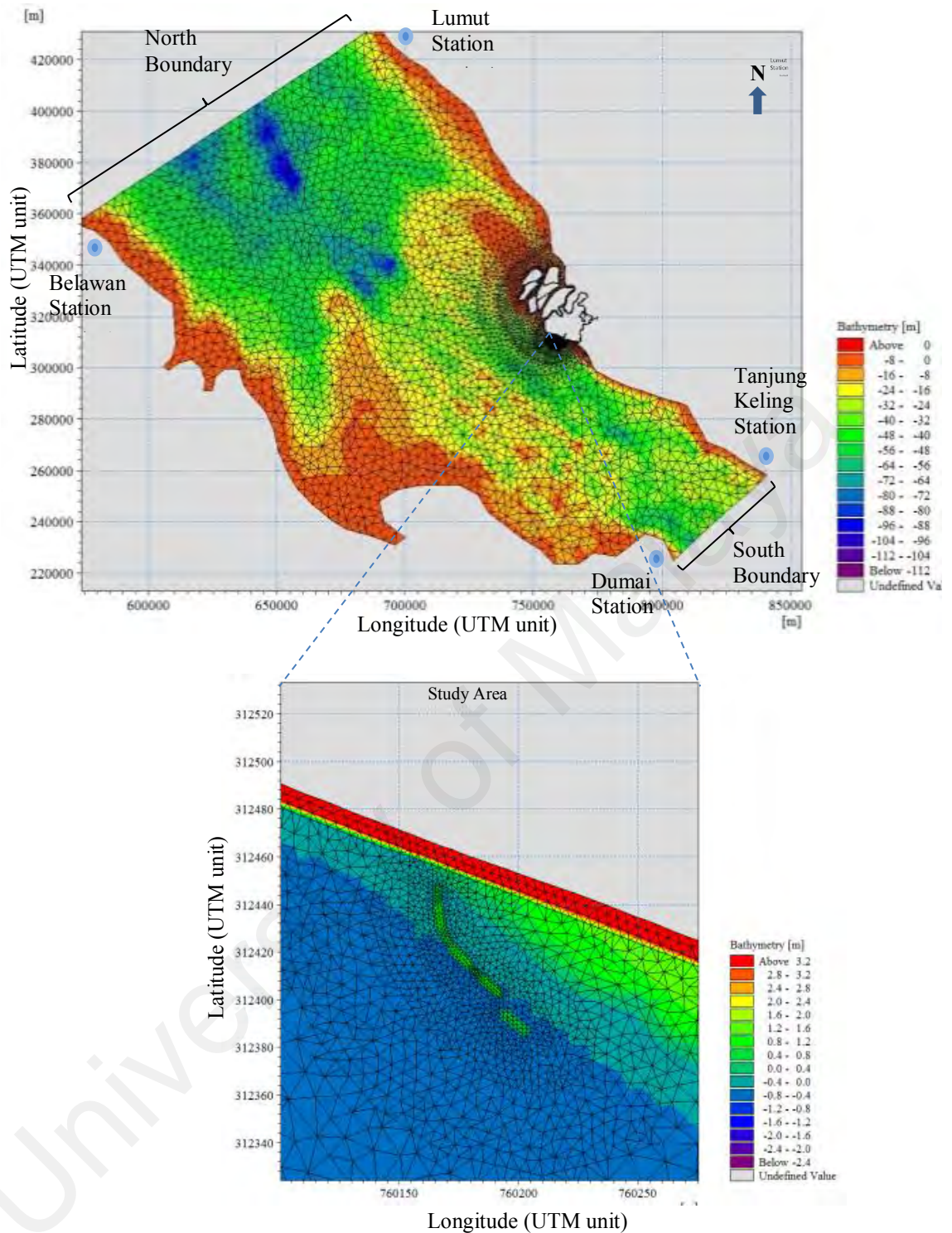
Figure 3.14: Computational domain for Hydrodynamic Simulation

3.3.1.2 Model Input

The input data required for the hydrodynamic model simulation programs comprised

bathymetry data of the years 2009 and 2014 (section 3.2.1.2 and section 3.2.3.3);

dominant values of the wind speeds and directions during northeast monsoon, southwest

monsoon and transition period based on 10-years period data; 3-hour interval data of wind in December 2014 to January 2015 (section 3.2.3.1) and wave radiation stresses obtained from wave spectra simulations.

3.3.1.3 Boundary Conditions

For the hydrodynamic simulation, water levels were used as boundary conditions. Tidal levels at Lumut station and Belawan station (obtained from the *Department of Meteorology, Malaysia)* were spatially interpolated to obtain the values at the north boundary condition, while tidal levels at Tanjung Keling and Dumai were spatially interpolated to find the values at the south boundary condition.

3.3.1.4 Model Setup

During the processes of the model calibration and validation, the model setup was prepared and run from 21 December 2014 to 8 January 2015. The water levels obtained from *Dinas Hidro-Oceanografi, Indonesia* and *Meteorology Department, Malaysia* were used as offshore boundary condition. 3-hour interval wind data obtained from *European Centre for Medium-Range Weather Forecasts* (ECMWF) were used as input wind data. Since the current conditions in the Carey Island coast is affected by wave conditions, wave radiation stresses obtained from simulation results of spectra wave model were included in simulations of hydrodynamic model to generate wave-induced currents.

In the process of determining the best model setup, varying values of Manning numbers and horizontal eddy viscosities were inputted in hydrodynamic model. It was done to find the proper parameters which suitable for study area conditions. The best model setup was determined based on comparison of the simulation results to field measurements.

After model calibration and validation processes were successfully carried out, the calibrated model setups were run with and without the existing detached breakwater for seven days (spring tide conditions) during different season"s conditions by inputting dominant winds based on climate data obtained from the years 2005 to 2014.

During northeast monsoon, the dominant wind speed used was 13 knots or 6.5 m/s and dominant wind direction was 310° (magnetic). During southwest monsoon, the dominant wind speed used was 8 knots or 4 m/s and dominant wind direction was 140° (magnetic). During transition period, the dominant wind speed used was 10 knots or 5 m/s and dominant wind direction was 10° and 280° (magnetic).

3.3.1.5 Model Calibration and Validation

The equations used in numerical models cannot be changed, but some of coefficients or parameters used inside numerical models can be varied from site to site. To minimize the error and give the best result in representing the hydrodynamic condition in the site area, the hydrodynamic model setup was initially calibrated against current speed, current direction and water levels measured in the field during 23rd December 2014 to 7th January 2015 (section 3.2.1.3) located at latitude 02˚ 48" 40.02" N and longitude 101˚ 20" 11.18" E (near study area).

The hydrodynamic model setup was further validated against field measurement of current speed, current direction, and water level on 23rd December 2014 to 7th January 2015 located at latitude 02˚ 49" 26" N and longitude 101˚ 18" 58.14" E. The hydrodynamic model calibration was carried out by adjusting the values of bed roughness/Manning number over the whole computation domain based on the depth relationship and condition of the area. Besides, the coefficient value of horizontal eddy viscosity was also specified.

Evaluating performance of the coastal numerical models is important to establish their credibility (Sutherland *et al.*, 2004). The usual practice used in evaluating the performance of a numerical model is by comparing the predicted results with the measured conditions inside the model domain (Sutherland *et al.*, 2004). In order to check the best performance of the simulation results, the *Root Mean Squared Error* (RMSE), *R Squared, and Theil's inequality coefficients* were calculated using following equation:

$$\text{RSME} = \sqrt{\frac{\sum_{i=1}^{n}(Y_p - Y_o)^2}{n}} \tag{3.6}$$

Where:

Yo   : observed values

Yp   : predicted values

$$R^2 = 1 - \frac{\sum_1^n (y_i - f_i)^2}{\sum_1^n (y_i - \bar{y})^2} \tag{3.7}$$

Where:

$\bar{y}$: mean of the observed data

y_i : observed values

f_i : predicted values

$$U = \frac{\left[\frac{1}{n} \sum_{i=1}^{n} (A_i - P_i)^2\right]^{1/2}}{\left[\frac{1}{n} \sum_{i=1}^{n} (A_i)^2\right]^{1/2} + \left[\frac{1}{n} \sum_{i=1}^{n} (P_i)^2\right]^{1/2}} \tag{3.8}$$

Where:

Ai   : actual observations

Pi   : corresponding predictions

The best prediction gives a R^2 values of closer to 1 and a theil's inequality coefficients of closer to 0.

3.3.2   MIKE 21 Spectra Wave FM Model

MIKE 21 spectral wave (SW) is a 3rd generation spectral wind-wave model developed by the *Danish Hydraulic Institute* to simulate the growth, decay and transformation of wind generated waves and swells in offshore and coastal area. It solves the spectral wave action balance equation formulated in either Cartesian or spherical coordinate (Komen *et al.*, 1994; I. Young, 1999). In horizontal Cartesian co-ordinates, the conservation equation for wave action reads:

$$\frac{\partial N}{\partial t} + \Delta(\vec{v}N) = \frac{(S_{in} + S_{nl} + S_{ds} + S_{bot} + S_{surf})}{\sigma} \tag{3.9}$$

Where:

$N(\vec{x}, \sigma, \theta, t)$: action density,

θ : direction of wave propagation,

$\sigma = 2\pi f$: relative angular frequency,

$\vec{v}$: propagation velocity of a wave group in the four-dimensional phase space $\vec{x}$, σ and θ,

Δ : four-dimensional differential operator in the space $\vec{x}$, σ, θ,

$S_{in}, S_{nl}, S_{ds}, S_{bot}, S_{surf}$: source term for energy balance equation,

S_{in} : momentum transfer of wind energy to wave generation,

S_{nl} : energy transfer due non-linear wave–wave interaction,

S_{ds} : dissipation of wave energy due to whitecapping (deep water wave breaking),

S_{bot} : dissipation due to bottom friction,

S_{surf} : dissipation of wave energy due to depth-induced breaking,

For wave propagation over slowly varying depth and currents, the relative angular frequency can be read as:

$$\sigma = \sqrt{gk \tanh(kd)} \qquad\qquad\qquad (3.10)$$

Where k is wave number

The spectra wave module includes diffraction process, which is especially important when considering wave transformations around breakwater. Diffraction is included using the phase-decoupled refraction-diffraction approximation proposed by (Holthuijsen *et al.*, 2003).

In this study, this model was used to investigate the changes of wave characteristics before and after construction of the detached breakwater. The changes of wave characteristics were investigated for three scenarios, which are during northeast monsoon, southwest monsoons and transition period. Besides, the changes of wave characteristics were also presented for different water level conditions which are when water levels (WL) are lower than 0.4 m of MSL; when water levels (WL) are higher than 0.4 m of MSL and lower than 0.9 m of MSL; and when water levels (WL) are higher than 0.9 m of MSL.

During northeast monsoon, dominant values of wind speed and direction, significant wave height and mean wave direction between November and March from 10 years" period data (section 3.2.3.1) were used. During southwest monsoon, dominant values of wind speed and direction, significant wave height and mean wave direction between May and September from 10 years period data were used. Besides, dominant values of wind speed and direction, significant wave height and mean wave direction in April and October from 10 years period were used for the scenario during the transition period.

Initially, the model setup was prepared using the latest bathymetry measured in December 2014 and generated by *C-MAP software* (section 3.2.1.2 and section 3.2.3.3), and climate condition (water level, wind and wave) in December 2014 to January 2015

(section 3.2.3.1 and section 3.2.3.2). The model was further calibrated and validated against field measurement in December 2014 to January 2015 (section 3.2.1.3). The calibration parameters used were bottom friction, wave breaking and white-chapping.

After obtaining the best model setup, the model was run using bathymetry condition of year 2009 and climate condition (water level, wind and wave) during northeast monsoon, southwest monsoons and transition period (section 3.2.3.1 and section 3.2.3.2). The model was simulated for two cases that are with breakwater and without breakwater. Finally, the simulation results were compared and analyzed. The steps required for completing the spectra wave simulation are shown in a flow chart as shown in Figure 3.15.
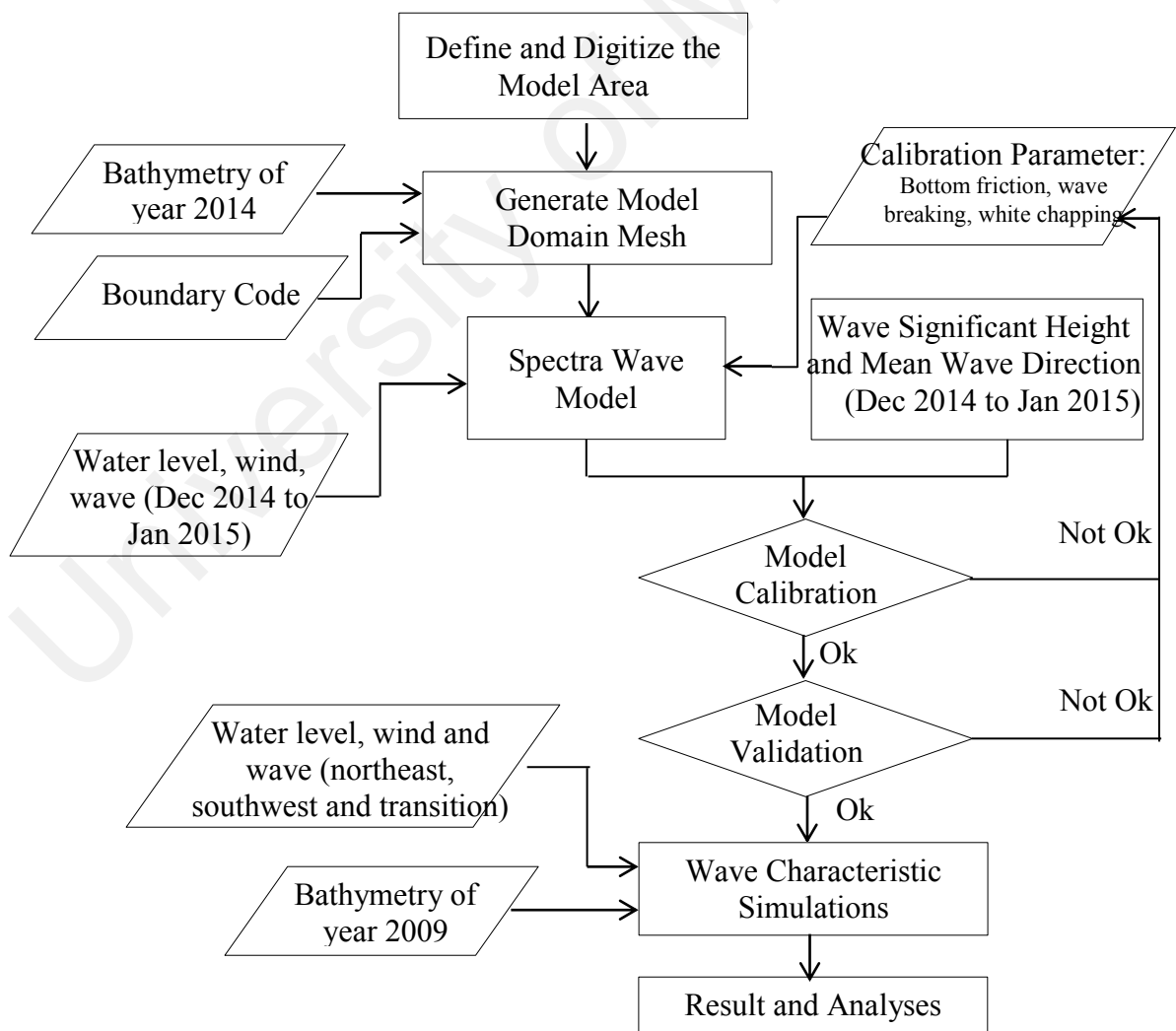
Figure 3.15: Flow chart of the Spectra Wave Simulations

3.3.2.1 Model Computational Domain

The model computation domain used in Spectra Wave model is similar to model computational domain used in Hydrodynamic model (section 3.3.1.1).

3.3.2.2 Model Input

The input data required for the spectra wave model simulation programs comprised of bathymetry data of the years 2009 and 2014 (section 3.2.1.2 and section 3.2.3.3), dominant values of wind speed and wind direction during northeast monsoon, southwest monsoon and transition period based on 10 years period data (section 3.2.3.1), 3-hours interval data of wind speed and wind direction in December 2014 to January 2015 (section 3.2.3.1), and water level in December 2014 to January 2015 (section 3.2.3.2).

3.3.2.3 Boundary Condition

For the spectra wave simulation, the significant wave height, mean wave direction and mean wave period based on 10 years wave data were used as boundary conditions (section 3.2.3.1) as well as 3-hours interval data of wave characteristics were also used.

3.3.2.4 Model Setup

During the processes of the model calibration and validation, the model setup was prepared and run from 21st December 2014 to 8th January 2015. 3-hour interval wave data obtained from *European Centre for Medium-Range Weather Forecasts* (ECMWF) were used as offshore boundary condition for spectra wave model. 3-hour interval wind data obtained from *European Centre for Medium-Range Weather Forecasts* (ECMWF) were used as input wind data.

In the processes of determining the best model setup, varying values of wave breaking parameters, bottom friction parameters and white-capping parameters were inputted in spectra wave model. It was done to find the proper parameters, which are

suitable for study area conditions. The best model setup of spectra wave models were determined based on comparison of the simulation results to field measurements.

After model calibration and validation processes were successful carried out, the calibrated model setups were run with and without the existing detached breakwater for seven days (spring tide conditions) during different seasons" conditions by inputting dominant winds and significant wave conditions based on climate data obtained from the year 2005 to 2014.

During northeast monsoon, the dominant wind speed used was 13 knots or 6.5 m/s and dominant wind direction was 310° (magnetic), while significant wave height was 1 m, mean wave direction was 250° (magnetic), and mean peak wave period was 4 s. During southwest monsoon, the dominant wind speed used was 8 knots or 4 m/s and dominant wind direction was 140° (magnetic), while significant wave height was 0.5 m, mean wave direction was 120° (magnetic) and mean peak wave period was 4 s. During transition period, the dominant wind speed used was 10 knots or 5 m/s and dominant wind direction was 10° and 280° (magnetic), while significant wave height was 0.5 m, mean wave direction was 330° and 230° (magnetic) and mean peak wave period was 4 s.

3.3.2.5 Model Calibration and Validation

The simulation results from spectra wave models were initially calibrated against measured conditions of significant wave height and mean wave direction on 23rd December 2014 to 7th January 2015 located at latitude 02˚ 48" 40.02" N and longitude 101˚ 20" 11.18" E. The spectra wave models were further validated against field measurement of significant wave height and mean wave direction on 23rd December 2014 to 7th January 2015 located at latitude 02˚ 49" 26" N and longitude 101˚ 18" 58.14" E.

The spectra wave module calibration was carried out by adjusting the values of wave breaking parameters, bottom friction parameters and white-capping (deep water wave breaking) parameters. Various statistical metrics, including the *Root Mean Squared Error* (RMSE), *R Squared*, and *Theil's inequality coefficients* were calculated to compare the predictive performance of the model.

3.3.3   MIKE 21 Mud Transport FM

MIKE 21 Mud transport FM model describes the erosion, transport and deposition processes of fine-grained material (< 63 μm) under the action of currents and waves in unstructured mesh domain. This model solves advection-dispersion equations, which essentially based on the principles in Mehta et al., (1989) and classically written:

$$\overline{\frac{\partial c}{\partial t}} + V_X \overline{\frac{\partial c}{\partial x}} + V_Y \overline{\frac{\partial c}{\partial y}} = \frac{1}{h}\frac{\partial}{\partial x}\left(hD_X \overline{\frac{\partial c}{\partial x}}\right) + \frac{1}{h}\frac{\partial}{\partial y}\left(hD_Y \overline{\frac{\partial c}{\partial y}}\right) + \sum_{i=1}^{n}\frac{S_i}{h} \qquad (3.11)$$

Where:

$\bar{c}$: depth averaged suspended sediment concentration (g/m³)

Vx,Vy   : depth averaged flow velocities (m/s)

Dx, Dy   : dispersion coefficients (m² /s)

H   : water depth (m)

Si   : source/sink term (gm² /s)

In the *MIKE 21 MT* model, a stochastic model for flow and sediment interaction is applied (first developed by Krone (1962). The terms for calculating the deposition or erosion are given by equations 3.12 and 3.13, respectively. Krone suggests that deposition rate can be expressed by:

$$S_D = w_s c_b P_d \qquad (3.12)$$

$$P_d = 1 - \frac{\tau_b}{\tau_{cb}} = \tau_b \leq \tau_{cb}$$

$$w_s = kc^m$$

$$\tau_b = \frac{1}{2}\rho_w f_w \left(U_b^2 + U_\delta^2 + 2U_b U_\delta \cos\beta\right)$$

$$f_w = \exp\left(5.213\left(\frac{\alpha}{k_b}\right)^{-0.194} - 5.977\right)$$

Where:

S_D	: deposition rate (g/m^2)
w_s	: sediment's settling velocity (m/s)
c_b	: near bottom concentration (g/m^3), dependent on the depth averaged sediment concentrations described in (Teeter, 1986)
p_d	: probability of deposition
τ_b	: bottom shear stress (N/m^2)
τ_{cb}	: critical bed shear stress for deposition (N/m^2)
k and m	: site-specific constants that have to be determined empirically
ρ_w	: density of water (kg/m^3)
U_b	: horizontal mean wave orbital velocity at the bed (m/s)
U_δ	: current velocity at the top of wave boundary layer (m/s)
β	: angle between the mean current direction and the direction of wave propagation.
f_w	: wave friction factor
α	: horizontal mean wave orbital motion at the bed (m)
k_b	: bed roughness (m)

The expression for erosion is as follows:

$$S_E = E_e\left(\sqrt[\alpha]{\tau_b - \tau_{ce}}\right) \tag{3.13}$$

Where:

S_E	: erosion rate (g/m^2)
E	: erodibility of the bed $(kg/m^2 s)$
τ_b	: bed stress for erosion (N/m^2)
τ_{ce}	: critical shear stress for erosion (N/m^2)
α	: erosion coefficient $(m\ N^{-0.5})$

MIKE 21 Mud Transport FM model was used to determine the patterns of sediment transport before and after construction of the detached breakwater. Besides, general patterns of sediment accretion and erosion were also investigated. Since the sediment transport patterns in the coast mainly influent by hydrodynamic and wave conditions, *MIKE 21 Mud Transport FM* model is interrelated with the *MIKE 21 Hydrodynamic FM* model. Beside wave radiation obtained from spectra wave simulation was inputted into the hydrodynamic parameter.

The same procedure was followed in order to get the best setup for sediment transport model. Erosion coefficients, critical shear stress for deposition, critical shear stress for erosion, power of erosion, settling velocity, and bed roughness were used as the calibration parameters. The model was run for three scenarios, which are during northeast monsoon, southwest monsoon and transition period based on 10 years period of climate data. The steps required for completing the mud transport simulation are described in flow chart as shown in Figure 3.16.
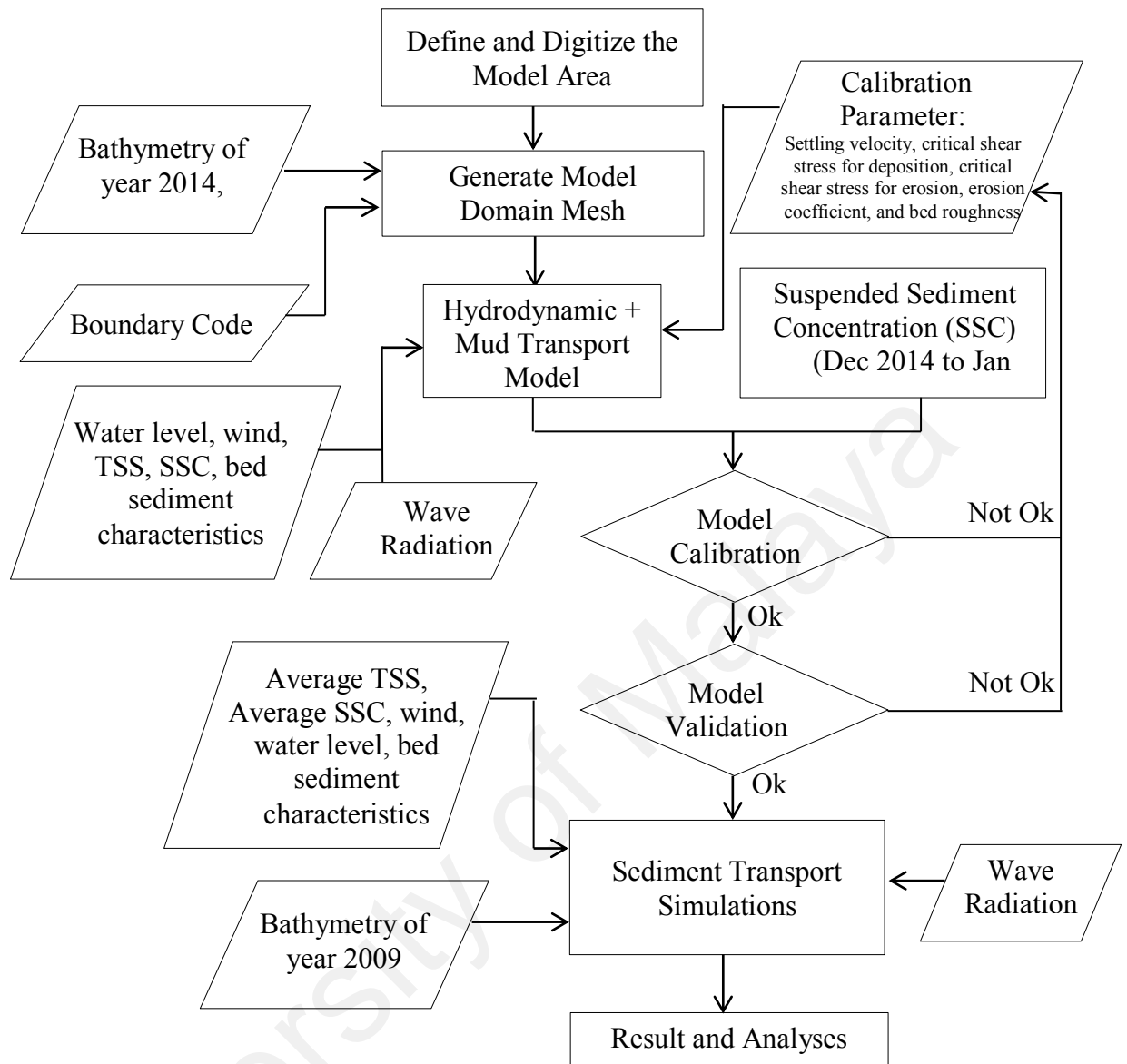
Figure 3.16: Flow chart of the Sediment Transport Simulations

3.3.3.1 Model Computational Domain

The model computational domain used in the suspended sediment transport simulations were made smaller than computation domain used in the hydrodynamic simulations. It further reduced the consuming time during run processes by significantly speeding up the computational time. However, the computational domain used was still sufficiently far away from the study site, so that the boundary condition would not

affect the area of interest. Figure 3.17 presents the computational domain used in the suspended sediment transport simulations.

The wider mesh along the Strait of Malacca covered an area of 70 km (longshore) and on average 26 km (cross-shore) with 3345 elements, 2173 nodes and length was on average 2 km to 500 m. The nearshore mesh around the Carey Island coast covered an area of 25 km (long-shore) and 17 km (cross-shore) with 6542 elements, 3271 nodes and length was on average 300 m to 1 m from offshore to near the detached breakwater structures.
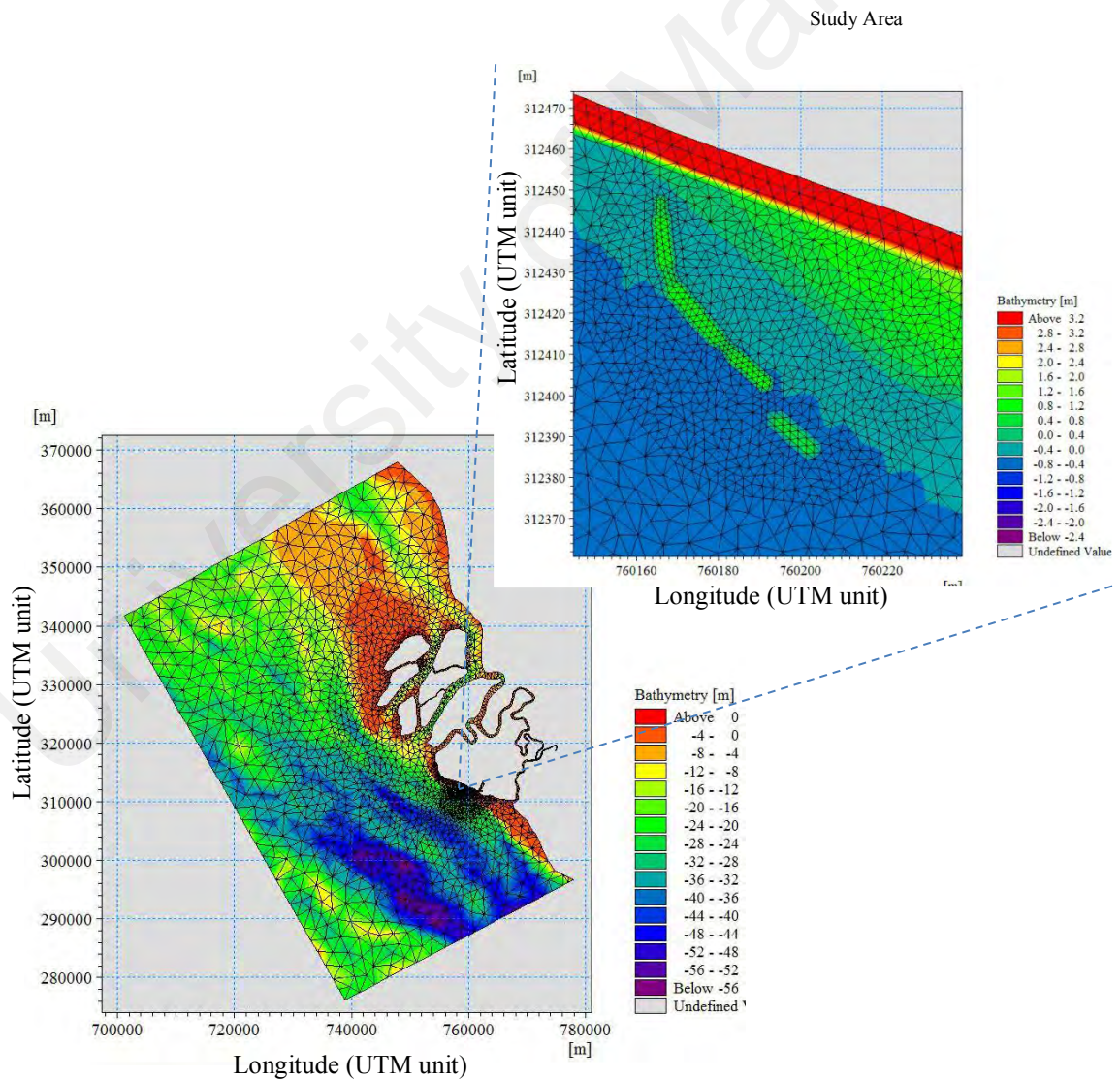
Figure 3.17: Computational domain for Mud Transport Simulation

The same scenarios (two scenarios) of computational domain were prepared in suspended sediment transport simulations. For the first scenario, the bathymetry conditions of the year 2009 surveyed by *National Hydrography Centre, Malaysia* were used. In the second scenario, the bathymetry conditions surveyed in December 2014 compiled with bathymetry generated by using *C-MAP* software were used. The first scenario of computational domain was used to simulate the changes of suspended sediment transport and accretion/erosion patterns before and after construction of the breakwater while the second scenario was used to simulate the suspended sediment transport for model calibration and validation purposes.

3.3.3.2 Model Input

The input data required for simulating the sediment transport patterns in the study area included bathymetry data of the years 2009 and 2014 (section 3.2.1.2 and section 3.2.3.3); dominant values of wind speeds and wind directions; wave radiation stresses from spectra wave simulations during December 2014 to January 2015, northeast monsoon, southwest monsoon and transition period based on 10 years period data (section 3.2.3.1), 3 hour interval data of wind speed, and wind direction in December 2014 to January 2015 (section 3.2.3.1); water level (section 3.2.3.2); suspended sediment concentration (SSC) (section 3.2.1.4); total suspended sediment (TSS) and sediment characteristic.

3.3.3.3 Model Setup

In the suspended sediment transport model setup, water level and conditions of current and wave characteristics along with boundary conditions were transferred from the hydrodynamic simulation results. Suspended sediment concentrations (SSC) recorded from 23rd December 2014 to 7th January 2015 were inputted along the

boundary conditions in mud transport module. In addition, total suspended sediments measured from the Langat River were inputted in sources part.

During model calibration and validation processes, the model setup was prepared and run from 23rd December 2014 to 7th January 2015. Here, varying values of settling velocity, erosion coefficient, critical shear stress for deposition, critical shear stress for erosion and power of erosion were inputted in mud transport model. The model setup were further run for two numbers of bed layer and one number of fraction distribution (100%). The upper layer, which is 0.4 m in depth was described as fluid mud, while the bottom layer, which is 1 m in depth was described as hard mud. The horizontal dispersion was scaled by eddy viscosity formulation.

After model calibration and validation processes were successfully carried out, the calibrated mud transport model setup was run for seven days during neap tide and seven days during spring tide. The model setup was also run for different season"s conditions. It was carried out to investigate the patterns of suspended sediment transport and accretion/erosion during full neap tide and full spring tide conditions on different seasons.

3.3.3.4 Model Calibration and Validation

In producing the best performance of simulation results and giving the confidence in presenting the patterns of suspended sediment transport and accretion/erosions in the vicinity of the existing detached breakwater, the simulation results obtained from the mud transport model were initially calibrated against measured conditions of suspended sediment concentration on 23th December 2014 to 7th January 2015 located at latitude 02° 48" 40.02" N and longitude 101° 20" 11.18" E. The mud transport models were further validated against field measurement of suspended sediment concentration on

23th December 2014 to 7th January 2015 located at latitude 02˚ 49" 26" N and longitude 101˚ 18" 58.14" E.

The mud transport model calibration was carried out by adjusting the values of settling velocity, erosion coefficient, critical shear stress for deposition, critical shear stress for erosion and power of erosion. In order to check the best performance of the simulation results, the *Root Mean Squared Error* (RMSE), *R Squared, and Theil's inequality coefficients* were calculated.

3.4 Morphodynamic changes in the vicinity of Existing Detached Breakwater

The coastal morphodynamic changes in the vicinity of the existing detached breakwater were investigated before and during six years of its installation from the year 2009 to 2014. The coastal morphodynamic changes discussed in this study include bed level changes in the vicinity of detached breakwater, accretion and erosion pattern around the existing detached breakwater and cumulative sediment deposition behind detached breakwater (in mangrove degradation areas) during its installation. The descriptions of these items are given the following sections.

3.4.1 Investigating the Seabed Level Changes

The bed surface elevations in the vicinity of detached breakwater at intertidal area of cohesive shore of Carey Island were monitored from just prior to building the structure in January 2009 until six years after construction of the breakwater. The method to collect the bed profiles was described in the previous section (section 3.2.1.6).

The bed surface elevations at cross section eleven (CS11) and cross section fourteen (CS14) from all consecutive surveys were compared and analyzed in order to investigate the bed profile changes due to the presence of existing detached breakwater. The CS11 (crossing the mainbody's breakwater) and CS14 (crossing the gap's

breakwater) were chosen to represent the bed level changes near mainbody''s and gap''s structures of the breakwater.

3.4.2 Determining the Accretion and Erosion Pattern around Detached Breakwater

In this section, the accretion and erosion patterns that occurred in the vicinity of the detached breakwater were produced based on the profiling results. The accretion and erosion patterns were obtained by calculating the differential elevations between the initial surface elevations (before construction of the breakwater in January 2009) and the surface elevations of each consecutive survey (after construction of the breakwater between years 2009 and 2014). The patterns of accretion and erosion were determined with durations of 4 months, 8 months, 1 year, 4 years, 5 years and 6 years after construction of the existing detached breakwater.

3.4.3 Calculating the Deposition Volume behind the Detached Breakwater

The bed surface elevations at all cross sections from every consecutive survey were interpolated to obtain the topography shapes around the existing detached breakwater at intertidal area of cohesive shore of Carey Island during consecutive survey between years 2009 and 2014. The topography conditions were further used to determine the amounts of sediment accumulations behind the detached breakwater in mangrove degradation area for every consecutive survey. It was done by calculating the differential sediment volumes between consecutive surveys. Sediment volume at behind detached breakwater for every consecutive survey was calculated using "*Area and volume statistic*" operation in *Arcview-GIS* with datum level of -0.6 m with respect to MSL. These results were further used to analyze the performance of the structure, and then to relate it to the mangrove rehabilitation purposes.

In producing the best topography shapes, one of three interpolation methods in Arcview-GIS, including *bilinear interpolation* method, *Inverse Distance Weighted (IDW) nearest interpolation* method and *spline interpolation* method was chosen based on the smallest value of *Root Mean Squared Error* (RMSE). This would help increasing the accuracy of the calculation of sediment deposition behind the breakwater.

3.5 Investigating the Seabed Level Changes at Various Configurations of Geometry and Position of Detached Breakwater

The existing detached breakwater was found to be able in trapping the sediment accumulations behind its structure and increasing the bed surface elevations in the mangrove degradation areas. Based on previous simulation results, it can be showed that position and geometry of the detached breakwater directly affected the hydrodynamic conditions and pattern of the sediment transport in the site areas. Therefore, it influenced the amount of sediment, which could be trapped in the mangrove degradation area.

The proper seabed elevations for suitable tidal regime for mangrove survival need to be provided around the mangrove degradation areas in order to support the success of mangrove rehabilitation project at intertidal cohesive area of Carey Island. Regarding this matter, better design parameters of the existing detached breakwater that can optimize the increase in the seabed elevations need to be worked out. It could be done by simulating *MIKE 21 Mud Transport* model for different cases by changing geometry and position of the existing detached breakwater. Due to the limitation of the SSC data, *Mud transport* model was run for two weeks period starting from 23rd December 2014 to 7th January 2015. The simulation results of seabed level changes were further compared and analyzed. The better design parameters of the breakwater were chosen based on sediment accumulation pattern behind its structure (mangrove degradation area).

CHAPTER 4: **RESULT AND DISCUSSION**

This chapter presents the results obtained from field monitoring and numerical model simulations. The impact of the presence of existing detached breakwater on the coastal hydro-morphodynamic conditions in the intertidal area of cohesive shore of Carey Island, Peninsular Malaysia that included currents and waves characteristics, suspended sediment transport, coastal bed profiles and patterns of accretion and erosion was discussed. Besides, the bed level changes due to the changes of geometry and position of the existing detached breakwater were also investigated.

4.1 Hydrodynamic Changes due to the Presence of Existing Detached Breakwater

This section presents the simulation results obtained from *MIKE 21 Hydrodynamic FM* and *MIKE 21 Spectra Wave FM* models. The simulation results were used to investigate the nearshore hydrodynamic changes before and after construction of the existing detached breakwater. Apart from that, the results obtained during the calibration and validations processes of *MIKE 21 Hydrodynamic and Spectra wave* models are also presented.

4.1.1 Model Calibration and Validation

The water levels and current characteristics showed the best calibration when the model setup of hydrodynamic simulations used values of bed roughness as presented in Figure 4.1 and Table 4.1. Here, the horizontal eddy viscosity was specified by using smagorinsky formulation with constant value of 0.28, while the minimum and maximum eddy values applied were based on default values. In the spectra wave model setup, the simulation results of wave characteristics showed the best calibration when the model used the parameters of wave breaking, bottom frictions and white-chapping as presented in Table 4.2.
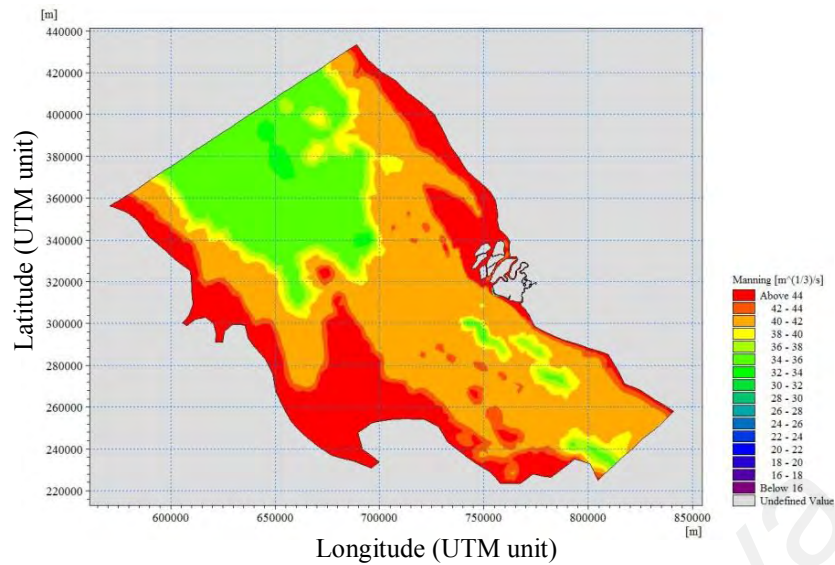
Figure 4.1: Bed roughness values used in the computation domain of hydrodynamic model setup

Table 4.1: **Bed Roughness values used in the computation domain of hydrodynamic model setup**

No	Depth Range (m) or Area Condition	Manning Number ($m^{1/3}/s$)
1	Less than 15 m	45
2	15 to 50 m	40
3	Greater than 50 m	35
4	Mangrove area	17.5 (DHI, 2008)

Table 4.2: **Parameters used in spectra wave model setup**

No	Item	Parameters name	Value
1	Wave breaking (Type of Functional form by Nelson, 1994)	Alpha	1
2	Bottom friction	Nikuradse roughness	0.04 m
3	White-chapping	Dissipation coefficient (Cd, Delta)	4.5, 0.5

Figure 4.2 shows a comparison of predicted and measured current speeds, current directions and water levels on 23rd December 2014 to 7th January 2015 at latitude 02˚

48" 40.02" N and longitude 101° 20" 11.18" E. While, Figure 4.3 shows the comparison of predicted and measured significant wave heights and mean wave directions on 23rd December 2014 to 7th January 2015 at latitude 02° 48" 40.02" N and longitude 101° 20" 11.18" E. The dash lines present the predicted values while the continuous lines present the observed values.
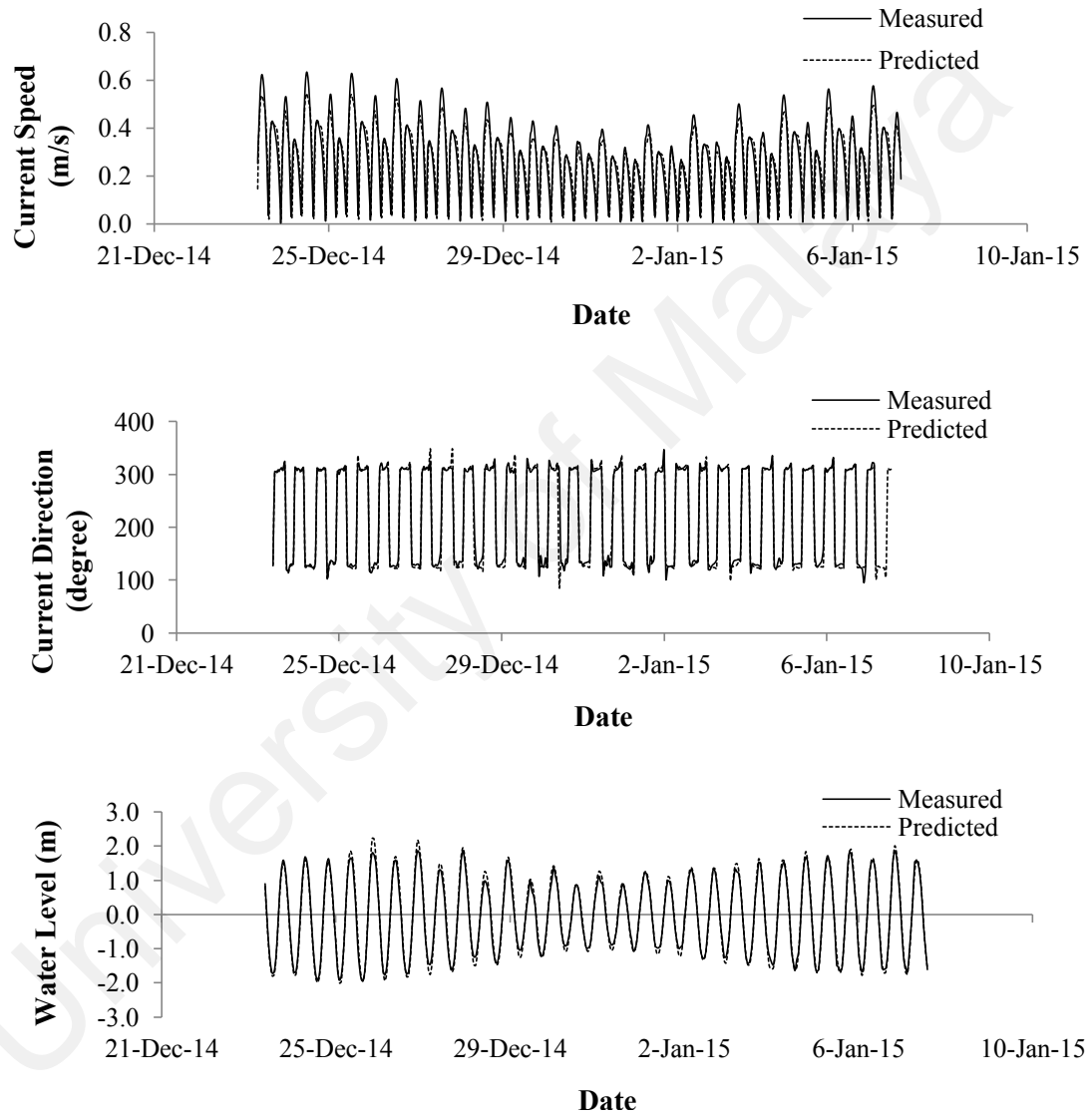
Figure 4.2: Measured and predicted current speeds, current directions and water levels on 23rd December 2014 to 7th January 2015 at latitude 02° 48' 40.02" N and longitude 101° 20' 11.18" E
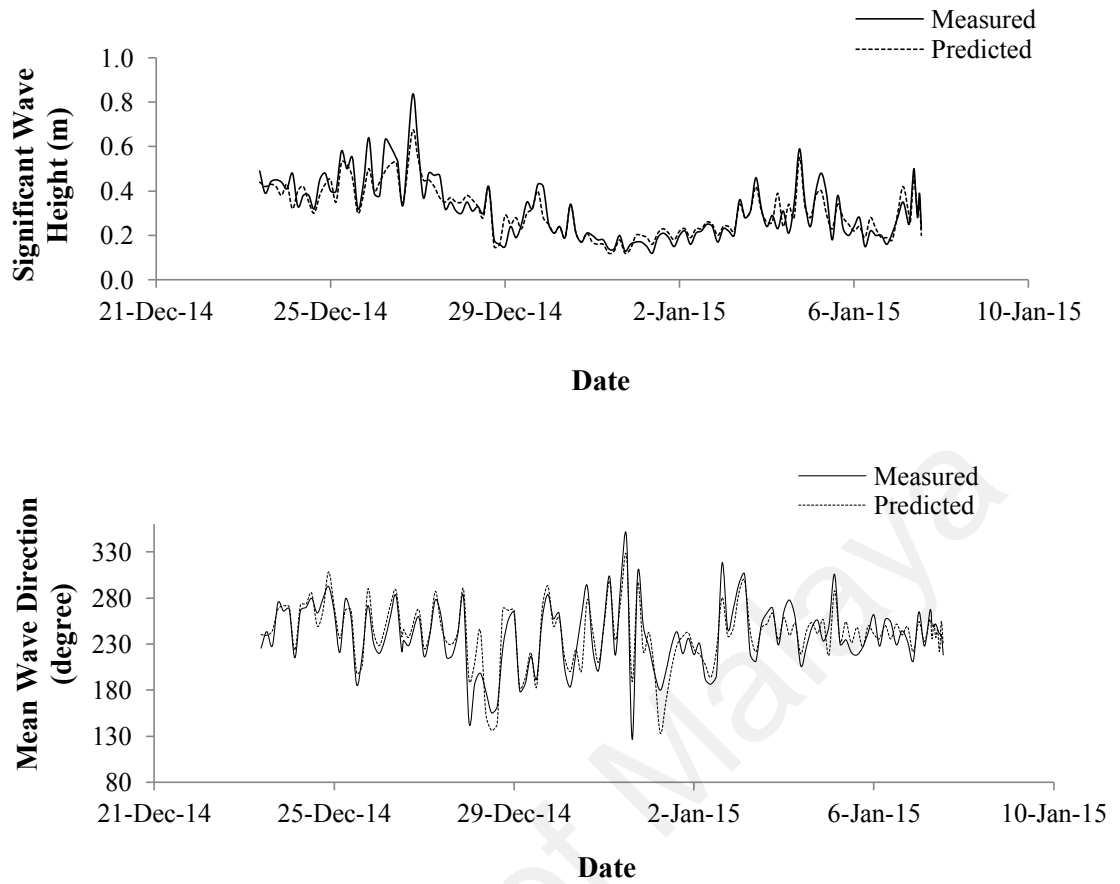
Figure 4.3: Measured and predicted significant wave heights and mean wave directions on 23rd December 2014 to 7th January 2015 at latitude 02° 48' 40.02" N and longitude 101° 20' 11.18" E

According to Figure 4.2, the current speeds, current directions and water levels obtained from hydrodynamic model simulations at latitude 02° 48" 40.02" N and longitude 101° 20" 11.18" E are very well compared to the field measurement conditions on 23rd December 2014 to 7th January 2015. Similar results are also shown in Figure 4.3 that the significant wave heights and mean wave directions obtained from spectra wave model simulations are quite well compared to the actual conditions on 23rd December 2014 to 7th January 2015 at latitude 02° 48" 40.02" N and longitude 101° 20" 11.18" E. However, the differences between the measured and predicted values of water levels and current characteristics are found to be smaller in comparison to significant wave heights and mean wave direction.

In addition, Figure 4.4 and Figure 4.5 show the comparison of predicted and measured current speeds, current directions, water levels, significant wave heights and mean wave directions on 23rd December 2014 to 7th January 2015 at latitude 02˚ 49" 26" N and longitude 101˚ 18" 58.14" E. The dash lines present the predicted values while the continuous lines present the observed values.
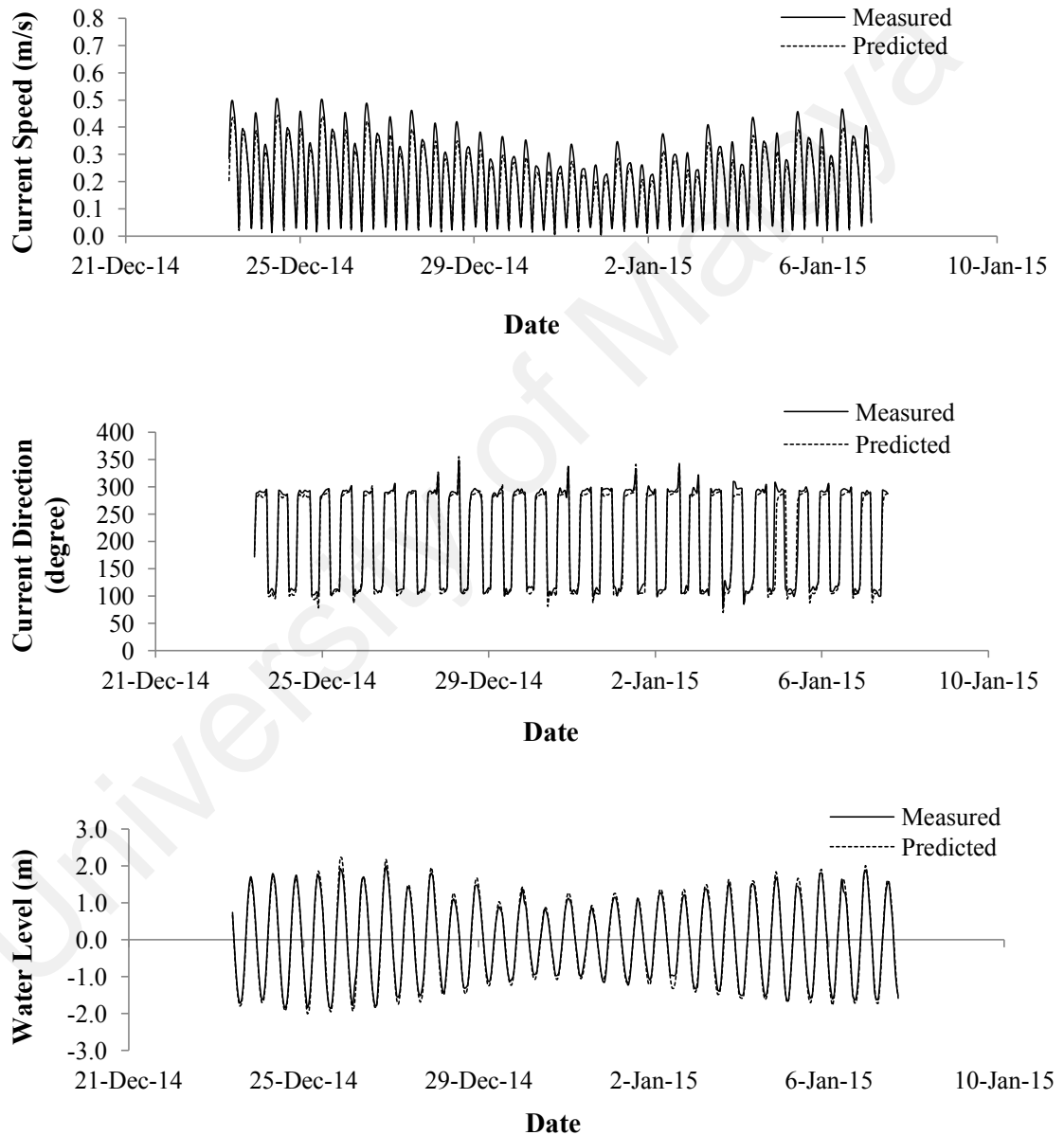
Figure 4.4: **Measured and predicted current speeds, current directions and water levels on 23rd December 2014 to 7th January 2015 at latitude 02˚ 49' 26" N and longitude 101˚ 18' 58.14" E**
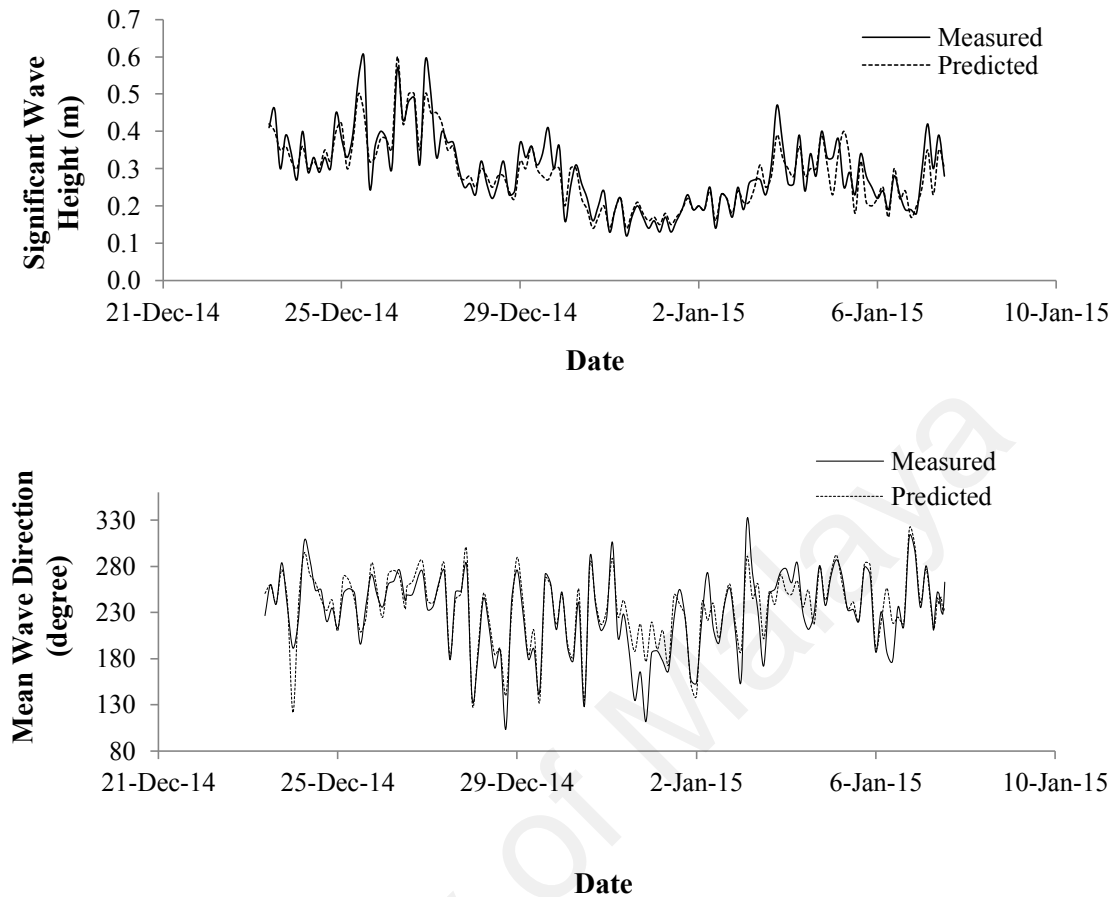
Figure 4.5: Measured and predicted significant wave heights and mean wave directions on 23rd December 2014 to 7th January 2015 at latitude 02° 49' 26" N and longitude 101° 18' 58.14" E

Based on Figure 4.4 and Figure 4.5, the current speeds, current directions, water levels, significant wave heights and mean wave directions at latitude 02° 49" 26" N and longitude 101° 18" 58.14" E obtained from hydrodynamic and spectra wave model simulations are also well compared to the measured conditions. It demonstrates that the model setup used in the hydrodynamic and spectra wave models is quite satisfactory to present the real condition in the study area.

The comparison between predicted and measured values of current speeds, current directions, water levels, significant wave heights and mean wave directions at latitude

02° 49" 26" N and longitude 101° 18" 58.14" E and at latitude 02° 49" 26" N and longitude 101° 18" 58.14" E during calibration and validation processes was done by using *Root Mean Squared Error* (RMSE), *R Squared, and Theil's inequality coefficientes.*

Table 4.3 provided the values of *Root Mean Squared Error* (RMSE), *R Squared, and Theil's inequality coefficients* obtained during the processes of model calibration and validation. The minimum value of RMSE for calibration and validation of current speeds was 0.07 m/s and 0.08 m/s, respectively, while the minimum values of RMSE for calibration and validation of significant wave heights was 0.11 m and 0.09 m, respectively. Based on standard error allowed for hydraulic study (DID, 2013), these *Root Mean Squared Error* (RMSE), *R Squared, and Theil's inequality coefficients* values proved that the models were well calibrated and validated.

Table 4.3: **Statistical Metrics for Hydrodynamic model performance**

No	Item	Calibration Process			Validation Process		
		RMSE	R Squared (R^2)	Thiel's inequality coefficient	RMSE	R Squared (R^2)	Thiel's inequality coefficient
1	Current Speeds	0.07 m/s	0.92	0.08	0.08 m/s	0.91	0.08
2	Current Directions	15°	0.94	0.05	17°	0.93	0.06
3	Water Levels	0.05 m	0.95	0.04	0.06 m	0.94	0.05
4	Significant wave heights	0.04 m	0.85	0.14	0.05 m	0.83	0.16
5	Mean Wave Directions	18°	0.81	0.18	19°	0.80	0.19

4.1.2 Hydrodynamic Changes during Northeast Monsoon

Figure 4.6 presents the conditions of current speeds and current directions before and after construction of the existing detached breakwater during northeast monsoon for different water level conditions, while Figure 4.7 presents the conditions of significant wave heights and mean wave directions before and after construction of the existing detached breakwater during northeast monsoon for different water level conditions.

Before construction of the detached breakwater, the current flow occurred to the site (mangrove degradation areas) from northwest direction approximately 302° (magnetic) towards southeast direction approximately 122° (magnetic) with speeds between 0.12 m/s and 0.22 m/s during northeast monsoon (Figure 4.6 (a, b, c)). In the same time, waves forced the mangrove degradation areas from southwest direction approximately 233° to 244° (magnetic) to northeast direction approximately 53° to 64° (magnetic) with significant heights between 0.09 m and 0.2 m (Figure 4.7 (a, b, c)). However, after construction of the existing detached breakwater, the current speeds, current directions, significant wave heights and mean wave direction are changed depending on water level conditions (Figure 4.6 (d, e, f) and Figure 4.7 (d, e, f)).

When the water levels are lower than gap"s breakwater crest levels (Figure 4.6 (d)), the current flow occurs to the mangrove degradation area through gaps between dyke and breakwater and between breakwater and stone. The current"s directions from available gaps are approximately 275° - 285° (magnetic) to the mangrove degradation areas. In the same time, waves force the mangrove degradation area through the same ways (Figure 4.7 (d)) without any obvious changes of wave directions. In this moment, current speeds and wave heights are reduced drastically behind the structure of the detached breakwater that are approximately from 0.14 m/s to 0.04 m/s and from 0.1 m to 0.04 m, respectively. Besides, the current speeds are found to be slightly increased

around the gaps from 0.14 m/s to 0.16 m/s because of turbulent flows due to the return flow occurrences in these areas, while wave heights are slightly increased at toe of the front of breakwater approximately from 0.12 m to 0.15 m due to the reflection incidences. Since the currents cannot flow through the breakwater structure, the current directions are changed at front of breakwater from 302° (magnetic) to be 311° (magnetic). Besides, the mean wave directions are also changed from 233° (magnetic) to 228° (magnetic) at toe of the front of breakwater affected by reflection occurrences.

Moreover, when the water levels are lower than mainbody"s breakwater crest levels and higher than gap"s breakwater crest levels, the currents flow to the mangrove degradation area over the gap"s breakwater and through the gaps between breakwater and dyke and between breakwater and stone (Figure 4.6 (e)). In the same time, waves force the mangrove degradation area through the same ways (Figure 4.7 (e)). At this moment, the current speeds behind breakwater decrease from 0.18 m/s to 0.10 m/s (approximately 20 m from breakwater structure to landward area) and from 0.18 m/s to 0.04 m/s (closest to the breakwater structure). The wave heights also decrease behind the breakwater approximately from 0.15 m to 0.06 m. Besides, the current speeds are found to increase around the gap"s breakwater, above the stone and gaps (between breakwater and dyke) from 0.18 m/s to 0.26 m/s because of turbulent flows in these areas due to the return flow occurrences, while the wave heights are found to increase slightly at toe of the front of mainbody"s breakwater from 0.15 m to 0.18 m due to reflection incidences.

Regarding the current and mean wave directions, current directions change from 302° (magnetic) to 311° (magnetic) at front of breakwater"s structure and 310° (magnetic) behind the breakwater. Mean wave directions also change from 240° (magnetic) to 236° (magnetic) at toe of the front of mainbody"s breakwater due to the

reflection occurrences when wave cannot pass through the mainbody"s breakwater. The diffraction occurrences are also found closest to the breakwater structure after waves enter the mangrove degradation areas through the gap"s breakwater. It further causes the changes of mean wave directions behind the breakwater from 240° (magnetic) to 210° and 266° (magnetic).

In addition, during full spring tide (when the water levels are higher than mainbody"s breakwater crest), the overall current speeds and wave heights behind the breakwater (mangrove degradation areas) are reduced approximately from 0.18 m/s to 0.16 m/s and from 0.18 m to 0.15 m, respectively. However, the current speeds behind and front of the first mainbody"s breakwater are found to be reduced higher from 0.18 m/s to 0.1 m/s (Figure 4.7 (f) and Figure 4.8 (f)). Besides, there are increasing values of the current speeds and wave heights around left side of mainbody"s breakwater (where the directions of currents/waves come from) from 0.18 m/s to 0.28 m/s and from 0.18 m to 0.24 m. It may be because of refraction occurrences (due to the differences of water depths) combined with reflection incidences when the currents and waves pass through mainbody"s breakwater with an angle to underwater contour and shallower depths.

When the water levels are higher than 0.9 m of MSL, the current and wave directions changed at front and behind the breakwater"s structure. Before construction of the detached breakwater, the current flow occurred from seaward at approximately 302° (magnetic) direction and waves force the mangrove degradation area from 244° (magnetic) direction. However, after construction of the detached breakwater, the current directions are changed to 305° (magnetic) at front of the structure and 308° (magnetic) behind the structure, while wave directions are changed to 240° (magnetic) behind the breakwater"s structure. It can happen because the currents and waves cross an obstacle (breakwater"s structure).
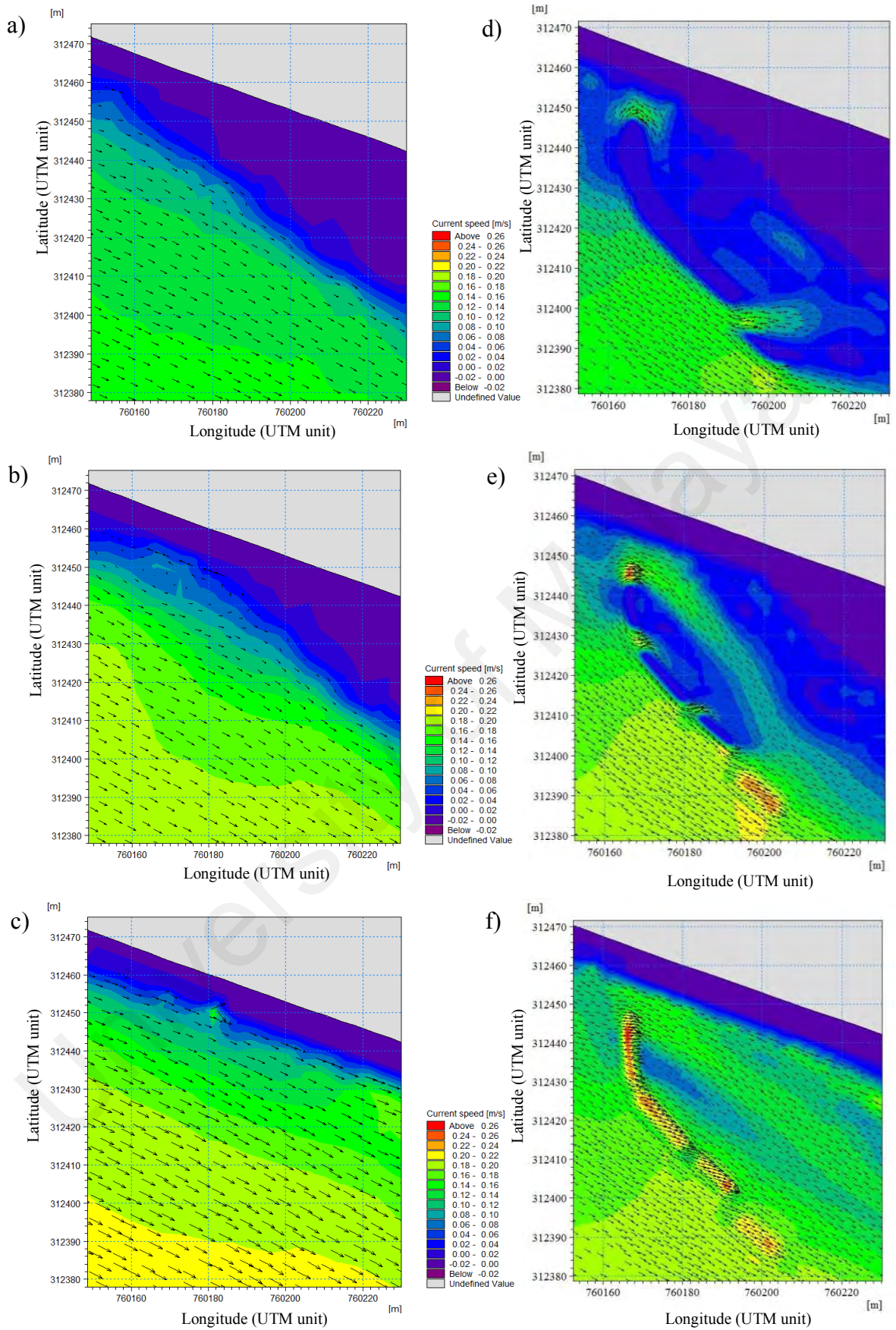
Figure 4.6: Current characteristics before and after construction of detached breakwater during northeast monsoon, (a, d) WL < 0.4 m of MSL, (b, e) 0.4 m of MSL < WL < 0.9 m of MSL, (c, f) WL > 0.9 m of MSL
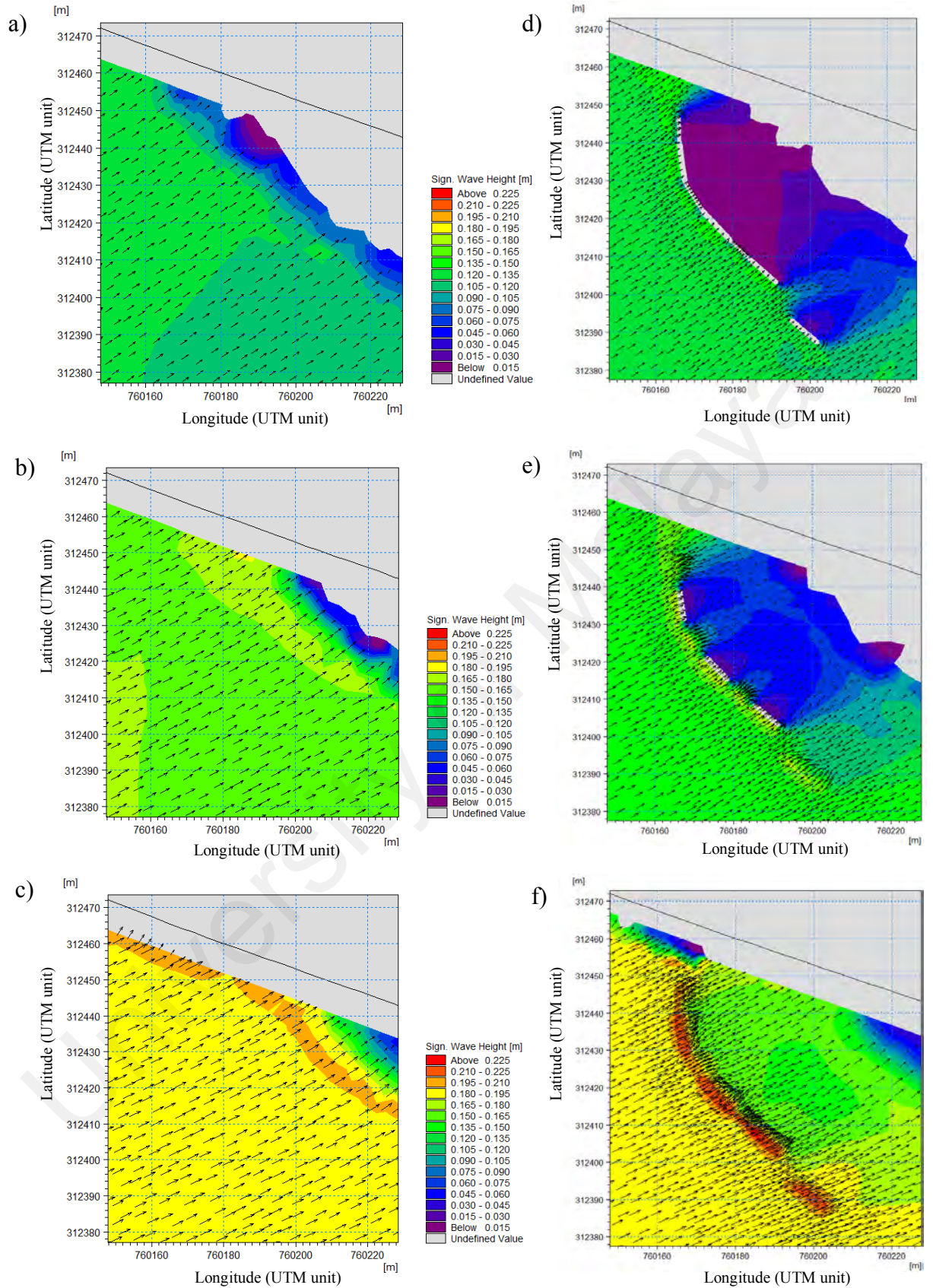
Figure 4.7: Wave characteristics before and after construction of detached breakwater during northeast monsoon, (a, d) WL < 0.4 m of MSL, (b, e) 0.4 m of MSL < WL < 0.9 m of MSL, (c, f) WL > 0.9 m of MSL

4.1.3 Hydrodynamic Changes during Southwest Monsoon

Figures 4.8 and 4.9 present the conditions of current speeds, current direction, wave heights and wave directions before and after construction of the existing detached breakwater during southwest monsoon for different water level conditions.

During southwest monsoon, the current flow occurred to the study site area from southeast direction approximately 116° (magnetic) towards northwest direction approximately 296° (magnetic) with speeds between 0.09 m/s and 0.18 m/s before construction of the existing detached breakwater (Figure 4.8 (a, b, c)). In the same time, waves forced the study site area from south direction approximately between 159° and 184° (magnetic) with significant heights between 0.1 m and 0.225 m (Figure 4.9 (a, b, c)). However, after construction of the existing detached breakwater, the current speeds, current directions, significant wave heights and mean wave direction have changed depending on water level conditions (Figure 4.8 (d, e, f) and Figure 4.9 (d, e, f)).

When the water levels are lower than gap"s breakwater crest levels (Figure 4.8 (d)), the currents, which come from southeast direction reach the mangrove degradation area having bed elevations lower than 0.4 m of MSL. Some of the currents then straightly flow to the seaward through a gap between breakwater and stone and some of them are trapped behind the breakwater structure. Slowly, the trapped currents flow back seaward after reaching breakwater"s structure through the gap between breakwater and stone. Here, current speed decreases behind the detached breakwater from 0.09 m/s to 0.03 m/s.

In the same time, waves force the mangrove degradation area through gaps between dyke and breakwater and between breakwater and stone (Figure 4.9 (d)). The wave heights decrease behind breakwater structure approximately from 0.1 m to 0.03 m. In contrast to northeast monsoon conditions, wave heights are found to decrease at front of

detached breakwater and also around the gaps between breakwater and dyke and between breakwater and stone. The mean wave directions change at toe of the front of breakwater"s structure due to reflection incidences that are from 184° (magnetic) to 200° (magnetic).

Moreover, when the water levels are lower than mainbody"s breakwater crest levels and higher than gap"s breakwater crest level (Figure 4.8 (e)), the currents, which come from 116° (magnetic) directions straightly reach the mangrove degradation areas having bed elevations lower than 0.9 m of MSL. The current flow occurs seaward above the gap"s breakwater, above the stone and gaps between breakwater and stone and between breakwater and dyke. At this moment, currents are reduced behind the breakwater structure approximately from 0.13 m/s to 0.04 m/s and they are increased above the gap"s breakwater and around the gaps between the breakwater and stone and between breakwater and dyke approximately from 0.04 m/s to 0.21 m/s.

At the same time, waves force the mangrove degradation area through gaps between dyke and breakwater and between breakwater and stone, above the stone and also above the gap"s breakwater (Figure 4.9 (e)). The wave heights are found to decrease behind breakwater structure approximately from 0.15 m to 0.03 m. Here, the wave heights are also found to increase slightly above the stone approximately from 0.15 m to 0.18 m. Regarding the mean wave directions, there are changes of the wave directions after construction of detached breakwater when water levels are lower than 0.9 m of MSL. The changes are found at the toe of front of mainbody"s breakwater approximately about 31° (magnetic) due to the wave reflection incidences. Besides, the wave directions are also changed from 173° (magnetic) to 164° (magnetic) and 214° (magnetic) behind breakwater due to wave diffraction incidences after the waves pass through the gap"s breakwater.

In addition, during full spring tide (when the water levels are higher than mainbody's breakwater crest) (Figure 4.8 (f)), the overall current speeds behind the breakwater (mangrove degradation area) are reduced approximately from 0.16 m/s to 0.13 m/s; reducing of current speed also occurs quite significantly around the first mainbody's breakwater that is approximately up to 0.6 m/s. Besides, there are increasing values of the current speeds around right side of mainbody's breakwater (the directions from which currents come) that are approximately from 0.16 m/s to 0.22 m/s.

For the wave characteristics (Figure 4.9 (f)), there is no reducing of wave heights at the mangrove degradation area after construction of the breakwater when the water levels are more than 0.9 m above MSL. However, there are increasing values of wave heights around left side of mainbody's breakwater (the directions from which wave come) and above the stone that are approximately from 0.2 m to 0.24 m due to the refraction and reflection incidences. Besides, slight decrease in wave heights is found that are approximately from 0.225 m to 0.195 m. Wave directions were found to change at the mangrove degradation area before construction of the breakwater and after its construction that are approximately from directions of 158° (magnetic) to 185° (magnetic).
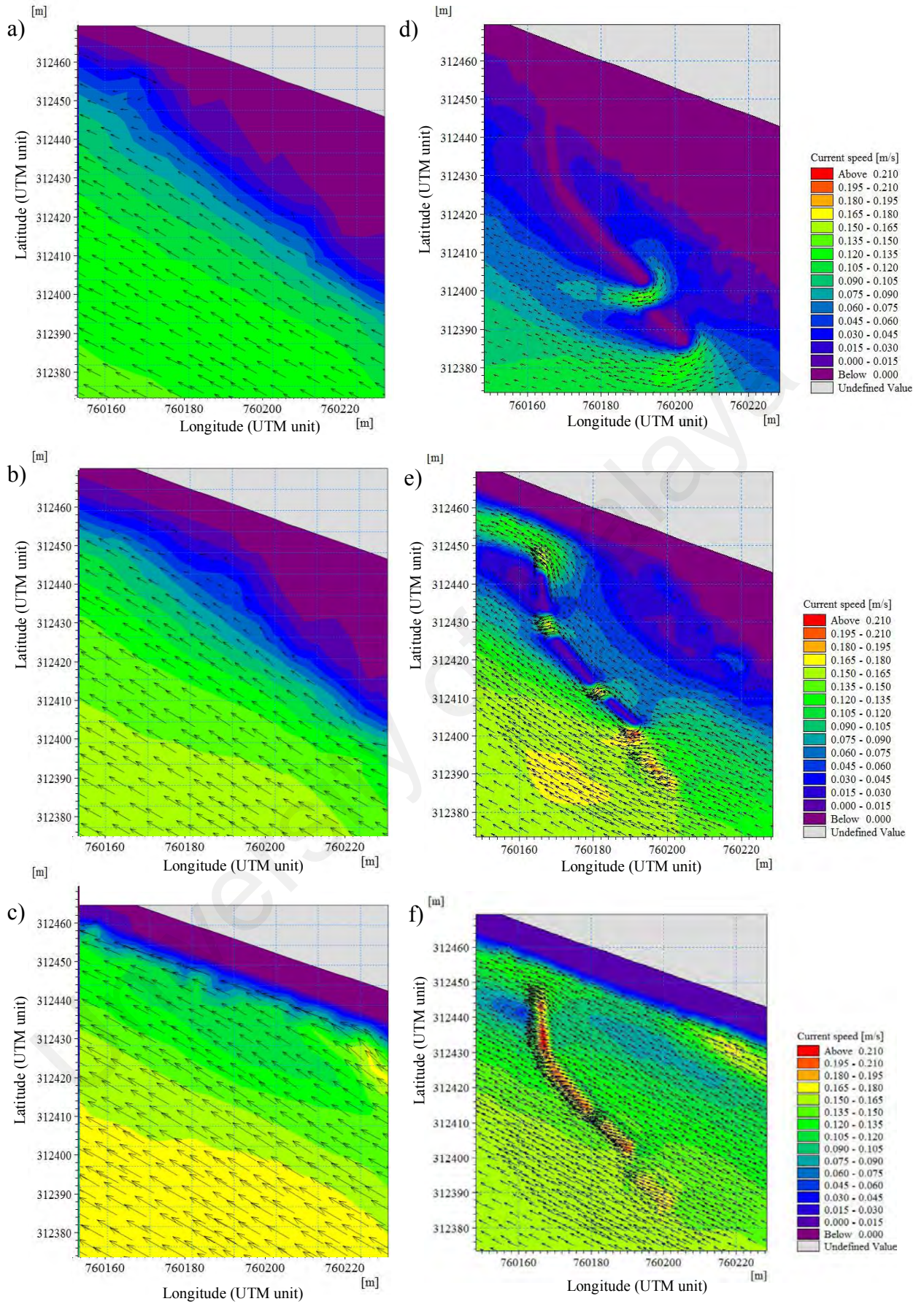
Figure 4.8: Current characteristics before and after construction of detached breakwater during southwest monsoon, (a, d) WL < 0.4 m of MSL, (b, e) 0.4 m of MSL < WL < 0.9 m of MSL, (c, f) WL > 0.9 m of MSL
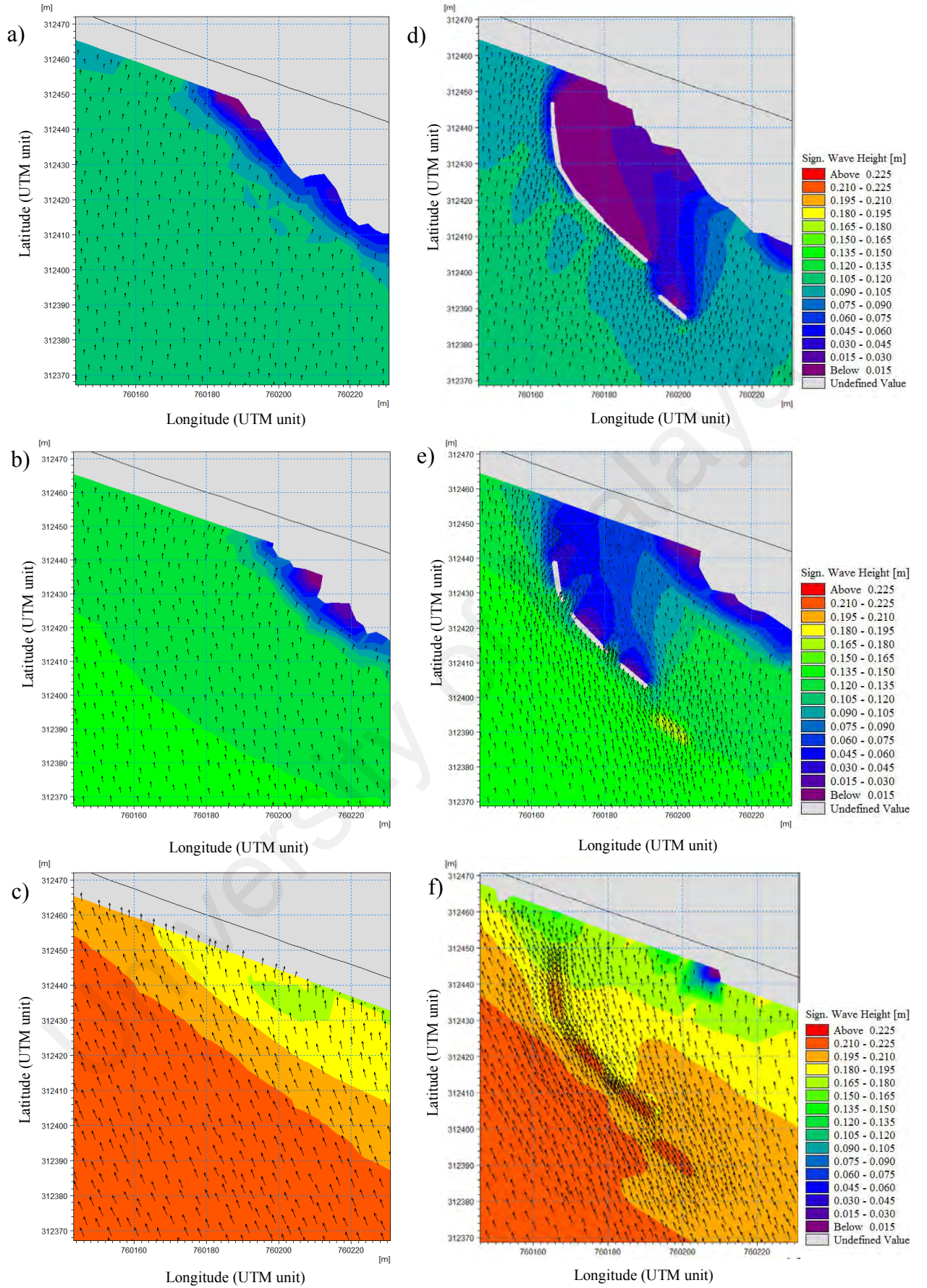
Figure 4.9: Wave characteristics before and after construction of detached breakwater during southwest monsoon, (a, d) WL < 0.4 m of MSL, (b, e) 0.4 m of MSL < WL < 0.9 m of MSL, (c, f) WL > 0.9 m of MSL

4.1.4 Hydrodynamic Changes during Transition Period

Figure 4.10 presents the conditions of current speeds and current direction before and after construction of the existing detached breakwater during transition period for different water level conditions, while Figure 4.11 presents significant wave heights and mean wave directions before and after construction of the existing detached breakwater during transition period for different water level conditions.

Based on Figure 4.10 and Figure 4.11, during transition period, the patterns of current flows and waves moving from seaward to the mangrove degradation area before and after construction of the detached breakwater are found to be quite similar to northeast monsoon duration. However, the values of current speeds and wave heights are found to be lower than during northeast monsoon with difference in current directions and mean wave directions of approximately about 16° (magnetic). Since the values of current and wave characteristics are significantly affected by values of wind and wave data, the values of current and wave characteristics during transition period are found to be lower than northeast monsoon due to the conditions that wind and wave during transition period are lower than during northeast monsoon.

In example, as shown in Figure (4.10 (a, b, c)), before construction of the detached breakwater, the current flow occurred to the mangrove degradation areas from northwest direction approximately 298° (magnetic) towards southeast direction approximately 117° (magnetic) with speeds between 0.10 m/s and 0.18 m/s. In the same time, waves force the mangrove degradation area from southwest direction approximately 245° to 260° (magnetic) with significant wave heights between 0.02 m and 0.05 m (Figure 4.11 (a, b, c)). However, after construction of the existing detached breakwater, the current speeds, current directions, significant wave heights and mean

wave direction were changed depending on water level conditions (Figure 4.10 (d, e, f) and Figure 4.10 (d, e, f)).

The presence of breakwater has totally obstructed the current flows and wave moving to the mangrove degradation area when the water levels are lower than 0.4 m of MSL (Figure 4.10 (d) and Figure 4.11 (d)). At this moment, the currents flow to the mangrove degradation area through gaps between dyke and breakwater and between breakwater and stone. Here, current speeds and wave heights are found to be reduced behind the structure of detached breakwater that are approximately 0.08 m/s and 0.02 m, respectively. Besides, the current speeds are found to increase around the gaps between breakwater and dyke and between breakwater and stone approximately from 0.12 m/s to 0.20 m/s. Since the currents cannot flow through the breakwater''s structure, the current directions are changed at front of breakwater from 298° (magnetic) to 315° (magnetic).

Moreover, when the water levels are lower than mainbody''s breakwater crest levels and higher than gap''s breakwater crest levels, the current flows and waves move from seaward to the mangrove degradation area above the gap''s breakwater and through the gaps between breakwater and dyke and between breakwater and stone (Figure 4.10 (e) and Figure 4.11 (e)). At this moment, the current speeds behind breakwater decrease approximately from 0.16 m/s to 0.10 m/s (approximately 20 m from breakwater structure to landward area) and from 0.16 m/s to 0.03 m/s (closest to the breakwater structure). The wave heights also decrease behind the breakwater approximately from 0.04 m to 0.02 m. Besides, the current speeds are found to increase around the gap''s breakwater, above the stone and gaps between breakwater and dyke approximately up to 0.225 m/s, while the wave heights are found to increase slightly at toe of front of breakwater and above the stone approximately from 0.02 m to 0.05 m.

Regarding the current and mean wave directions, current directions are found to change from 298° (magnetic) to 315° (magnetic) at front of breakwater's structure. Mean wave directions also change behind the detached breakwater from 253° (magnetic) to 206° (magnetic) and 279° (magnetic) due to the diffraction occurrences when waves move to the mangrove degradation area through the gap's breakwater.

In addition, during full spring tide (when the water levels are higher than 0.09 m of MSL), the overall current speeds and wave heights at the mangrove degradation areas are slightly reduced. However, the current speeds and wave heights increase at the left side of mainbody's breakwater (the directions from which currents/waves come) that are approximately from 0.15 m/s to 0.225 m/s and from 0.04 m to 0.058 m, respectively. The current and mean wave directions have changed after construction of the breakwater to 301° (magnetic) and 262° (magnetic) at front of breakwater's structure.
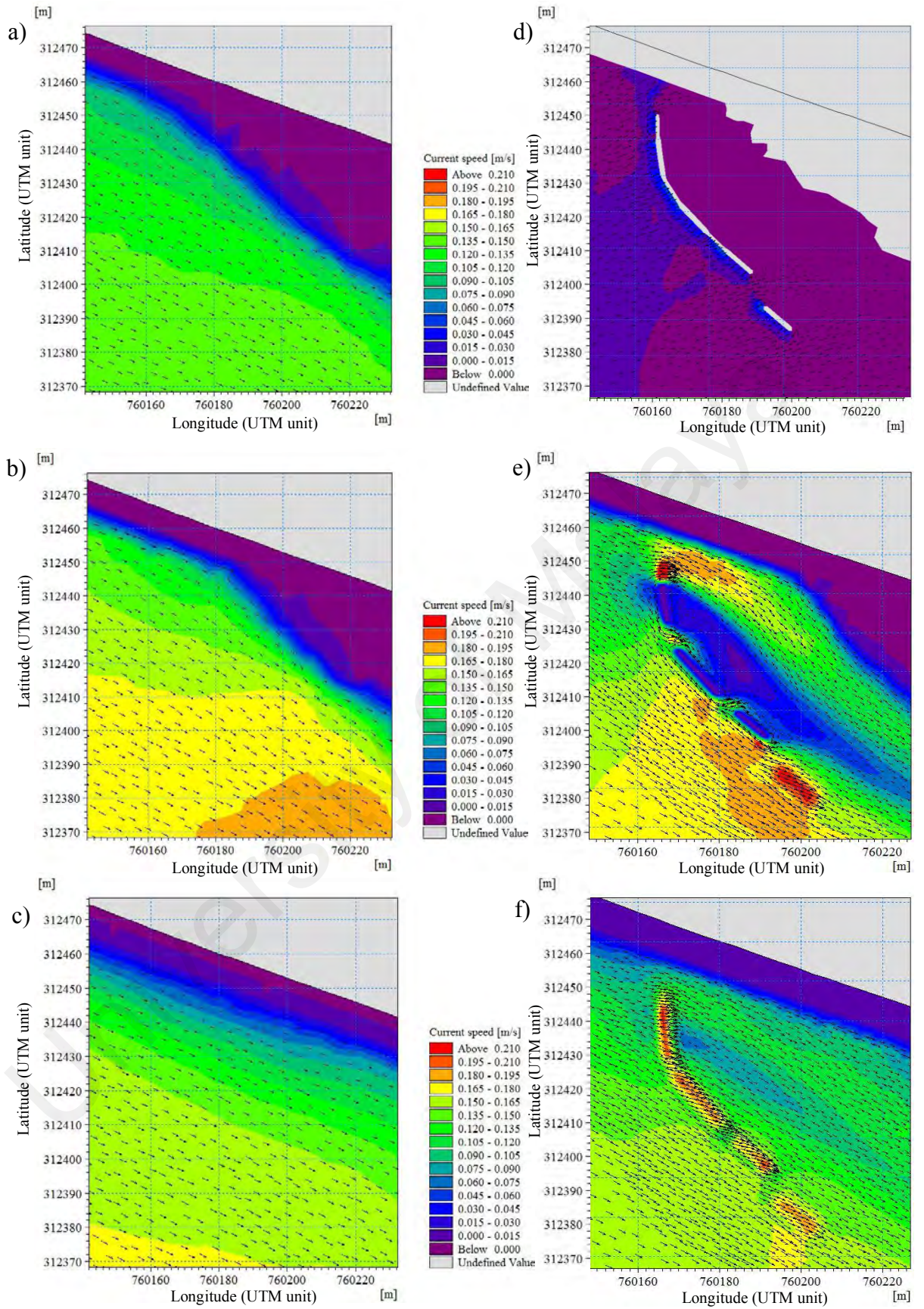
Figure 4.10: Current characteristics before and after construction of detached breakwater during transition period, (a, d) WL < 0.4 m of MSL, (b, e) 0.4 m of MSL < WL < 0.9 m of MSL, (c, f) WL > 0.9 m of MSL
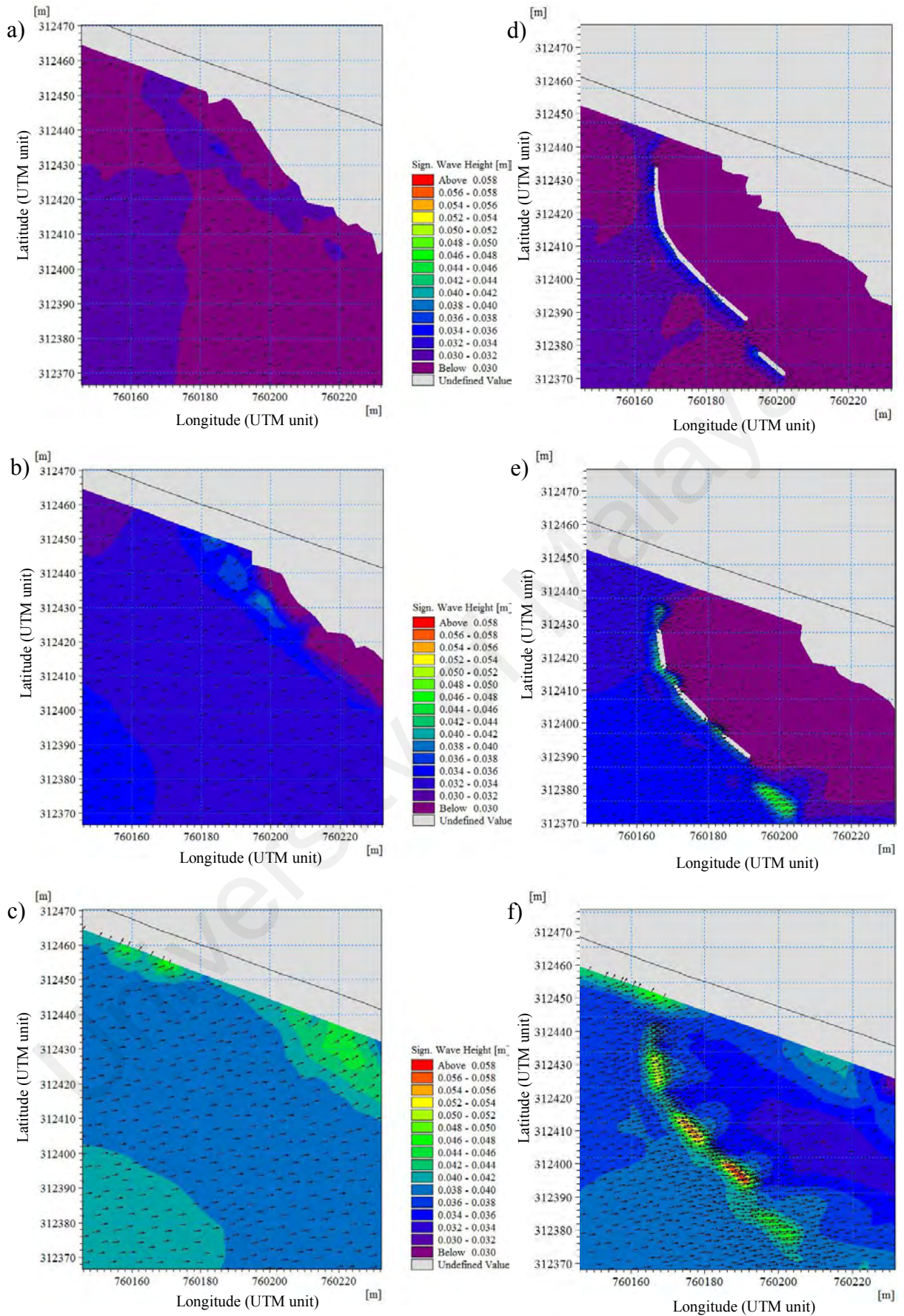
Figure 4.11: Wave characteristics before and after construction of detached breakwater during transition period, (a, d) WL < 0.4 m of MSL, (b, e) 0.4 m of MSL < WL < 0.9 m of MSL, (c, f) WL > 0.9 m of MSL

4.1.5 Summary

The coastal hydrodynamics are strongly affected by local climate and environment conditions. Carey Island coastline is imposed by three main monsoon seasons every year that are northeast monsoon, southwest monsoon and transition period. During northeast monsoon, the currents flow to the study site from northwest direction towards southeast direction with speeds approximately between 0.12 m/s and 0.22 m/s, while waves force the study site from southwest direction to northeast direction with significant heights between 0.09 m and 0.2 m. During southwest monsoon, the currents flow to the study site from southeast direction towards northwest direction with speeds between 0.09 m/s and 0.18 m/s, while waves force the study site from south direction with significant heights between 0.1 m and 0.225 m. In addition, during transition period, the patterns of current flow and wave movement from seaward to study site are found to be quite similar to northeast monsoon duration. However, the values of current speeds and wave heights are found to be lower than during northeast monsoon with difference in current directions and mean wave directions which are approximately 16° (magnetic).

Before construction of the existing detached breakwater, the energy of currents and waves straightly forces the study site and made it exposed to tidal inundation and current/wave actions. For long term, it further raised erosion problems and caused worse condition in the mangrove degradation area. However, after construction of the detached breakwater, the presence of breakwater"s structure has reduced the current speeds and wave heights in the study site/mangrove degradation area.

When the breakwater"s structure is emerged, currents and waves move to the study site through available gaps between dyke and breakwater and between breakwater and stone. In this condition, the current and wave energies are pretty much reduced behind

the breakwater's structure in the mangrove degradation area; however, some increase in current speeds in the available gaps between breakwater and dyke, and between breakwater and stone are found. The increases of current speeds in the available gaps are suspected due to the turbulence occurrences of return flows, which are caused by narrow pathway created in these areas after construction of the detached breakwater and presence of stones. For example, the current speeds in the mangrove degradation area decrease to approximately 0.06 m/s to 0.1 m/s, while the current speeds around the available gap reach 0.225 m/s during northeast monsoon season.

When the breakwater's structure is submerged, current and wave energies also can pass the study site through overtopping the breakwater's structure. At this condition, the current and wave energies are slowly reduced in the mangrove degradation area; however, a slightly higher reduction of current speeds is found behind the first segment of mainbody's breakwater.

4.2 Suspended Sediment Transport around Existing Detached Breakwater

Fine sediments are characterized by low settling velocities. Therefore, the sediments may be transported over long distance by water flow before settling. However, the cohesive properties of fine sediments allow them to stick together and form larger aggregates named by flocs with settling velocities much higher than individual particles within the floc. In this way, they are able to deposit in areas where the individual fine particles would never settle (DHI, 2014). The formation and destruction of flocs are depending on the amount of sediment in suspension as well as the turbulent properties of the flows. Generally, the formation of flocks can occur when the amount of suspended sediments in water column is more than 0.01 kg/m^3 (DHI, 2014).

Fine-grained suspended sediment plays an important role in the estuarine environment. Conceptually, patterns of suspended sediment transports in the specific

areas are strongly affected by local hydrodynamic conditions. Besides, the presence of obstacle structures such as detached breakwater also influence the transport of local suspended sediments. Since the site area is located in a mesotide, therefore both current and wave actions strongly influence the patterns of suspended sediment in the vicinity of existing detached breakwater. Moreover, the suspended sediment transports could affect the variation of coastal morphologic changes at the mangrove degradation area in the Carey Island coast, Peninsular Malaysia.

In this study, *MIKE 21 Mud Transport FM* model combined with *MIKE 21 Hydrodynamic* model were used to simulate the patterns of suspended sediment transport and erosion/accretion around the existing detached breakwater during each monsoon season. The suspended sediment transports are also presented for different water level conditions, while the accretion/erosion patterns in the vicinity of the existing detached breakwater are described during full neap tide and full spring tide conditions at every monsoon season.

The results obtained during the model calibration and validation processes and simulation results of suspended sediment transport and accretion/erosion patterns before and after construction of the detached breakwater are described in the following sections.

4.2.1 Model Calibration and Validation

Figure 4.12 shows the comparison of predicted and measured suspended sediment concentrations at latitude 02° 48" 40.02" N and longitude 101° 20" 11.18" E on 23rd December 2014 to 7th January 2015 for the calibration purpose, while Figure 4.13 shows the comparison of predicted and measured suspended sediment concentrations on 23rd December 2014 to 7th January 2015 at latitude 02° 49" 26" N and longitude 101° 18" 58.14" E for validation purpose. In addition, Table 4.4 presents the proper values of

settling velocity, erosion coefficient, critical shear stress for deposition, critical shear stress for erosion and power of erosion inputted into mud transport model setup to represent the real condition of suspended sediment transport in the study area. The dash lines describe the predicted values, while the continuous lines describe the measured values.
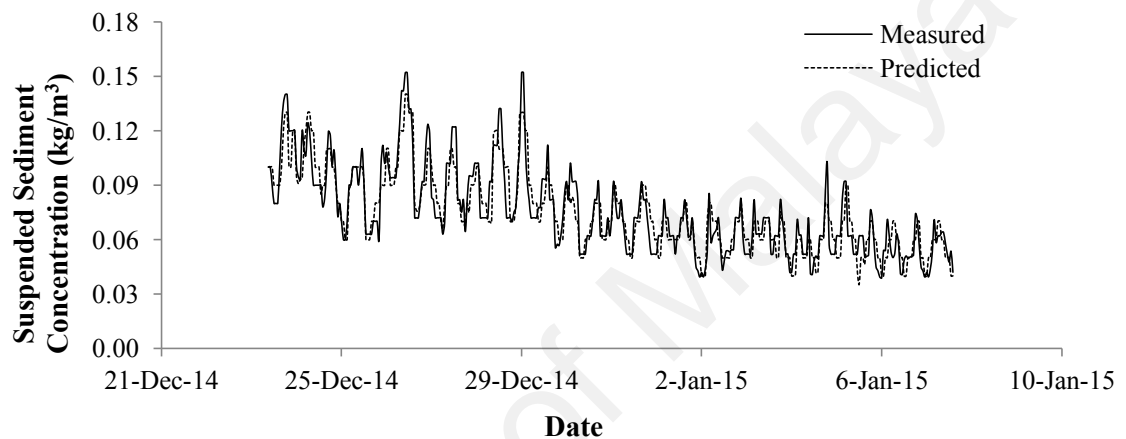
Figure 4.12: Measured and predicted of suspended sediment concentration on 23rd December 2014 to 7th January 2015 at latitude 02° 48' 40.02" N and longitude 101° 20' 11.18" E
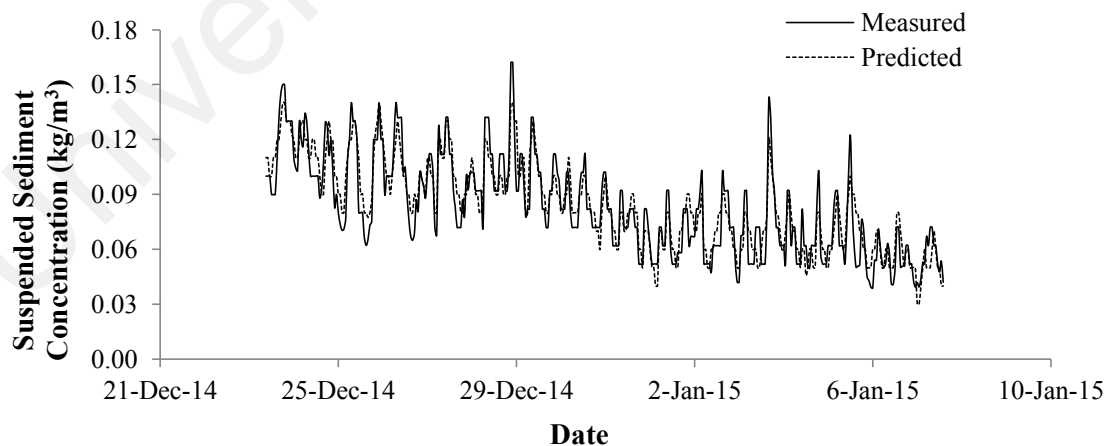
Figure 4.13: Measured and predicted of suspended sediment concentration on 23rd December 2014 to 7th January 2015 latitude 02° 49' 26" N and longitude 101° 18' 58.14" E

Table 4.4: Parameters used in mud transport model setup

No	Item	Parameters name	Value
1	Erosion parameters	erosion coefficient	0.0001 (kg/m^2/s)
		critical shear stress for erosion	1.5 N/m^2 (layer 1) 3.3 N/m^2 (layer 2)
		power of erosion	4 (layer 1) 1 (layer 2)
2	Deposition parameters	critical shear stress for deposition	0.09 N/m^2
3	Water column parameters	settling velocity	Includes flocculation calculations, with settling velocity coefficient = 7 m/s

Figure 4.12 and Figure 4.13 reveal that the overall values of suspended sediment concentrations obtained from simulations of the mud transport model are well compared to the suspended sediment concentration recorded in the field (5 km from the study site). Besides, based on both Figures, it presents that the average suspended sediment concentrations at the Strait of Malacca which is around 5 km from the study site is approximately 0.09 kg/m^3. It demonstrates that the suspended sediments conveyed from the Langat River (approximately 0.15 kg/m^3 in average) is not fully transported to the study area while some amount of sediment concentrations may be settled down on the seabed before arriving the area around the site.

To check the performance of the simulation results of *MIKE 21 Mud Transport*, the differences between predicted and measured values of suspended sediment concentrations are calculated by using *Root Mean Squared Error* (RMSE), *R Squared*, and *Theil's inequality coefficients*.

Table 4.5 provides the minimum values of *Root Mean Squared Error* (RMSE), *R Squared*, and *Theil's inequality coefficients* obtained during the model calibration and

validation process. The minimum values of Thiel"s inequality coefficient for the calibration and validation are 0.16 and 0.17, respectively. Based on standard error allowed for hydraulic study (DID, 2013), the *Root Mean Squared Err*or (RMSE), *R Squared, and Theil's inequality coefficients* values proved that the model were well calibrated and validated.

Table 4.5: Statistical Metrics for Mud Transport Model

Statistical Metric	Calibration Process	Validation Process
RMSE	0.010	0.011
R Squared (R^2)	0.83	0.82
Thiel"s inequality coefficient	0.16	0.17

4.2.2 Suspended Sediment Transport and Pattern of Accretion/Erosion in the vicinity of Detached Breakwater during Northeast Monsoon

Figure 4.14 presents the amount of suspended sediment concentrations in the vicinity of detached breakwater during northeast monsoon season for different water levels. The water levels were conditioned as discussed in hydrodynamic simulations (section 4.1). In addition, Figure 4.15 presents the patterns of accretion/erosion near the detached breakwater during full tide condition and neap tide condition at northeast monsoon.

According to Figure 4.14, the maximum concentrations of suspended sediment brought and transported by current and wave actions from seaward to the mangrove degradation area are approximately 0.048 kg/m^3 (Figure 4.14 (a, b, c)) during northeast monsoon. It means that there is a possibility of individual particles of suspended sediments in water column to stick together and form flocs in the areas, which have enough calm hydrodynamic conditions. In addition, the concentrations of suspended sediments brought from seaward are reduced in line with mean wave directions to

landward area. However, the amounts of suspended sediment concentrations are found to be slightly increased around the gap between breakwater and stone (Figure 4.14 (b)), which has higher current speeds due to the return flow occurrences in this area. Since the current speeds are influenced by wave radiations, it can be demonstrated that the current and wave actions significantly affect the pattern of suspended sediments transport in the intertidal areas.
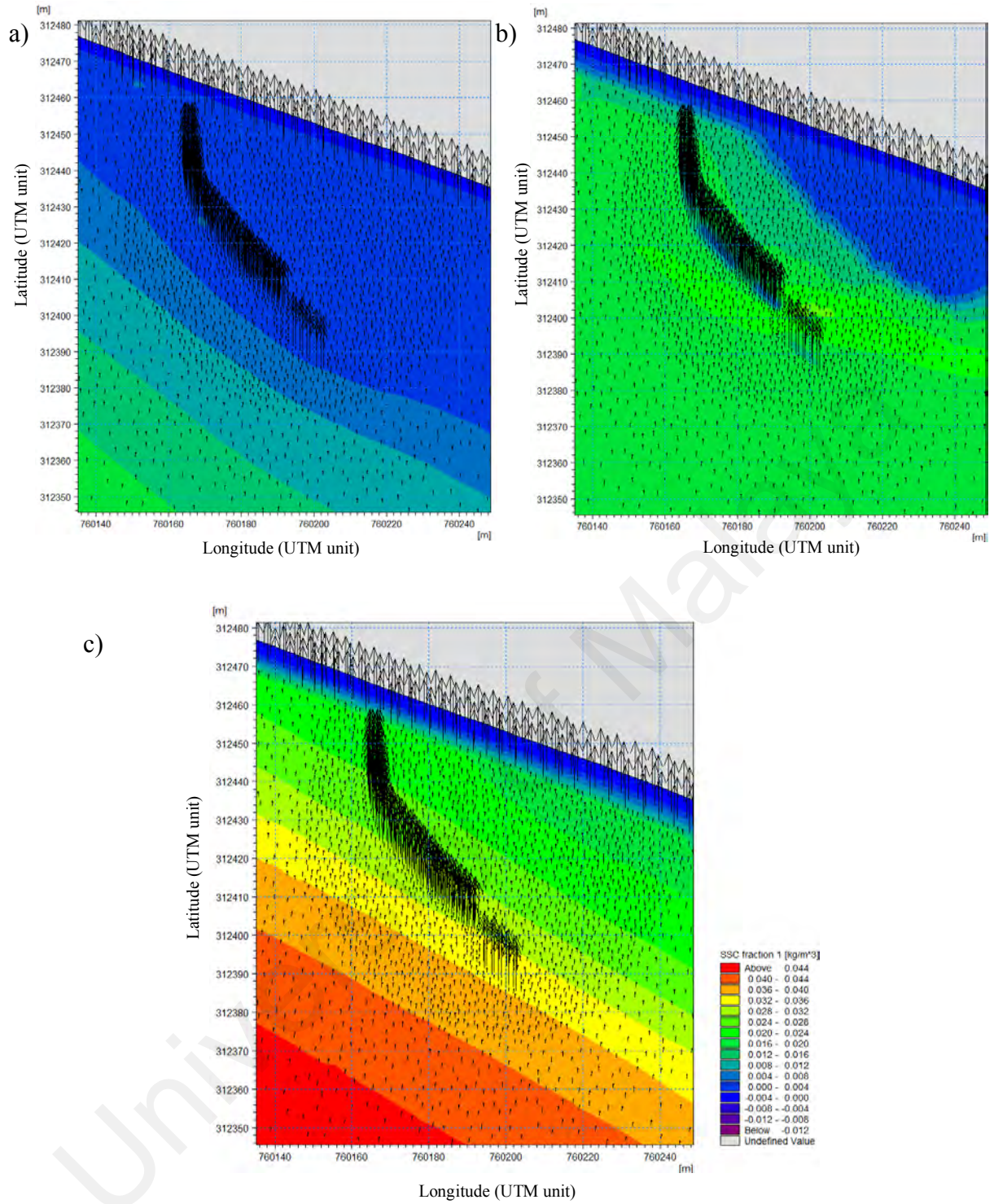
Figure 4.14: Suspended sediment transport in the vicinity of detached breakwater during Northeast Monsoon, (a) WL < 0.4 m of MSL, (b) 0.4 m of MSL < WL < 0.9 m of MSL, (c) WL > 0.9 m of MSL

Figure 4.15: **Accretion/erosion patterns around the detached breakwater during Northeast Monsoon, (a) neap tide, (b) spring tide**

When the water levels are lower than 0.4 m of MSL (flood tide conditions < 0.4 m of MSL), the presence of detached breakwater obstructs the transportation of suspended sediment from the seaward to the mangrove degradation area and it is found that the concentrations of suspended sediments are higher at front of breakwater than behind the

breakwater structure. The formations of flocs may occur at front of breakwater when the hydrodynamic conditions around this area are calm enough to settle down the sediments. However, some of the suspended sediments from seaward (individual size or floc size) can be transported into the mangrove degradation area through the gaps between breakwater and dyke and between breakwater and stone with smaller concentrations. Therefore, during ebb tide, the suspended sediments behind the breakwater that have individual particles might be brought back seaward by return flows due to small settling velocities; however, some flocs may settle down behind the breakwater because of small velocities of return flows and higher settling velocities of the sediments.

When the water levels are lower than 0.9 m of MSL (flood tide conditions < 0.9 m of MSL), the suspended sediments can enter the mangrove degradation area through overtopping the gap"s breakwater and through the available gaps between breakwater and stone and between breakwater and dyke with concentrations approximately 0.012 kg/m³. At this moment, floc formations of suspended sediment are possible at front and behind the breakwater during the calm hydrodynamic conditions. Besides, some of the suspended sediments (single particle size and floc size) which enter the mangrove degradation area can be trapped behind the mainbody"s breakwater. Therefore, it can increase the bed levels in the mangrove degradation area, especially near the structure of mainbody"s breakwater. Further, during ebb tide, some suspended sediments (individual particles or floc size) in water column can be transported back to seaward through the available gaps and above the gap"s breakwater together with current flows.

However, there is increasing concentrations of suspended sediment around the gap between breakwater and stone. It is suspected because of the higher current velocities recorded in this area due to the occurrences of return flows, which causes some of deposited individual particles to be re-suspended.

In addition, when the water levels are higher than 0.9 m of MSL (flood tide condition > 0.9 m MSL), the currents can fully flow to the mangrove degradation area with concentration approximately 0.012 kg/m^3 during flood tide. At this moment, flock formations of suspended sediment are possible at front and behind the breakwater. Besides, during ebb tide, some or all suspended sediments (individual particles or flock size) in water column can be transported back to seaward from the mangrove degradation area depending on turbulent properties of the flows. Since suspended sediments with floc size having higher settling velocities compared to individual size, some of the suspended sediments with floc size can be settled and deposited faster behind and front of the breakwater's structure.

Regarding Figure 4.15, it can be demonstrated that during neap tide (when the maximum water levels are at 1 m of MSL), there is no erosion was recorded around the gap between the breakwater and stone. While, small amount of accretion was found at front of breakwater.

During the spring tide, very small amount of erosions are recorded at the beginning from the available gap areas and linearly up to some part in the mangrove degradation areas. Besides, small amount of erosions are also found at left side of gap's breakwater. However, accretions are found mostly at mangrove degradation area behind the breakwater's structure and some part at front of breakwater.

4.2.3 Suspended Sediment Transport and Pattern of Accretion/Erosion in the Vicinity of Detached Breakwater during Southwest Monsoon

Figure 4.16 presents the amount of suspended sediment concentrations in the vicinity of detached breakwater during southwest monsoon season for different water levels. In addition, Figure 4.17 presents the patterns of accretion/erosion around the detached breakwater during full tide and neap tide conditions at southwest monsoon.

Figure 4.16: Suspended sediment transport in the vicinity of detached breakwater during Southwest Monsoon, (a) WL < 0.4 m of MSL, (b) 0.4 m of MSL < WL < 0.9 m of MSL, (c) WL > 0.9 m of MSL
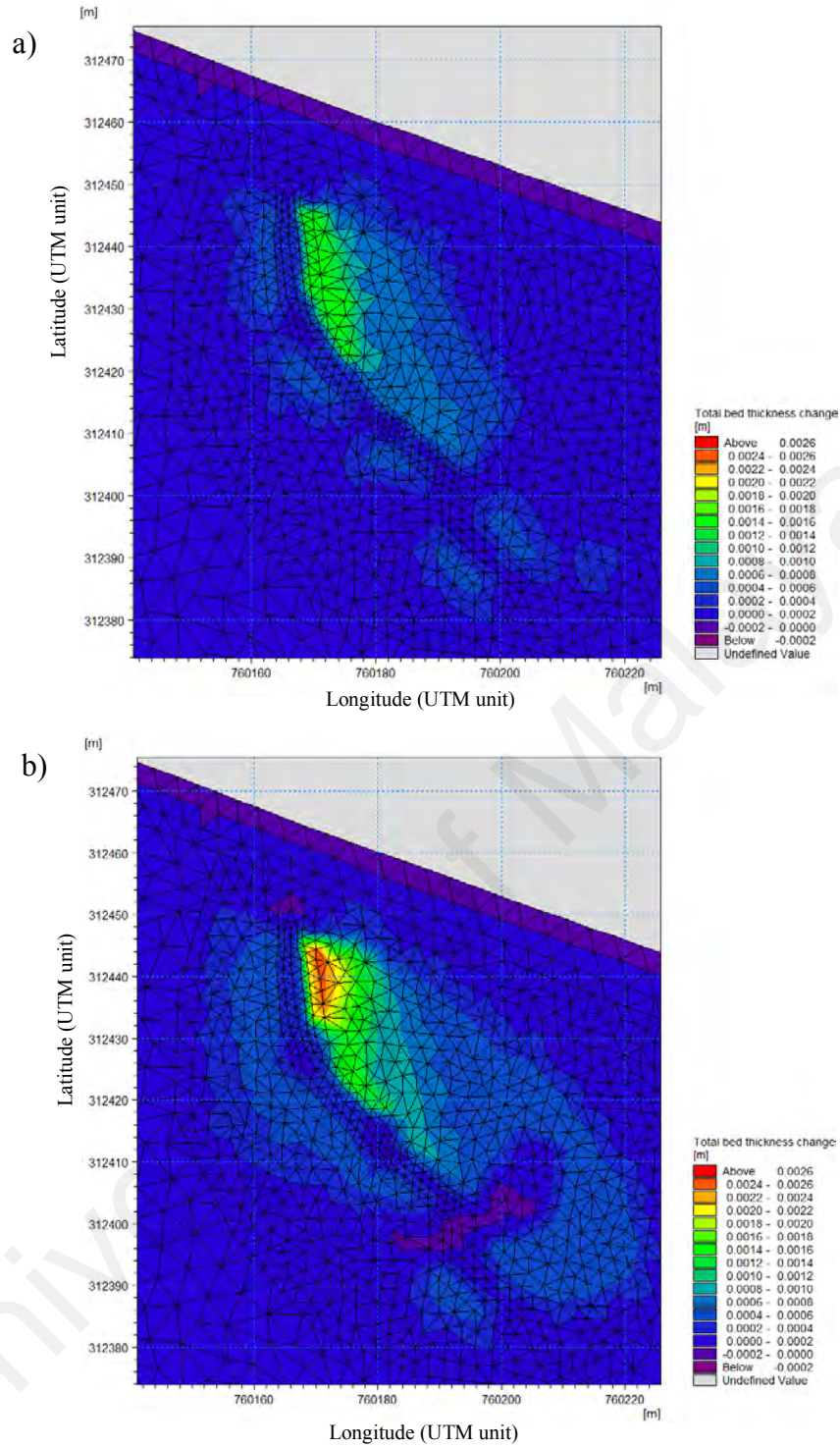
Figure 4.17: Accretion/erosion patterns in the vicinity of detached breakwater during Southwest Monsoon, (a) neap tide, (b) spring tide

According to Figure 4.16, the maximum concentrations of suspended sediment brought and transported by current and wave actions from seaward to the mangrove

degradation area during the southwest monsoon are slightly smaller compared to concentrations during northeast monsoon, which is 0.04 kg/m^3. However, the concentrations of suspended sediment are found to be higher in the mangrove degradation area when the water levels are less than 0.9 m of MSL. It might be because of the current conditions, which flow toward northwest from the southeast directions during southwest monsoon and make them pass over mangrove degradation area before they reach the breakwater structure. Therefore, the formations of flocs from the individual particle of suspended sediments in water column are possible to occur at the mangrove degradation area even when the water levels are lower than 0.4 m below MSL.

When the water levels are lower than 0.4 m below MSL (flood tide conditions < 0.4 m of MSL), the presence of detached breakwater can help in trapping some suspended sediments (floc size) before they flow seaward through the gaps between breakwater and stone and between breakwater and dyke. However, when the water levels are higher than 0.4 m above MSL and lower than 0.9 m above MSL (flood tide conditions < 0.9 m of MSL), more suspended sediments can flow seaward from the mangrove degradation area since they also can flow by overtopping the gap"s breakwater. At this moment, the turbulent conditions of water flow are a bit higher around the gap"s breakwater and make it possible to re-suspend the deposited individual particles around the gap"s breakwater.

In addition, when the water levels are higher than 0.9 m above MSL (flood tide condition > 0.9 m above MSL), the suspended sediments in water column can flow seaward from the mangrove degradation area by overtopping the breakwater"s structure. Then, all of the individual particles of suspended sediments in water column can pass the breakwater and flow seaward; however, some amounts of suspended sediments

(flocs size) can be trapped behind the breakwater's structure that significantly depended on settling velocities of suspended sediments (flocs size) and turbulent conditions of water flow.

Figure 4.17 demonstrates that during neap tide (when the maximum water levels are 1 m above MSL), there is no erosion/accretion recorded around the gaps between the breakwater and stone and between breakwater and dyke. Besides, small amount of accretion is found at front and behind breakwater's structure.

In addition, during the spring tide, there is very small amount of accretion recorded at starting from the available gap areas (between breakwater and stone) up to some parts in the seaward and forward of this area. While, very small amount of erosion is found at side of gap's breakwater. However, the significant accretions are found mostly at mangrove degradation area behind the breakwater's structure and the front of the first mainbody' breakwater.

4.2.4 Suspended Sediment Transport and Pattern of Accretion/Erosion in the Vicinity of detached Breakwater during Transition Period

Figure 4.18 presents the amount of suspended sediment concentrations in the vicinity of detached breakwater during transition period for different water levels. The water levels are conditioned as discussed in hydrodynamic simulations (section 4.1). In addition, Figure 4.19 presents the patterns of accretion/erosion around the detached breakwater during full tide condition and neap tide condition at southwest monsoon.
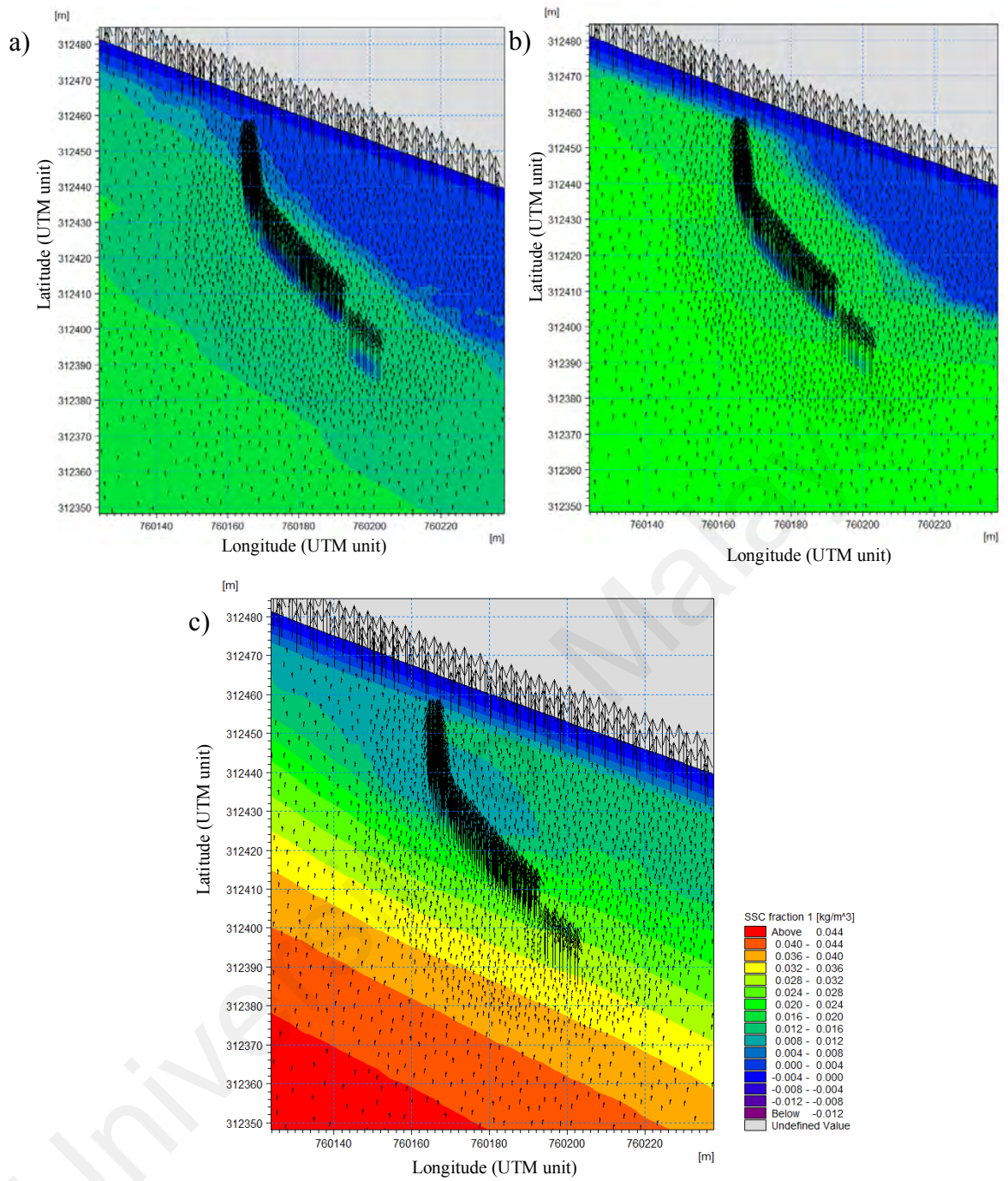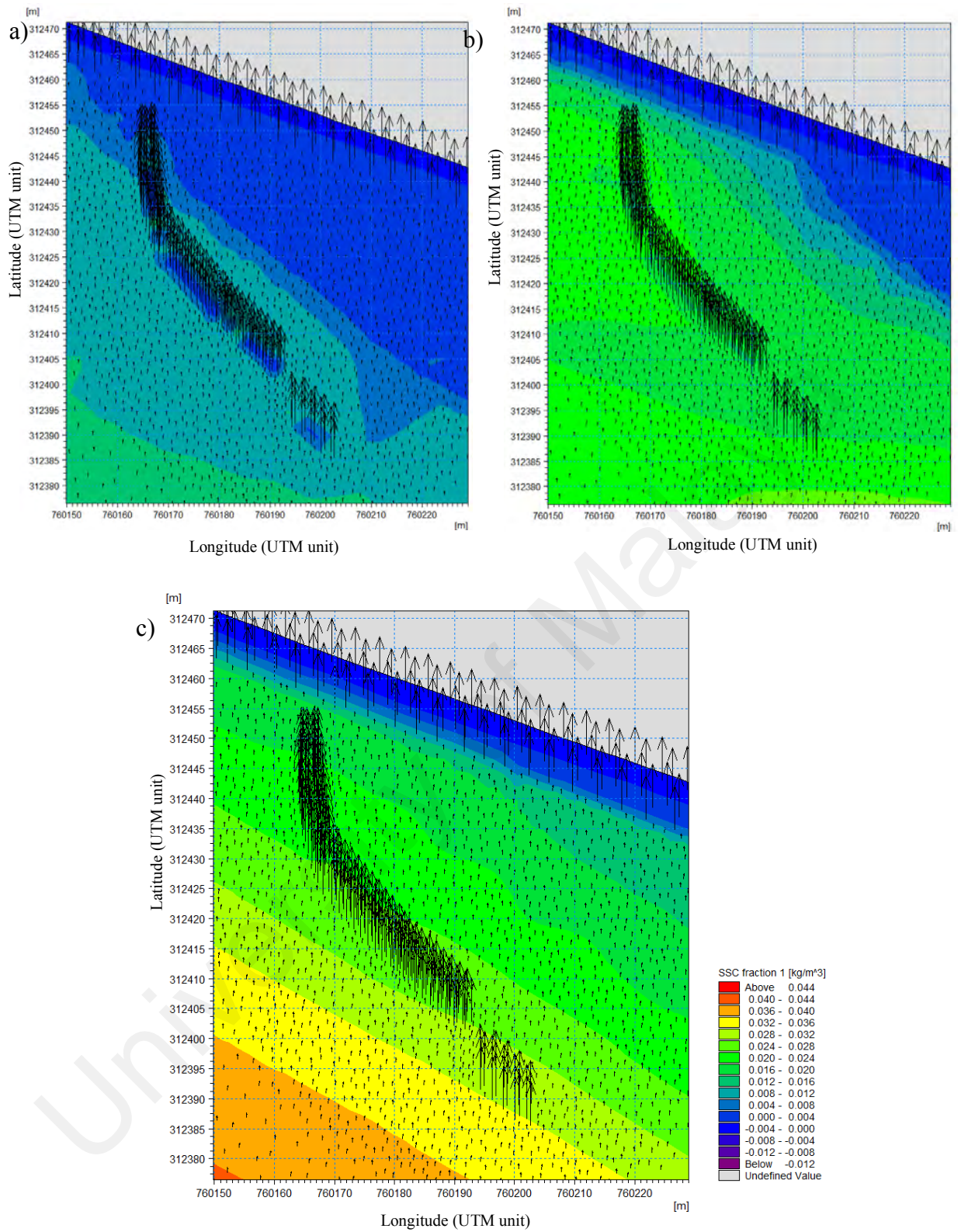
Figure 4.18: Suspended sediment transport in the vicinity of detached breakwater during Transition Period, (a) WL < 0.4 m of MSL, (b) 0.4 m of MSL < WL < 0.9 m of MSL, (c) WL > 0.9 m of MSL
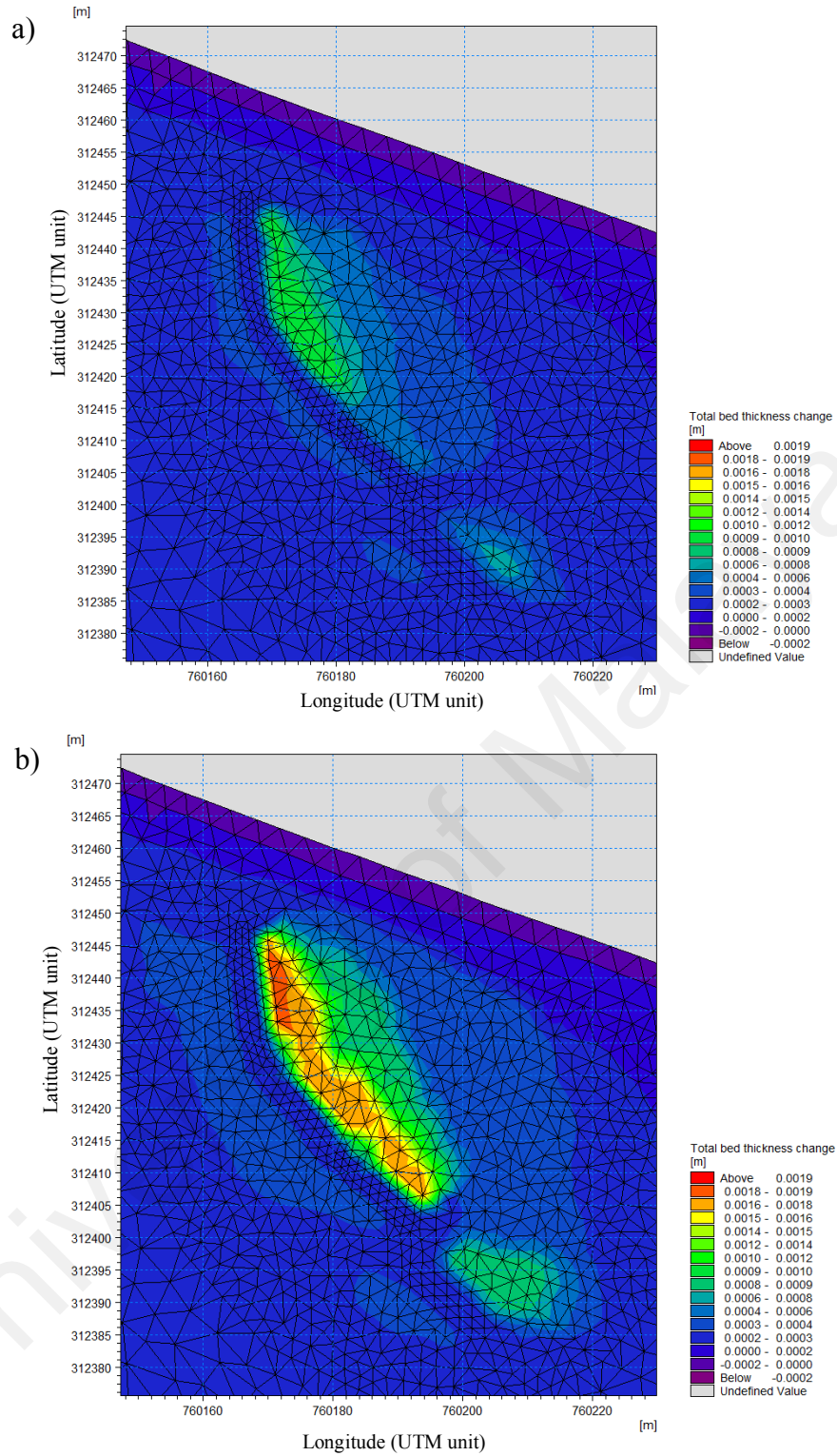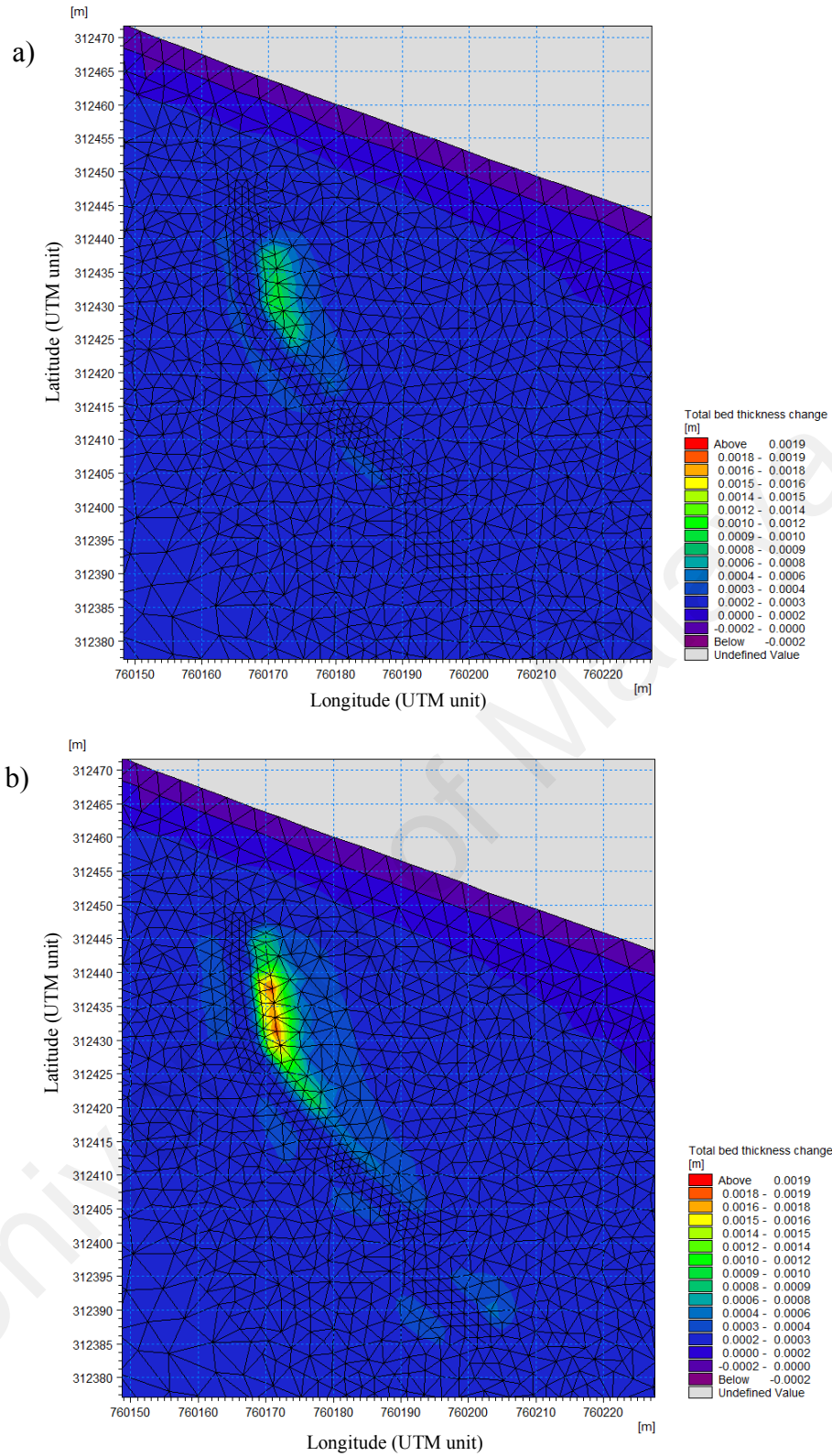
Figure 4.19: Accretion/erosion patterns in the vicinity of detached breakwater during Transition Period, (a) neap tide, (b) spring tide

The concentrations of suspended sediments around the existing detached breakwater (front and behind its structure) are found to be less than 0.01 kg/m^3 during transition

period when the water level is lower than 0.4 m of MSL (Figure 4.18 (a)). Therefore, the individual particles of suspended sediments in water column have less possible to stick together and form flocs around this area. It means that there is small possibility of suspended sediments in the water column to be deposited around the breakwater including mangrove degradation area in this moment due to the settling velocities of individual particles of fine sediment are small.

Besides, the concentrations of suspended sediments are found to be more than 0.01 kg/m^3 around the breakwater"s structure when the water levels are more than 0.4 m of MSL (Figure 4.18 (b, c)). Therefore, the floc formations of individual particles of suspended sediments in water column are highly possible around the existing detached breakwater. In this moment, some of suspended sediment (floc size) could be trapped behind the breakwater, while some of suspended sediment (individual and floc sizes) could be transported back to the seaward through the available gaps and through overtopping the gap"s breakwater/and mainbody"s breakwater.

Based on Figure 4.19, during neap tide (when the maximum of water levels are 1 m MSL), there is small accretion without any erosion occurrences in the vicinity of the detached breakwater in transition period (Figure 4.19 (a). However, there small amount of accretion is found around the breakwater structure while the higher values of depositions are found behind the first mainbody"s breakwater (Figure 4.19 (b)). In addition, very small accretion is recorded around the gaps between breakwater and stone and between breakwater and dyke during spring tide conditions (Figure 4.19 (b)).

4.2.5   Summary

The processes of sediment transport and pattern of accretion/erosion in the coastal zone are mostly dominated by ocean dynamic and environmental conditions. Strong currents/waves can readily suspend and re-suspend nearshore sediments, while the

higher settling velocities of sediments make them to be easier to settle down. In addition, the presence of a coastal structure in the coastal zone changes more complexity of the sediment dynamics, especially in the vicinity of the structure.

Fine sediments are characterized by low settling velocities that have possibility to be transported over long distance by the water flow before settling. However, the cohesive properties of fine sediments allow them to stick together when their concentrations are more than 0.01 kg/m^3 during the calm hydrodynamic conditions. It further makes possible for them to form larger aggregates name by flocks with settling velocities much higher than individual particles within the flock. In this way, they are able to be deposited in areas where the individual fine particles would never settles (DHI, 2014).

Based on simulation results of sediment transport model, it can be demonstrated that the concentrations of suspended sediments transported to the study area from the Strait of Malacca are found to be quite significant. The amount of sediment concentrations from the Strait of Malacca that enter the mangrove degradation area are increased as well as by increasing of tidal ranges and the maximum concentrations of suspended sediments are up to 0.048 kg/m^3 during full spring tide conditions of northeast monsoon, southwest monsoon and transition period. These results illustrate that there are possibility of single fine particles of suspended sediments to stick together and form flocks during calm hydrodynamic conditions. Further, the flock sizes of suspended sediments can easily settle down due to their higher settling velocity.

Before construction of the detached breakwater, the ocean dynamics straightly forced the mangrove degradation area with considerable energies of current and wave. The local conditions of current speeds and wave heights did not allow the suspended sediments to stick together and did not allow to settle down easily. However, after construction of the detached breakwater, there are reductions in current speeds and

wave heights in the mangrove degradation area, especially at the protected area behind breakwater"s structure. It further allows the single particles of suspended sediments in water column to form flock sizes during the calm hydrodynamic conditions and when the sediment concentrations are more than 0.01 kg/m^3. Moreover, the floc sediments can be easier to be settled down at the protected area behind the breakwater"s structure.

In detail, when the water levels are lower than 0.9 m below MSL (during neap tide condition), the suspended sediments in water column (individual particles size or floc size) from the seaward can enter the mangrove degradation area through overtopping the gap"s breakwater and through the available gaps between breakwater and stone and between breakwater and dyke with maximum concentrations approximately 0.012 kg/m^3. At this time, floc formations of suspended sediment are possible at front and behind the breakwater during the calm hydrodynamic conditions.

Since the current speeds behind the breakwater structure are reduced quite significantly, there is a possibility of the suspended sediments (single particle size or floc size) to be settled down behind the breakwater, especially near the mainbody"s structure. Therefore, it can increase the bed levels in the mangrove degradation area mainly near to the structure of mainbody"s breakwater. Further, during ebb tide, some suspended sediments (individual particles or floc size) in water column can be transported back seaward through the available gaps and above gap"s breakwater together with current flows. In addition, the higher return flow velocities around the gaps between the breakwater and stone can cause some of individual particle sizes of bottom sediments to be re-suspended and therefore causing small amount of erosion, which is recorded around the gap between the breakwater and stone.

When the water levels are higher than 0.9 m above MSL (during spring tide condition), the breakwater is fully submerged. The whole concentrations of suspended

sediments transported from the Strait of Malacca can enter the study site area through available gaps as well as through overtopping breakwater"s structure. During this time, there is a high possibility for single particles of suspended sediments to stick together and form the floc sizes and further, the floc sizes of suspended sediments can settle down at the protected area behind the breakwater"s structure during calm hydrodynamic condition. However, during ebb tide, there are also possibilities of some or all concentrations of suspended sediments (individual particles or floc size) in water column can be transported back seaward from the mangrove degradation area through overtopping breakwater"s structure depending on turbulent properties of the flows. Therefore, it can reduce the possibility of more sediment to be trapped in the mangrove degradation area.

Moreover, since the hydrodynamic condition around the first segment of mainbody"s breakwater is calmer during spring tide condition, the higher amounts of sediment accumulation are found around this area. In addition, some erosion which is found around the available gaps, may be due to re-suspension of the deposited sediments around the gaps areas because of turbulences of return flows.

4.3 Morphodynamic Changes in the Vicinity of Existing Detached Breakwater

The evaluation of morphodynamic changes includes the changes of seabed levels in the vicinity of the detached breakwater at every consecutive survey, the patterns of accretion and erosion in the vicinity of the detached breakwater before and after construction of detached breakwater (at every consecutive surveys), and volume changes at the mangrove degradation areas between consecutive surveys.

4.3.1 Bed Level Changes in the Vicinity of Detached Breakwater

Seabed profiles in the vicinity of the existing detached breakwater at intertidal area of Carey Island coast have been monitored during the year 2009 to 2014. In this section,

the seabed surface elevations at cross-section of profile CS11 and CS14 were plotted

out to presents the seabed level changes near to the gap''s breakwater and near to the

mainbody''s breakwater. Figure 4.20 presents the seabed level changes near the

mainbody''s breakwater (CS11) from the year 2009 to 2014 and Figure 4.21 indicates

bed level changes near the gap''s breakwater from the year 2009 to 2014.
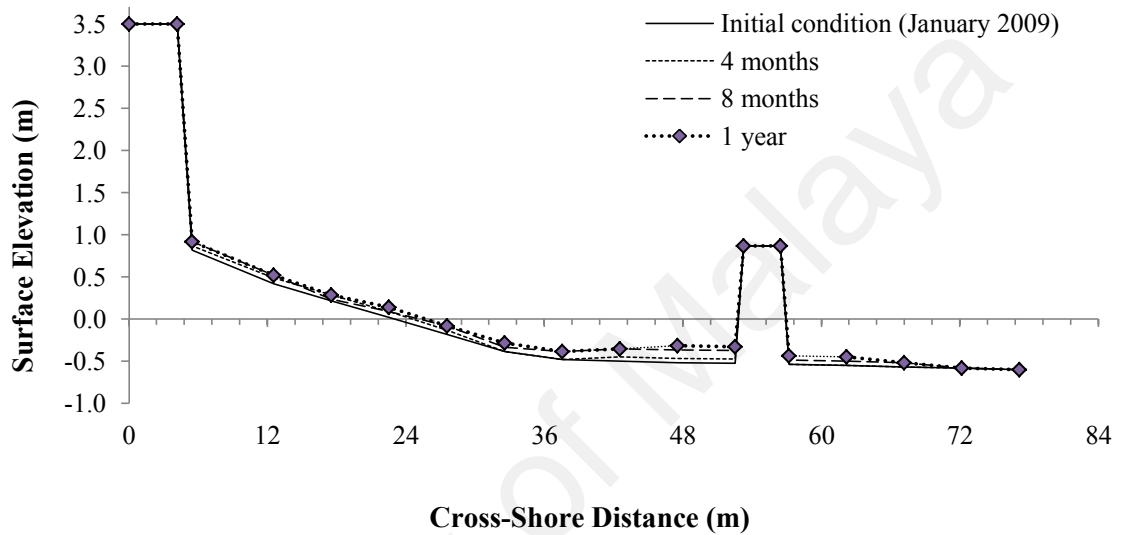
a) Comparison of seabed elevations during the first year construction of the
breakwater (monitoring interval: 4 months)
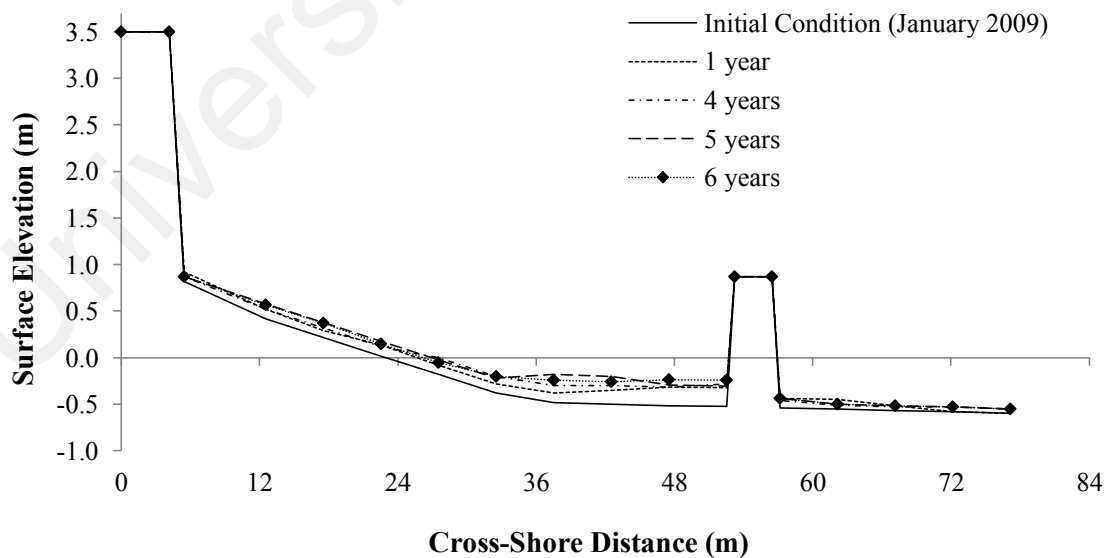
b) Comparison of seabed elevations between years 2009 and 2014
(monitoring interval: 12 months)

**Figure 4.20: Seabed surface elevations at profile line CS11 between years 2009 and
2014 (before and after the construction of breakwater)**
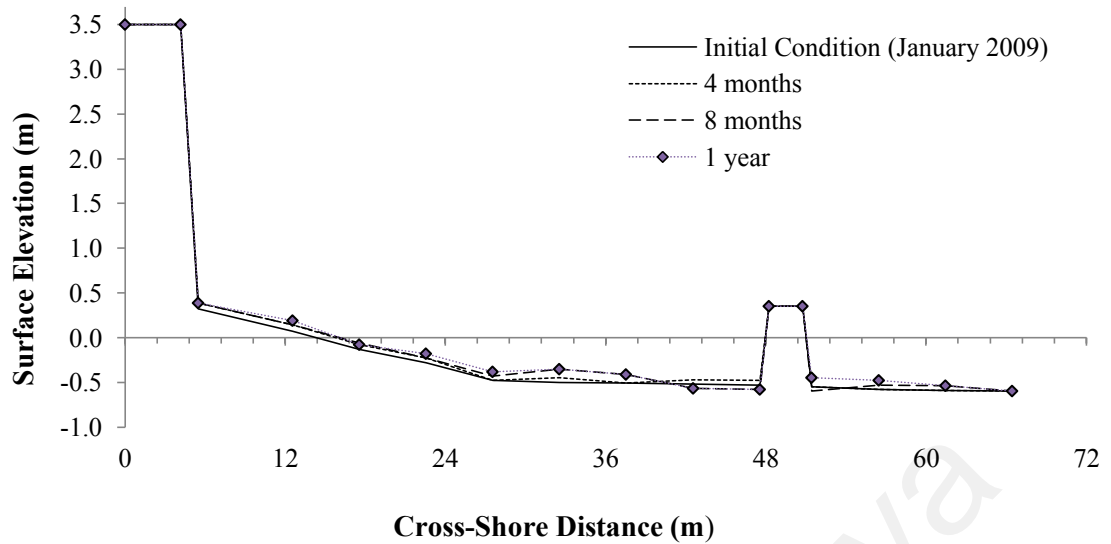
a) Comparison of seabed elevations during the first year construction of the breakwater (monitoring interval: 4 months)
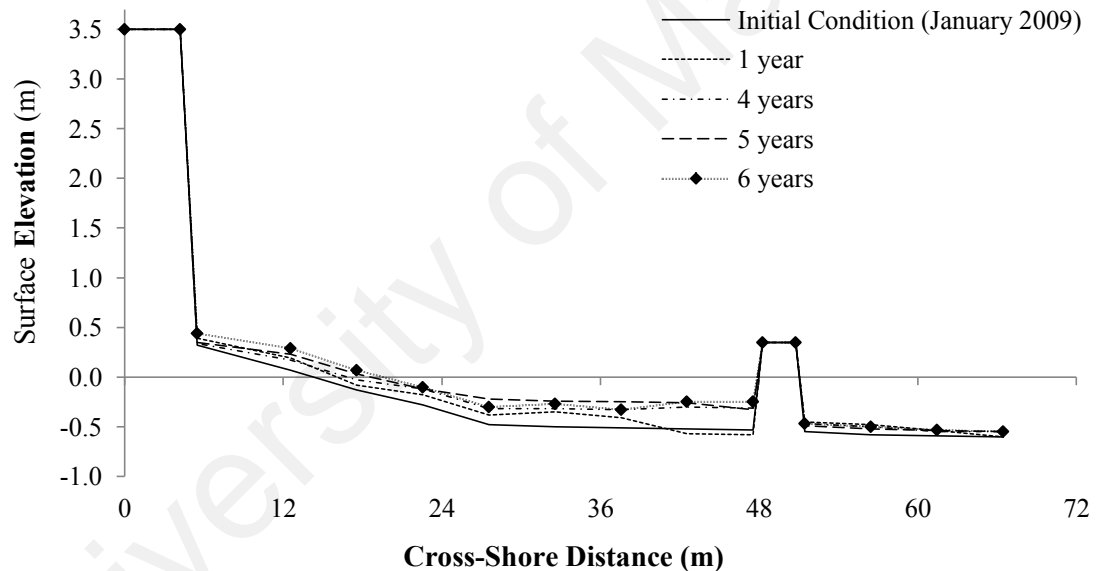
b) Comparison of seabed elevations between years 2009 and 2014 (monitoring interval: 12 months)

Figure 4.21: Seabed surface elevations at profile line CS14 between years 2009 and 2014 (before and after the construction of breakwater)

There is increase in seabed levels in the mangrove degradation areas, especially near the breakwater''s structure during six years of installation of the detached breakwater. The increase of the seabed levels was recorded to be quite considerable extended to 18 m behind the mainbody''s breakwater area during one year of its construction (Figure 4.20). The maximum increase of bed levels is 20 cm while the average increase of bed

levels is approximately 10 cm. The seabed levels are further rising slowly every year during the years 2010 to 2014. The maximum increase of the seabed levels in the mangrove degradation area after six years of construction of the detached breakwater is reaching 30 cm near its structure while the average increase of bed levels behind the breakwater"s structure is approximately 24 cm. Subsequently, the increments of the bed levels has reduced the bottom slope in the mangrove degradation area.

In contrast, the seabed levels around the gap"s breakwater are recorded to be slightly reduced during one year installation of the existing detached breakwater that are reaching 5-10 cm (Figure 4.21). However, the increase of the seabed levels is recorded in the mangrove degradation area behind the gap"s breakwater after one year implementation of the detached breakwater at intertidal area of cohesive shore of Carey Island.

Overall, the presence of detached breakwater at the study site has been found to be able in trapping sediment accumulation and increasing the bed levels in the mangrove degradation area. The increases of the seabed levels at profiles CS11 and CS14 during the years 2009 to 2014 were between 5 cm and 30 cm. Even though the presence of the existing detached breakwater has given an advantage for the mangrove rehabilitation purposes due to the increasing seabed elevations behind its structure and reduced erosion problem at the site, the average seabed elevations at most parts in the mangrove degradation areas after six years of its installation at intertidal area of Carey Island, Malaysia are less than 1.2 m below MSL. It means that the increase of the seabed elevations due to the presence of existing design of the detached breakwater over six years is too little to achieve the minimum target elevations required to provide a suitable hydraulic regime for mangrove survival in the intertidal area of Carey Island coast, Malaysia. Further, it is assumed that more than 20 years is required to establish a

suitable hydraulic regime for mangrove rehabilitation project at the site by using existing design of detached breakwater if the equilibrium rate is still not yet reached.

4.3.2   The Pattern of Accretion/Erosion around the Detached Breakwater

The erosion and accretion patterns caused by the 80-m long detached breakwater (with low crest levels) at the intertidal area of cohesive shore of Carey Island are evident. Figure 4.22 shows the erosion and accretion patterns in the vicinity of the existing detached breakwater after its construction during the years 2009 to 2014. In this figure, the positive mark represents the accretion, whereas the negative mark represents the erosion.

Based on Figure 4.22, it is evident that the shoreline positions in the intertidal area of cohesive shore are dynamic due to the presence of the existing detached breakwater. The results prove that erosion occurred in the vicinity of the gaps during the first year into the construction of the breakwater on the intertidal flat, whilst there was no erosion recorded in the vicinity of neither gaps nor main bodies one to six years after its implementation. For example, during January 2009 to January 2010, the bed surface elevations around the gaps reduced by 5 to 10 cm.

A linear increase in accretion was recorded every year near the lee of the structure especially after one year of its installation. The results showed that dynamic accretions occurred at any time and space behind and at front of the structure on the intertidal area of the cohesive shore (Figure 4.22).

It is generally accepted that erosion and accretion patterns in the cohesive shores are strongly affected by the sediment characteristic and physical forces, such as waves and tidal current (Le Hir *et al.*, 2000; Liu *et al.*, 2011). Regarding the sediment characteristics, the cohesive sediments exhibit cohesion behavior due to the electrochemical forces acting between their particles that can prevent the bed load

transport and resist the erosion (Franz *et al.*, 2014).

Friend *et* al. (2005) stated that waves and tidal currents play important roles in the sediment dynamics in the intertidal systems. Naturally, waves are generated by local winds. Strong waves re-suspend sediments, produce longshore as well as cross-shore currents and move the sediment from seaward to the onshore. In a cohesive shore, the wave heights at the intertidal area are much lower than the offshore. The wave height decreases as the wave moves towards the shoreline through the wave attenuation due to the friction effect of the increasing viscosity by the soft fluid mud (Awang, 2010; Jiang & Mehta, 1995; Lee & Mehta, 1997).

Tide is also the most important process in the intertidal area. As the tide rises (filling) and falls (emptying) at the flat, the water is forced to generate currents. Tidal currents carry the suspended sediment from the upstream during the flood tide and from downstream during the ebb tide.

Besides the physical forces, the accretion and erosion patterns on the cohesive shore are also affected by the presence of coastal structures. When a breakwater is placed in a shoreline system, it interacts with wind-generated waves, wave-generated currents and tidal currents (Chang *et al.*, 2012). This is because the breakwater attenuates the energy of the wind-generated waves, reduces the currents" velocities and dissipates them before approaching the shoreline.

Here, 80-m long detached breakwater with low crest levels was located in the intertidal zone and its first segment was designed like a groyne (perpendicular to the shoreline) to effectively block the longshore transport of sediment from the onshore to the sea. It resulted in the sediment accumulation to be formed in the protected area near the structures of the first segment. Because the detached breakwater is positioned in the

intertidal zone, the breakwater becomes submerged in high tide and emerged in low tide.

When the tide rises, the breakwater is submerged and water flows are allowed through the top of the structure and available gaps. In general, wave and currents carry the suspended sediment from seaward and allow the sediment to enter the protected area behind the breakwater. The existing detached breakwaters reduce the velocities of cross-shore currents behind its structure and prevents offshore transport, especially if there is no gap between the main bodies (Kamali, 2011). In this condition, velocities of the return flows will be smaller above the breakwater and higher at the gaps between breakwater and stone and between breakwater and dyke.

The sediment deposits are allowed to build up behind the breakwater"s structure (protected area) when the hydrodynamic conditions are calm enough to settle down the sediment. Besides, some deposited sediments are allowed to be eroded around the gaps between breakwater and stone and between breakwater and dyke due to the turbulent conditions of water flows in these areas. Further, during the ebb tide, water columns that contain suspended sediment flow back seaward through the top of the structures and gaps between breakwater and stone and also between breakwater and dyke. This condition forces some of the suspended sediments to return back seaward before deposition. It further reduces the chance to deposit more sediments behind the structures.

It is apparent that when the breakwater emerges, wave and currents from seaward are reflected back seaward as soon as they reach the structure, except there are gaps available. This is why slight erosion can be observed at the front of the breakwater. However, erosion will not occur around the area where the current velocities are not strong enough to re-suspend the cohesive sediment.
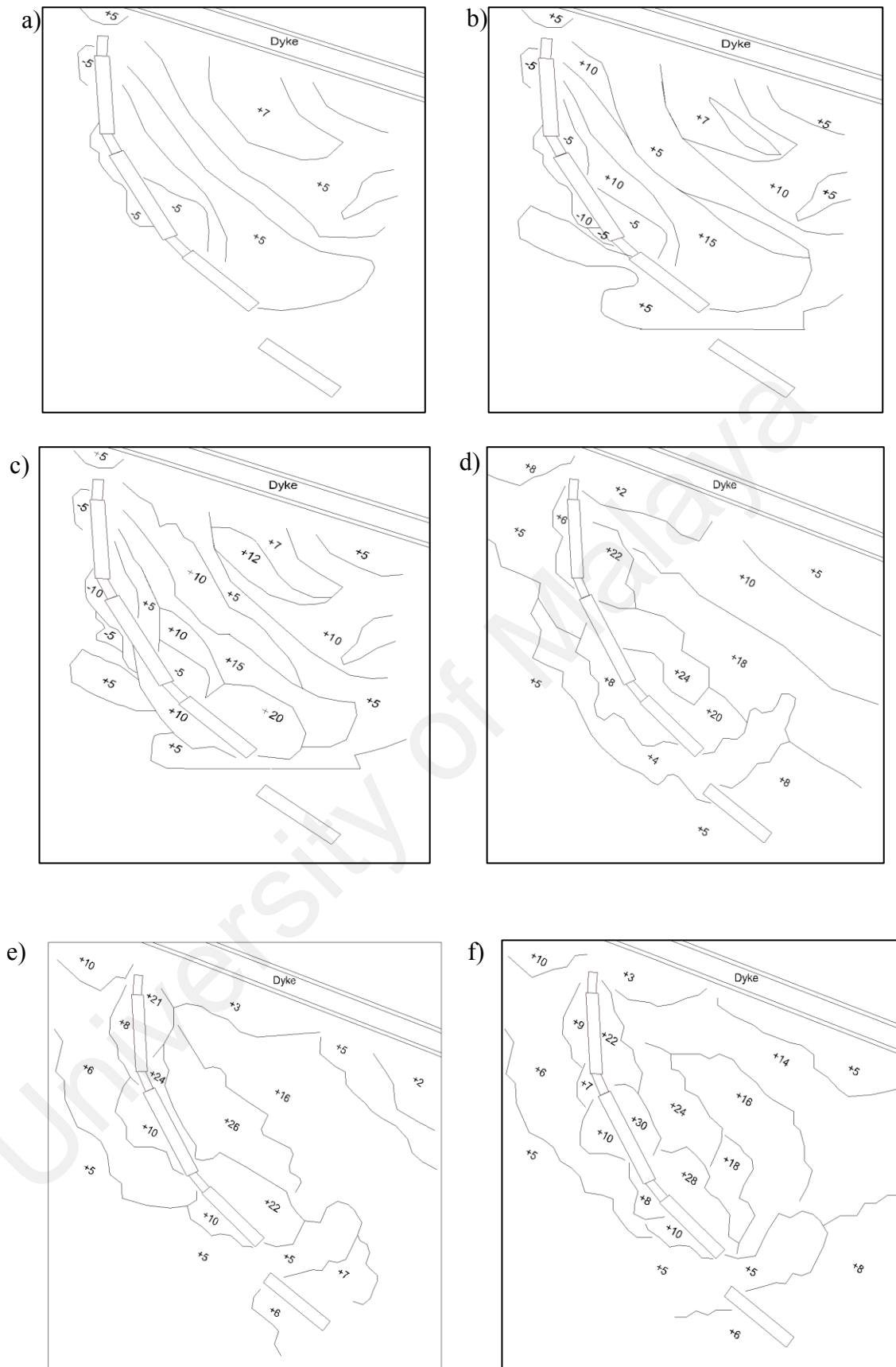
Figure 4.22: Erosion and accretion patterns in the vicinity of the detached breakwater after some period of its installation, (a) 4 months, (b) 8 months, (c) 1 year, (d) 4 years, (e) 5 years, (f) 6 years, note: (+) presenting the accretion in unit of cm and (−) presenting the erosion in unit of cm

4.3.3   Deposition Volume behind the Detached Breakwater

The comparison of smoother seabed elevations at cross-section CS11 obtained after interpolation processes using the *bilinear, IDW nearest and spline interpolation* methods is presented in Figure 4.23. The elevation values at the known points before and after interpolation"s processes were inputted in equation 3.6 to get RMSE values for every interpolation method. The comparison of RMSE values obtained from every interpolation method is presented in Table 4.6. The best interpolation method, which results in the smallest error was finally chosen to be applied in *Arc-view GIS* software in order to represent the topographic conditions at every consecutive survey.
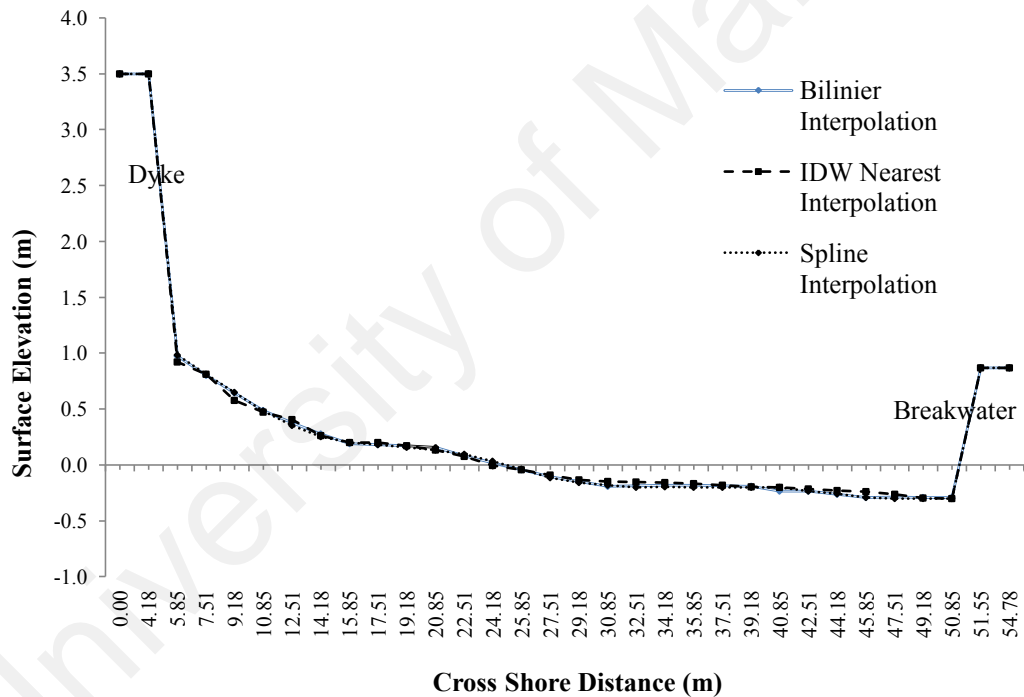
Figure 4.23: Comparison of seabed elevations at cross section CS11 in January 2009 produced by interpolation with bilinear, IDW nearest and spline methods

Table 4.6: RMSE value for each interpolation methods

No	Interpolation Method	RMSE (m)
1	Bilinear	0.011424
2	IDW nearest	0.028190
3	Spline	0.015534

Based on Figure 4.23, the seabed elevations obtained from the *bilinear and spline interpolation* methods are quite similar, while the surface elevations obtained from the *IDW nearest* are somewhat different. From Table 4.6, it is evident that whilst the bilinear and spline interpolations have small RMSE values, the bilinear interpolation method has the smallest value of RMSE. Thus, the bilinear interpolation method was used to generate the topography maps of the intertidal area of cohesive shore of Carey Island at every consecutive survey.

After producing the smooth topographic conditions at every consecutive survey, the volume changes of sediments at the seabed of mangrove degradation area (before and after construction of the detached breakwater) were calculated between the years 2009 and 2014 using the *ArcView-GIS* software. Figure 4.24 and Table 4.7 present the accumulative sediment deposition trapped locally behind the existing detached breakwater on the cohesive shore of Carey Island.
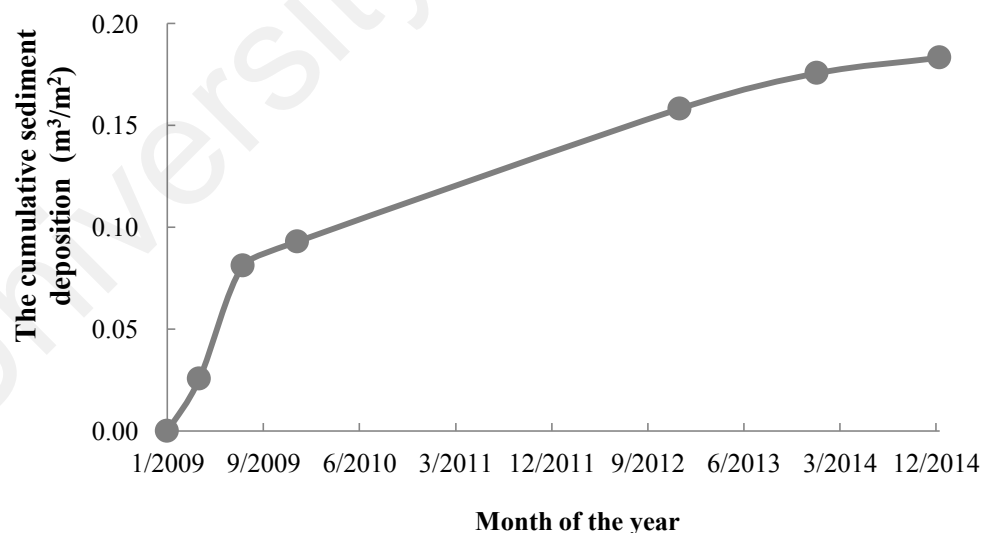
**Figure 4.24: Cumulative sediment deposition behind
existing detached breakwater**

Table 4.7: Sediment accumulation behind the breakwater

No	Time	Cumulative sediment deposition behind the breakwater (m^3/m^2)	Volume changes between consecutive surveys (m^3/m^2)
1	Jan-2009	0.000	0.000
2	Apr-2009	0.026	0.026
3	Aug-2009	0.081	0.055
4	Jan-2010	0.093	0.012
5	Jan-2012	0.158	0.029
6	Jan-2013	0.176	0.017
7	Jan-2014	0.183	0.008

The results show that the existing detached breakwater has locally succeeded in trapping the accumulation of sediment in the mangrove degradation area. The volumes of sediment accumulation behind the structure increased rapidly during the first year after the breakwater construction. Furthermore, this value increased gradually every year at a constant rate of 0.02075 m^3/year.m^2. Based on experiment study done by Nikmanesh and Telebbeydokhti (2013), they showed that the wave height is much influent the accretion/erosion pattern of muddy seabed. They mentioned that "by increasing wave height, muddy bed effects are significant because water waves have more interaction with seabed" and thus will reduce the occurrence of seabed accretion. In the previous section (section 3.2.3.1, Figure 3.10), it shows that the average wave heights at the year 2009 are lower than 2010 to 2014. The higher wave heights at year 2010 to 2014 seem effect the amount of sediment accretion around the breakwater.

Based on Table 4.7, the increase of sediment accumulation reached 0.183 m^3/m^2 at six years after the construction of the breakwater. This finding demonstrates that the obtained volumetric budgets are positive every year after the construction of the existing

detached breakwater, while the sediment equilibrium rate is not yet reached after six years of installation of the existing detached breakwater.

Overall, the amount of 0.183 m^3/m^2 recorded in the mangrove degradation areas after six years of installation of the existing detached breakwater illustrates that the existing detached breakwater was raising the seabed levels slowly in the mangrove degradation area on the cohesive shore of Carey Island. Therefore, it might slowly help in reducing the erosion problem. Besides, the increase of the seabed levels due to the presence of existing detached breakwater can also be an advantage for the mangrove restoration purposes.

4.4 Seabed Level Changes at Various Configurations of Geometry and Position of Detached Breakwater
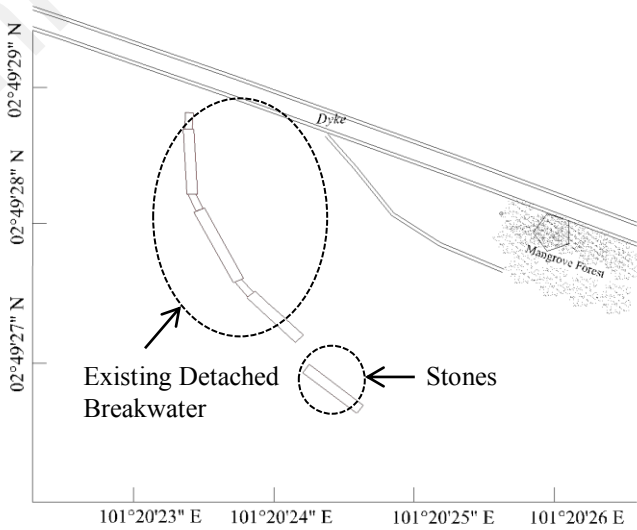
The coastal hydro-morphodynamic responses to the existing design of detached breakwater have been presented in the previous section through simulations and field monitoring. Based on the simulation results and field monitoring, it demonstrates that the existing design of detached breakwater has reduced the current speeds and wave heights and changed the suspended sediment transport in the mangrove degradation area. Besides, the presence of detached breakwater has also increased the bed elevations at the site during six years of its implementation. Therefore, it can give positive impact for mangrove rehabilitation project at the Carey Island.

However, the annual increase in bed elevations in the mangrove degradation area after installation of the existing design of detached breakwater is found insignificant. Based on results of bed elevation changes, it can be assumed that the suitable bed elevations required for mangrove survival only be achieved approximately after more than 20 years implementation of existing design of the detached breakwater if the equilibrium rate is still not reached yet.

Simulation results of suspended sediment transport have shown that the amount of suspended sediments, which are transported from seaward to the study area are quite considerable. Therefore, it is suspected that more sediment can be trapped in the mangrove degradation area due to the presence of detached breakwater in the study site. Since the different geometry and position of the detached breakwater can give different responses to the local hydro-morphodynamics and in order to optimize the function of the detached breakwater in trapping more sediments, bed level changes for various configuration of geometry and position of detached breakwater were investigated and related to the mangrove rehabilitation project in the Carey Island.

For this, nine cases by changing the parameters (position and geometry) of the existing detached breakwater were examined. Table 4.8 presents the various configurations of geometry and position of detached breakwater that were used to find out the better design parameters of detached breakwater for mangrove rehabilitation project.

Table 4.8: Adjustment of geometry and position of detached breakwater

Case No	Case Illustration/Sketch	Description
0		**Actual Condition**

Case No	Case Illustration/Sketch	Description
1		Actual condition without stones (existing design of detached breakwater)
2		The location of existing detached breakwater is moved linearly seaward to a distance of 15 m.
3		The location of existing detached breakwater is moved linearly seaward to a distance of 15 m and then moved again linearly to East direction to a distance of 15 m.

Table 4.8 Continued

132

Case No	Case Illustration/Sketch	Description
4		The location of existing detached breakwater is moved linearly seaward to a distance of 15 m and then moved again linearly to West direction to a distance of 15 m.
5		The position of existing detached breakwater is rotated to East direction by 15°.
6		The position of existing detached breakwater is rotated to East direction by 25°.

Table 4.8 Continued

Case No	Case Illustration/Sketch	Description
7	Noted: The same height for gap and mainbody = 1.5 m	The heights of the gap's and mainbody's structures are increased to 1.5 m
8	Noted: Mainbody = 2.5 m height gap = 1.5 m height	The heights of the gap's and mainbody's structures are increased to 1.5 m and 2.5 m, respectively
9	1.5 m height 2.5 m height 1.5 m height Noted: Total length : 130 m (30,70, 30) Gap's/Mainbody's widths : same	The width of the gap's and mainbody's structures is equaled, the heights of the structure are adjusted to be 1.5 m (at right and left segments) and 2.5 m (at middle segment), respectively and the length of the breakwater is increased to be 130 m.

Table 4.8 Continued

The simulation results of bed thickness changes in the vicinity of the detached breakwater for every case are presented in Figure 4.25. This figure presents the impact of the changes of position and geometry of the existing detcahed breakwater on the sediment erosion/accretion patterns as well as bed elevations changes in the mangrove degradation area.
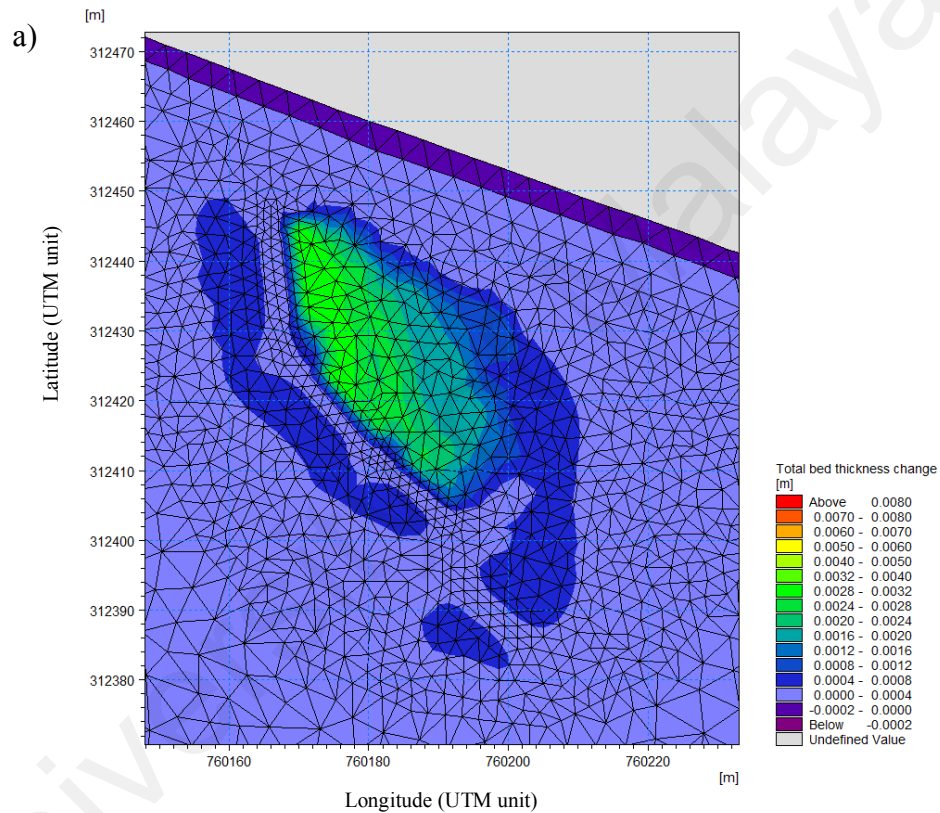
Figure 4.25 Bed thickness changes in the vicinity of the detached breakwater for 2 weeks period at every case, (a) actual condition
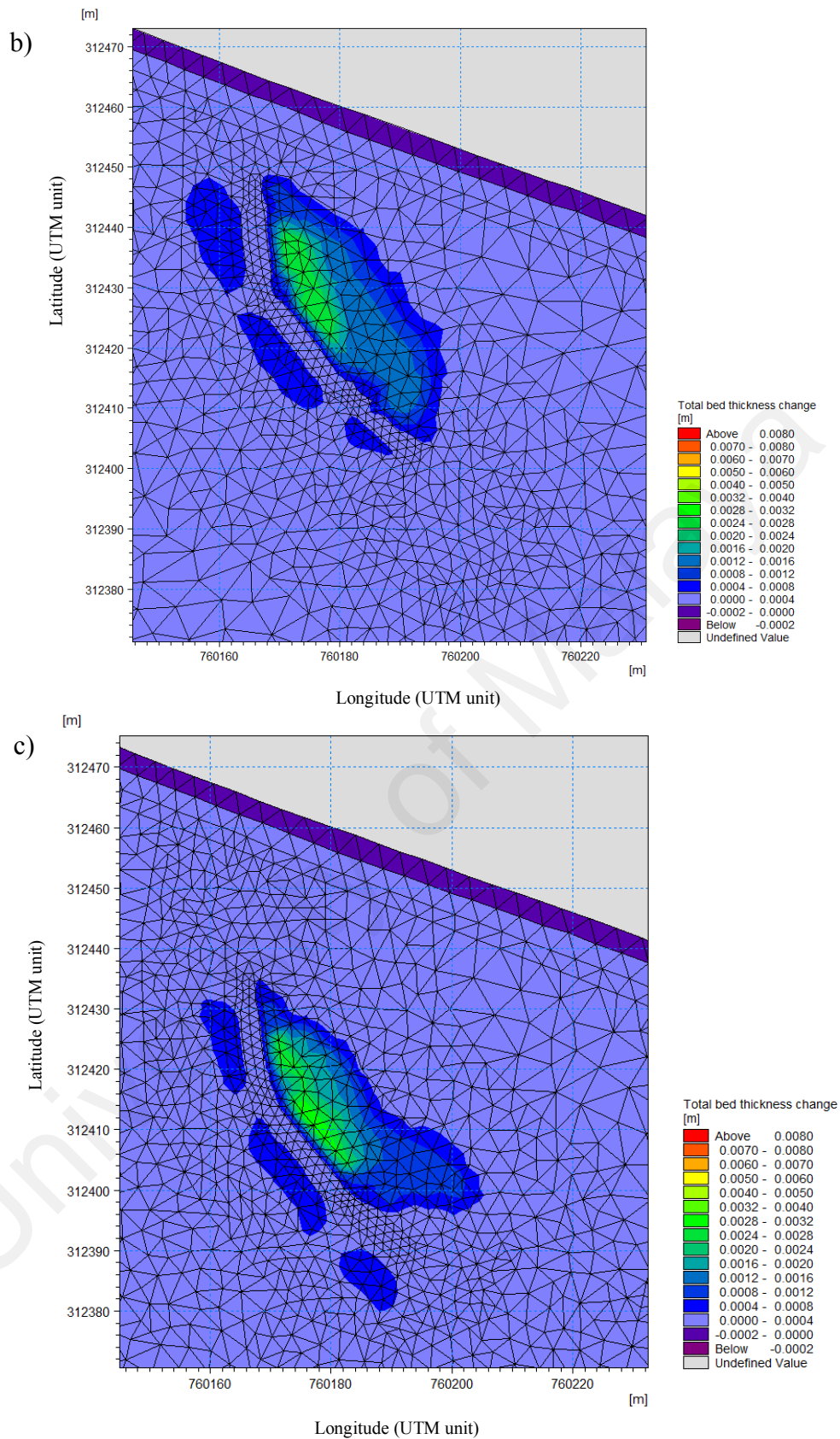
Figure 4.25 Continued,
(b) case 1, (c) case 2
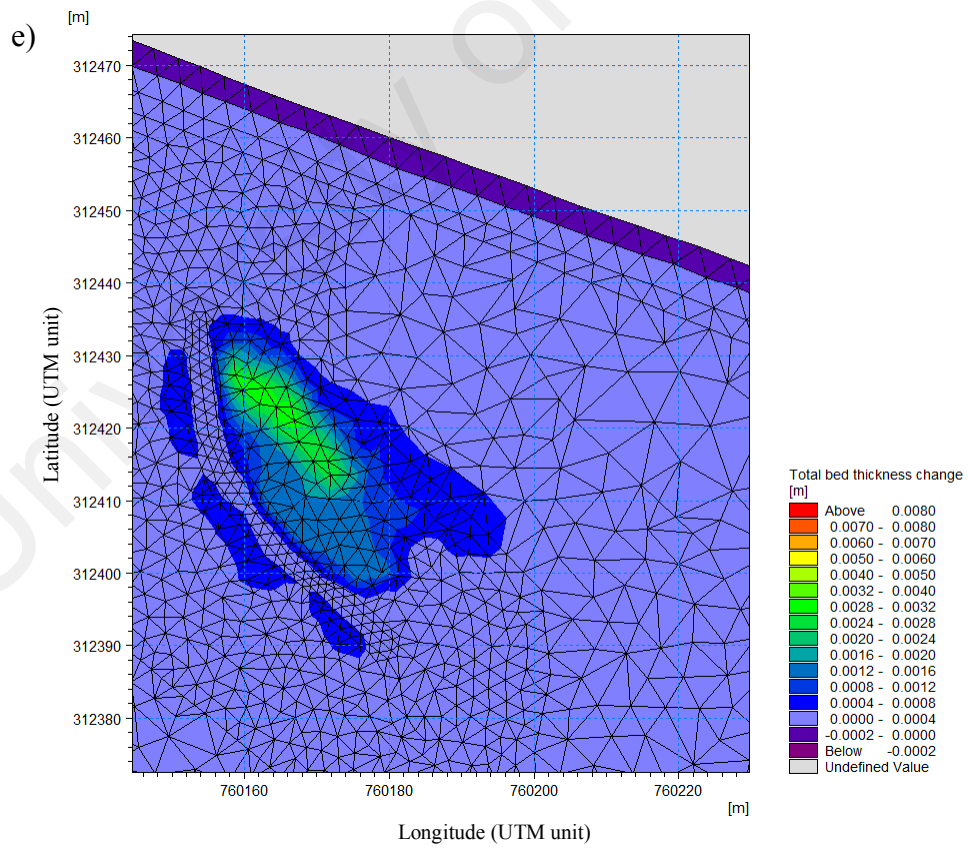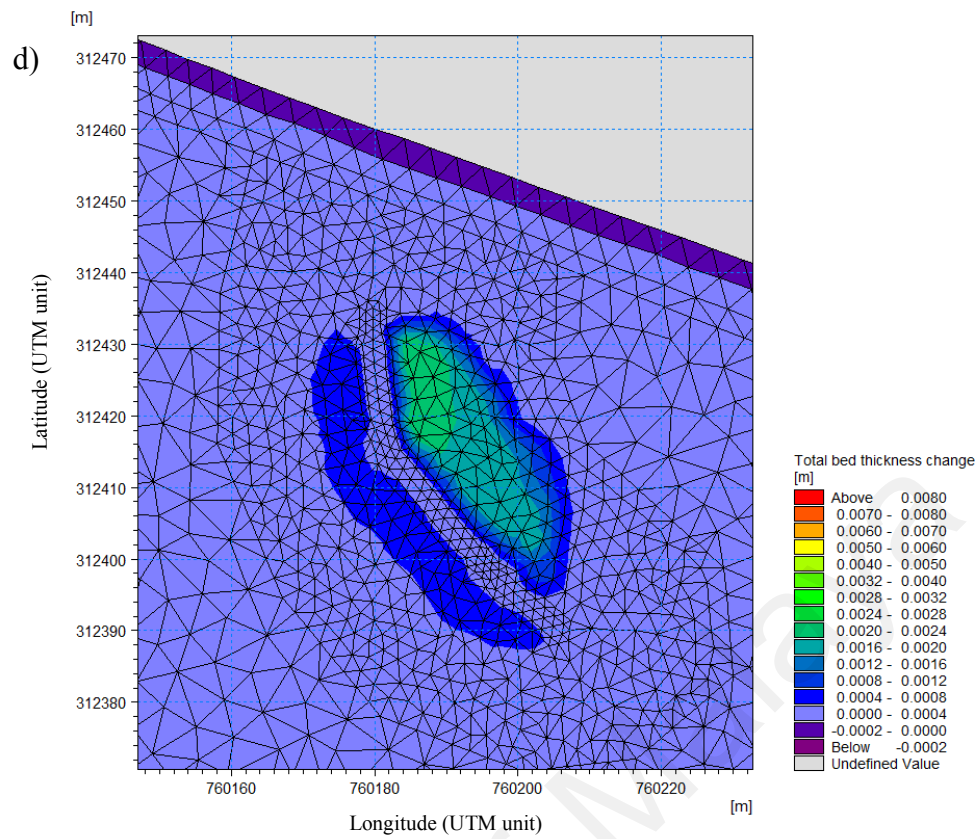
Figure 4.25 Continued,
(d) case 3, (e) case 4
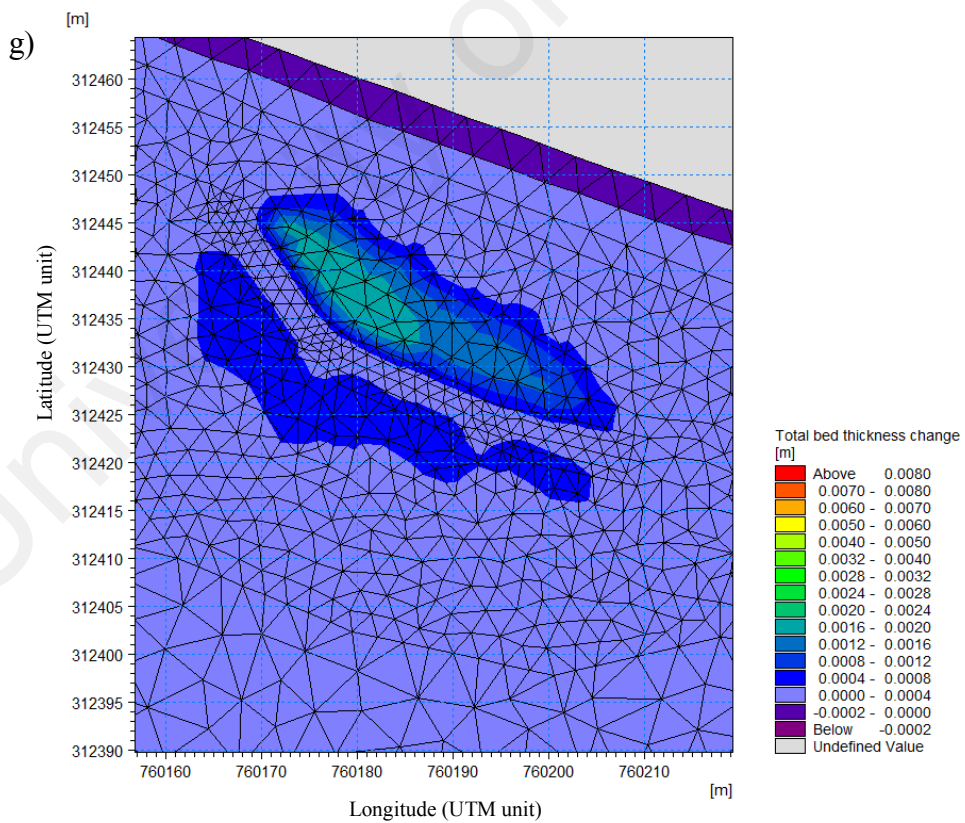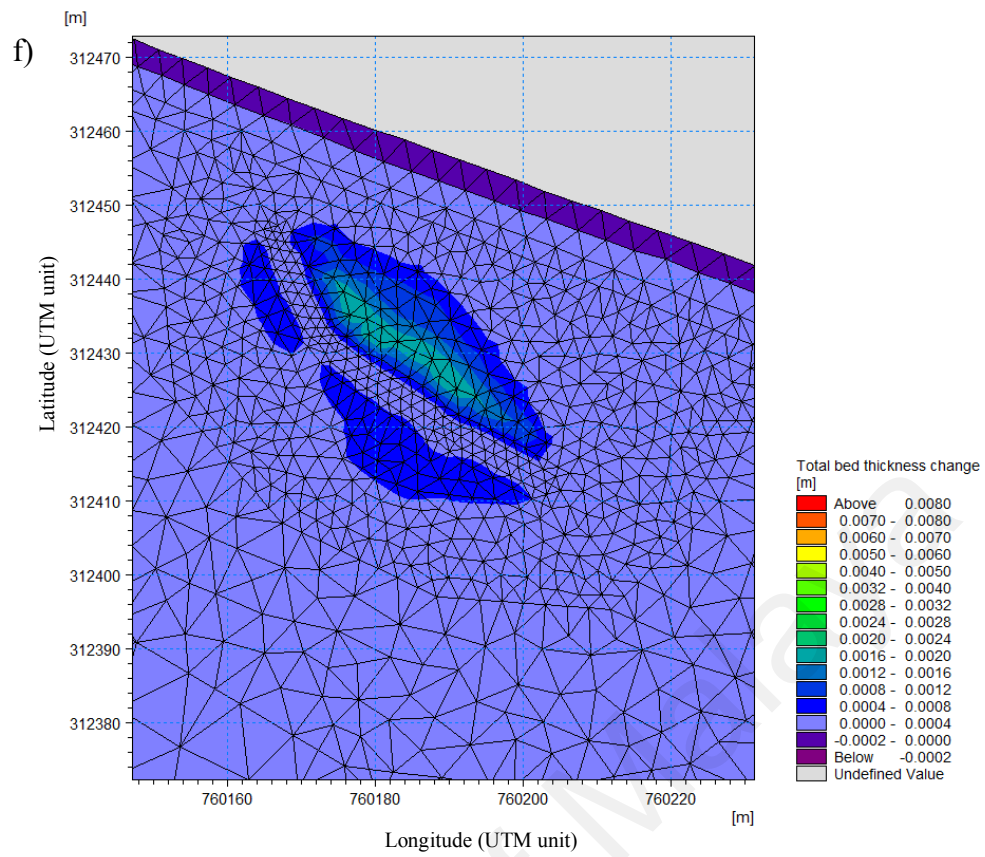
Figure 4.25 Continued,
(f) case 5, (g) case 6
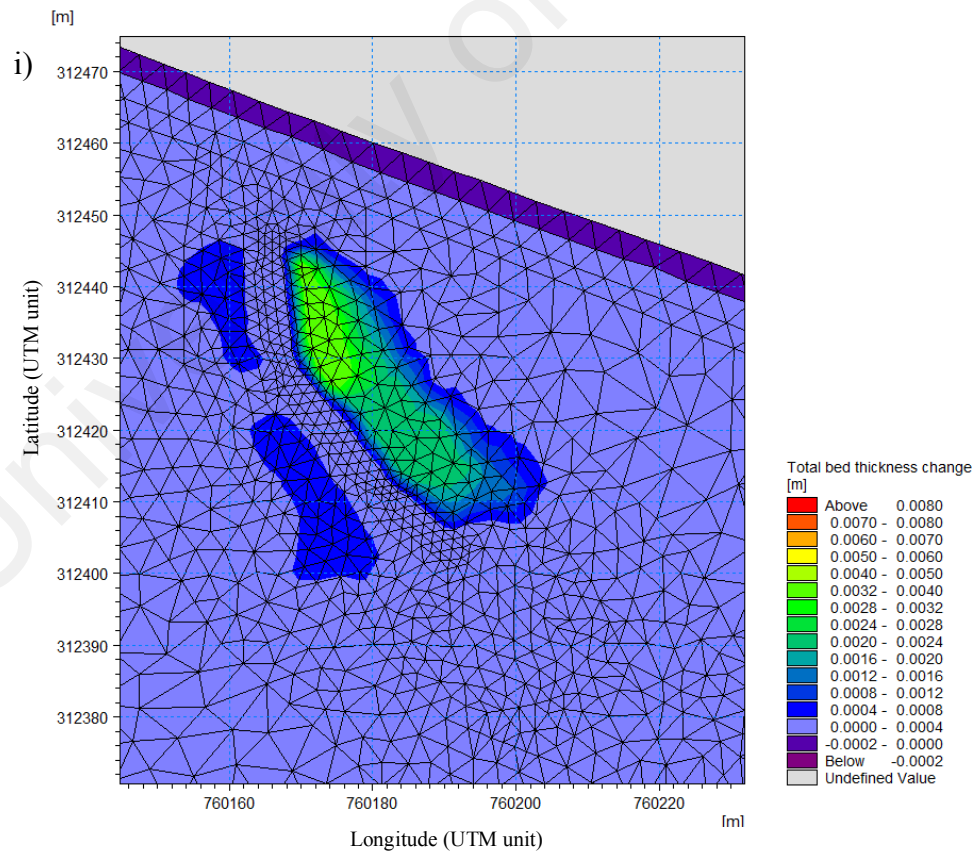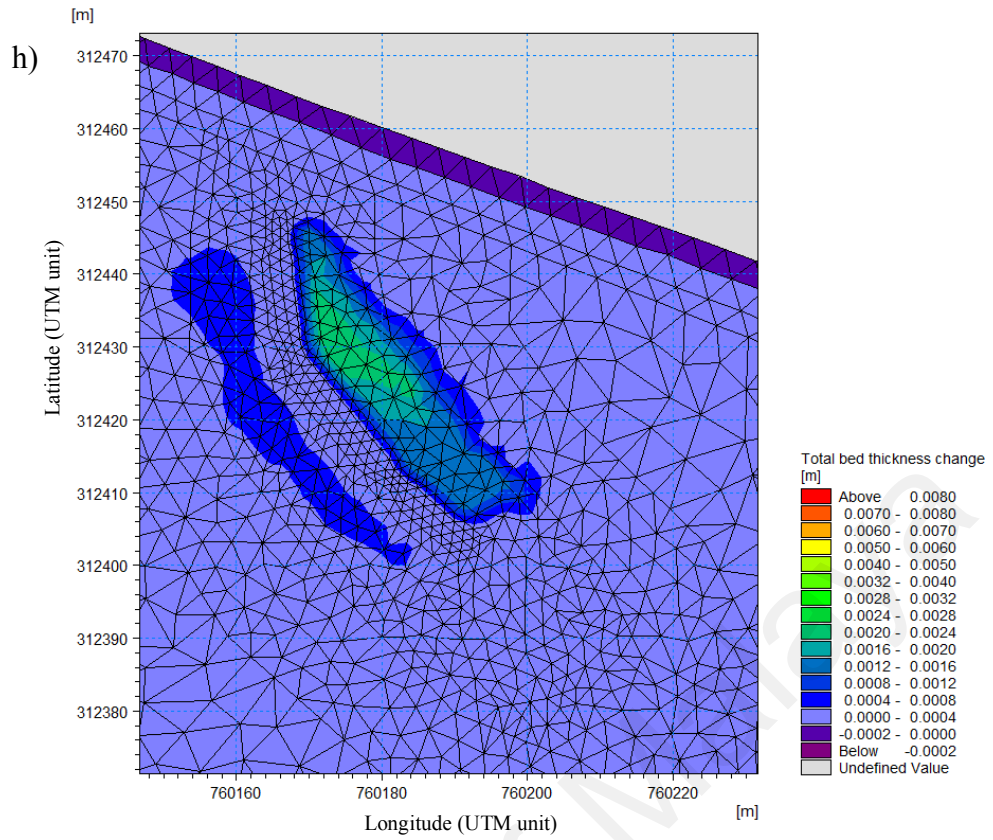
Figure 4.25 Continued,
(h) case 7, (i) case 8

j)
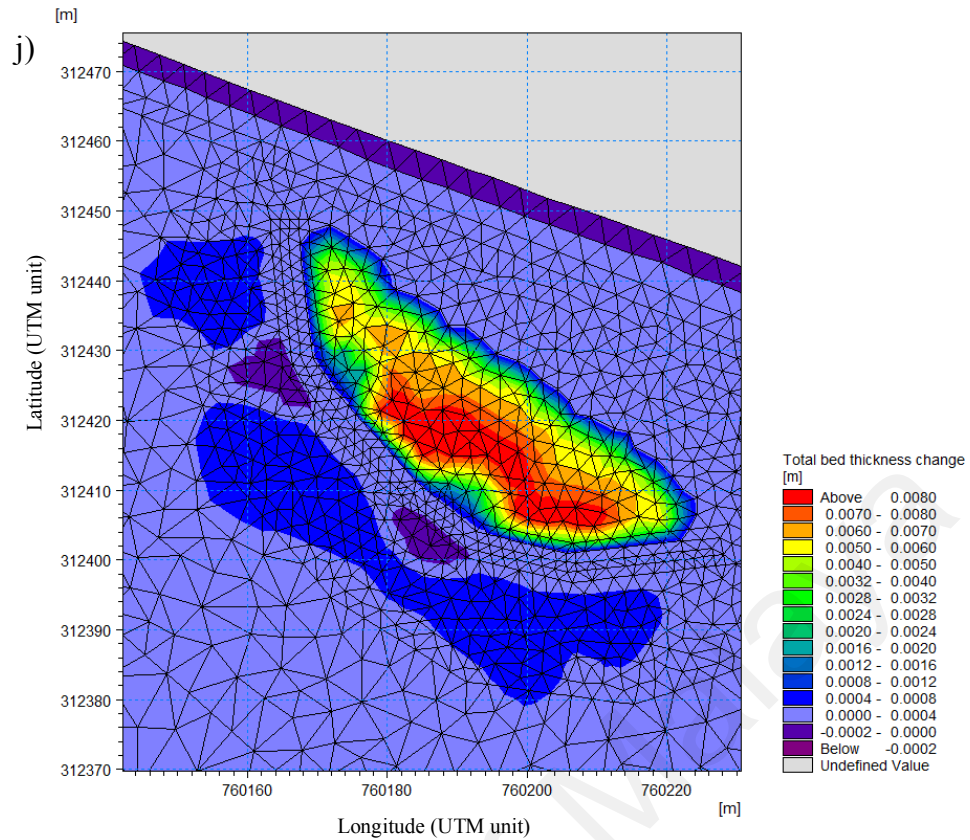
Figure 4.25 Continued,
(j) case 9

Based on Figure 4.25, the simulation results of bed thickness changes from all cases (case 0 to case 9) show that by constructing the detached breakwater at intertidal area of cohesive shore of Carey Island, the coastal bed elevations are found to increase mostly in the vicinity of the first segment of mainbody"s structure and at the protected area behind the breakwater"s structure. When the stones are taken out form the environment (case 1), the sediment accumulations behind the breakwater are found to decrease a bit. It means that the presence of the stones in the environment has helped in trapping more sediments in the mangrove degradation area (case 1).

Based on simulation results of bed thickness changes (case 1 to case 4), after moving the position of the detached breakwater approximately by 15 m linearly to seaward (case 2) or 15 m linearly to west direction (case 4), the coastal bed elevations in the mangrove degradation area are found to increase a bit. However, when the position of

the existing detached breakwater is moved closer to the mangrove degradation area approximately by 15 m to east direction (case 3), the coastal bed elevations behind the breakwater"s structure are found to be quite smaller to case 1.

Besides, when the positions of the existing detached breakwater are rotated approximately by 15° and 25° to east direction (case 5 and case 6), there is a bit reduction of the coastal bed elevations in the mangrove degradation area. In addition, there is increasing of the coastal bed elevations after increasing the height of the existing detached breakwater (case 7 and case 8). However, there is a surprising result when the height and length of the existing detached breakwater is increased at the same time: 2.5 m height and 130 m length (case 9). The simulation results of bed thickness changes from case 9, revealing almost four times increment of the coastal bed elevations in the mangrove degradation area after adding the length and height of detached breakwater.

Overall, the results show that by only changing the position of the existing detached breakwater around the study site (case 1 to case 7) does not improve the performance of the detached breakwater much in trapping the sediment accumulations as well as increasing the bed elevations in the mangrove degradation area, while the performance reductions are found when the position of existing detached breakwater was rotated to east direction. Besides, the performance of detached breakwaters is also not improved by only changing the structure"s height of the existing detached breakwater (case 8).

However, when the structure"s height of the existing detached breakwater is increased together with addition of structure"s length, the performance of the detached breakwater in increasing the coastal bed elevations is found to be dramatically improved, especially at the protected area behind the higher structure. But, very small reducing sediment accretion were recorded at front of the detached breakwater"s

structure. Based on these results, it can be demonstrated that the function of detached breakwater in trapping the sediment accumulations in the Carey Island coastline can be optimized by increasing dimensions of the existing detached breakwater that include its height and lengths together. It further can give a big contribution in supporting the success of mangrove rehabilitation project at the Carey Island coastline.

Since the suspended sediment transport were estimated for two weeks period of simulations, the bed level changes for every case are obtained for two weeks period only. Bed level changes after 1 and 6 years of implementation of new design of the detached breakwater are assumed based on linear interpolation to the results obtained from actual condition at the case 0. Table 4.9 presents the prediction of bed thickness changes for every case after 1 and 6 years of their implementation in the study site.

Table 4.9: Prediction of bed level thickness after 6 years implementation of new design parameters of detached breakwater

Case No.	Amount of bed thickness changes for 2 weeks period (cm)	Prediction of bed thickness changes after 1 year period (cm)	Prediction of bed thickness changes after 6 year period (cm)
0 (actual condition)	**0.25**	**10**	**24**
1	0.20	8.00	19.20
2	0.23	9.20	22.08
3	0.18	7.20	17.28
4	0.22	8.80	21.12
5	0.18	7.20	17.28
6	0.18	7.20	17.28
7	0.22	8.80	21.12
8	0.27	10.80	25.92
9	0.76	30.40	72.96

Based on Table 4.9, it can be demonstrated that by changing the position of the existing detached breakwater (case 1 to case 7), the average bed thickness changes in the mangrove degradation area after 6 years of implementation of the detached breakwater are less than 24 cm and below. Besides, there is increment of bed thickness when the structure"s height of the existing detached breakwater is increased two times (case 8). Further, when the structure"s height and structure"s length of existing detached breakwater are increased (case 9) at the same time, approximately two times, the average bed thickness change after 6 years of its implementation reaches 73 cm. It means that the presence of detached breakwater with higher and longer dimensions can optimize the increase of the bed level elevations in mangrove degradation area required for mangrove rehabilitation project at Carey Island.

CHAPTER 5: **CONCLUSIONS AND RECOMMENDATIONS FOR FUTURE**

WORK

5.1   Conclusions

Based on results of field monitoring and simulation using *MIKE 21 numerical model*, some conclusions are drawn in the next sections.

5.1.1   The Coastal Hydrodynamic Changes due to the Presence of Existing Detached Breakwater

Before construction of the detached breakwater at intertidal area of Carey Island, the energies of waves and currents from the Strait of Malacca have significantly influenced the mangrove degradation area with heights and speeds of approximately 0.2 m and 0.22 m/s, respectively. These energies were reduced approximately up to 0.09 m and 0.12 m/s, respectively after the presence of existing design of breakwater" structure in the study site especially at the protected area behind the structure. However, an increase of current speeds and wave heights was found at the available gaps between breakwater and dyke and between breakwater and stones, approximately up to 0.06 m and 0.10 m/s due to turbulences of return flows in these areas.

5.1.2   Suspended Sediment Transport and General Pattern of Accretion and Erosion around the Existing Detached Breakwater

Long-shore waves and cross-shore currents carry suspended sediments from the Strait of Malacca to the study site. The normal hydrodynamic conditions in the Carey Island did not allow the suspended sediments inside the water column to form flock sizes and settle down in the site areas before they flow back seaward. After construction of the detached breakwater, calm hydrodynamic conditions were created behind the structure and front of the first segments of mainbody"s breakwater. This allows some suspended sediments to stick together forming flock sizes and then settle down in these

areas. However, some seabed sediments re-suspend around the available gaps between breakwater and dyke and between breakwater and stone due to turbulent hydrodynamic conditions in these area. Therefore, accretions were presented at front of the first segments of mainbody"s breakwater and behind the breakwater"s structure while erosion were present at available gaps.

5.1.3 Morphodynamic Changes in the Vicinity of Existing Detached Breakwater

The increases of seabed elevations in the mangrove degradation area were recorded after construction of the detached breakwater at intertidal area of Carey Island. The considerable increases of seabed elevations were recorded during one year of detached breakwater"s installation approximately up to 10 cm on average or 20 cm on maximum. Further, the seabed elevations were raised slowly every year during the years 2010 to 2014 with constant rate of sediment accumulations, approximately 0.02075 m^3/year.m^2. The seabed elevations were recorded to increase up to 30 cm near the breakwater"s structure after six years of its implementation (by the end of year 2014). In contrast, the seabed elevations were found to be slightly reduced around the gap"s breakwater during one year of installation of the existing detached breakwater approximately between 5 cm and 10 cm while there was no reduction of seabed elevations in the vicinity of neither gaps nor the main bodies after one year to six years of breakwater"s installation. This finding demonstrates that the obtained volumetric budgets are positive every year after the construction of breakwater and the breakwater can slowly help in reducing the erosion problem at the Carey Island coastline.

5.1.4 Seabed Level Changes at Various Configurations of Geometry and Position of the Detached Breakwater

The increment of seabed elevations was found insignificant after six years of implementation of existing design of detached breakwater. Since the suspended

sediments transported from seaward to the study area are quite considerable, the changes of geometry and/or position of the detached breakwater can optimize sediment trapping in the mangrove degradation area.

Based on simulation results, changing only position or height of the detached breakwater does not improve the performance of the detached breakwater in trapping more suspended sediments. However, when the structure"s height and length of the detached breakwater are increased at the same time by about 1 m and 50 m, respectively, the performance of breakwater in trapping sediment accumulation in the mangrove degradation area, especially near its structure is very significant. The increase in seabed levels is predicted up to 240 cm during 6 years of breakwater installation and therefore, the suitable tidal regime for mangrove survival can be provided in the mangrove degradation area for mangrove rehabilitation project at the Carey Island.

5.2   Recommendation for Future Work

The present study has investigated the coastal hydro-morphodynamic changes at intertidal area of Carey Island due to the presence of a detached breakwater through field monitoring and numerical simulations. In order to provide more precise and detail of the obtained results, some limitations in the present study are recommended to be improved in the future works as mentioned below:

1)   The simulation results of hydrodynamic and sediment transport models are mainly influenced by the seabed topography conditions and quality of the conditions of the local weather, current, wave and suspended sediment concentration. Therefore, higher resolution of the bathymetry; measurements of water levels, current characteristics, wave characteristics and suspended sediment concentration at more points nearest to the study site for model calibration and validation purposes; and installing a device in the study site to provide precise

local weather conditions can provide more detail and precise of the simulation results.

2)   In this study, seabed profiling has been focused on mangrove degradation area especially in the vicinity of the breakwater"s structure. By extending the monitoring area around the breakwater"s structure to seaward directions will facilitate more detail of the coastal morhodynamic changes impacted by the presence of the existing detached breakwater.

In addition, the obtained results from the field monitoring and simulations are further related to the mangrove rehabilitation project. The simulation results have showed that by installing a detached breakwater (with low crest and short length) in the study site, the small amount of sediment accumulations has been recorded to be trapped in the mangrove degradation area while the higher structure with the longer length can trap more suspended sediments behind its structure. However, when the higher and longer structure is applied, there is an erosion issue recorded at front of detached breakwater"s structure. Regarding the mangrove rehabilitation purposes, it is recommended to try applying other engineering approaches, such as beach nourishment in the same time when the detached breakwater was applied.

When a low crested detached breakwater (with short length) installed, the beach nourishment may be applied behind the breakwater structure to create the suitable bed elevations required for mangrove survival in the mangrove degradation area. Further, when the higher and longer structure of detached breakwater is installed, the beach nourishment might be applied at front of breakwater"s structure to reduce the erosion problems created after breakwater installation in the study area.

REFERENCES

Affandi, N. A. M., Kamali, B., Rozainah, M. Z., Mohd Tamin, N., & Hashim, R. (2010). Early growth and survival of Avicennia alba seedlings under excessive sedimentation. *Scientific Research and Essays, 5*(18), 2801-2805.

Airoldi, L., Abbiati, M., Beck, M. W., Hawkins, S. J., Jonsson, P. R., Martin, D., . . . Åberg, P. (2005). An ecological perspective on the deployment and design of low-crested and other hard coastal defence structures. *Coastal engineering, 52*(10), 1073-1087.

Anders, F. J., & Byrnes, M. R. (1991). Accuracy of shoreline change rates as determined from maps and aerial photographs. *Shore and Beach, 59*(1), 17-26.

Anthony, E. J. (2004). Sediment dynamics and morphological stability of estuarine mangrove swamps in Sherbro Bay, West Africa. *Marine Geology, 208*(2–4), 207-224.

Archetti, R., & Zanuttigh, B. (2010). Integrated monitoring of the hydro-morphodynamics of a beach protected by low crested detached breakwaters. *Coastal Engineering, 57*(10), 879-891.

Awang, N. A. (2010). *Hydrodynamic modelling for mangrove afforestation at Haji Dorani, West Coast Peninsular Malaysia.* (MSc Thesis), Waikato University, New Zealand.

Baas, J. H., Davies, A. G., & Malarkey, J. (2013). Bedform development in mixed sand-mud: The contrasting role of cohesive forces in flow and bed. *Geomorphology, 182*, 19-32.

Baran, E., & Hambrey, J. (1999). Mangrove conservation and coastal management in southeast Asia: What impact on fishery resources? *Marine Pollution Bulletin, 37*(8), 431-440.

Barbaro, G., & Foti, G. (2013). Shoreline behind a Breakwater: Comparison between Theoretical Models and Field Measurements for the Reggio Calabria Sea. *Journal of Coastal Research, 29*(1), 216-224.

Barbier, E. B. (2015). Valuing the storm protection service of estuarine and coastal ecosystems. *Ecosystem Services, 11*, 32-38.

Birben, A. R., Ozolcer, I. H., Karasu, S., & Komurcu, M. I. (2007). Investigation of the effects of offshore breakwater parameters on sediment accumulation. *Ocean Engineering, 34*(2), 284-302.

Black, K. P., Kurian, N.P., Mathew, J. and Baba, M. (2008). Open coast monsoonal beach dynamics. *Journal of Coastal Research, 24*(1): 1-12.

Blasco, F., Saenger, P., & Janodet, E. (1996). Mangroves as indicators of coastal change. *CATENA, 27*(3–4), 167-178.

Boak, E. H., & Turner, I. L. (2005). Shoreline definition and detection: a review. *Journal of Coastal Research*, 688-703.

Boothroyd, J. C. (1978). Mesotidal inlets and estuaries *Coastal Sedimentary Environments* (pp. 287-360): Springer

Borsje, B. W., van Wesenbeeck, B. K., Dekker, F., Paalvast, P., Bouma, T. J., van Katwijk, M. M., & de Vries, M. B. (2011). How ecological engineering can serve in coastal protection. *Ecological Engineering, 37*(2), 113-122.

Bosire, J. O., Dahdouh-Guebas, F., Walton, M., Crona, B. I., Lewis, R. R., Field, C., . . . Koedam, N. (2008). Functionality of restored mangroves: A review. *Aquatic Botany, 89*(2), 251-259.

Bricio, L., Negro, V., & Diez, J. J. (2008). Geometric detached breakwater indicators on the Spanish Northeast Coastline. *Journal of Coastal Research*, 1289-1303.

Burcharth, H. F., Kramer, M., Lamberti, A., & Zanuttigh, B. (2006). Structural stability of detached low crested breakwaters. *Coastal Engineering, 53*(4), 381-394.

Cáceres, I., Sánchez-Arcilla, A., Zanuttigh, B., Lamberti, A., & Franco, L. (2005). Wave overtopping and induced currents at emergent low crested structures. *Coastal Engineering, 52*(10), 931-947.

Campbell. (2008). Turbidity and temperature monitoring system-operator's manual. Campbell Scientific, Inc 815 West 1800 North, Logan, USA. 52p.

CEM. (2006). *Coastal Sediment Processes*. Washington DC: Army Corps of Engineers.

Chang, K.-H., Tsaur, D.-H., & Huang, L.-H. (2012). Accurate solution to diffraction around a modified V-shaped breakwater. *Coastal Engineering, 68*, 56-66.

Chaplot, V., Darboux, F., Bourennane, H., Leguédois, S., Silvera, N., & Phachomphon, K. (2006). Accuracy of interpolation techniques for the derivation of digital elevation models in relation to landform types and data density. *Geomorphology, 77*(1), 126-141.

Chen, L. C. (1998). Detection of shoreline changes for tideland areas using multi-temporal satellite images. *International Journal of Remote Sensing, 19*(17), 3383-3397.

Chiang, Y.-C., & Hsiao, S.-S. (2011). *Coastal morphological modeling*: INTECH Open Access Publisher.

De Jong, R. J. (1996). *Wave transmission at low crested structures* (MSc Thesis), Delf University of Technology, Netherlands.

De Vriend, H. J., Zyserman, J., Nicholson, J., Roelvink, J. A., Pechon, P., & Southgate, H. N. (1993). Medium-term 2DH coastal area modelling. *Coastal Engineering, 21*(1), 193-224.

Dean, R. G., Chen, R. J., & Browder, A. E. (1997). Full scale monitoring study of a submerged breakwater, Palm Beach, Florida, USA. *Coastal Engineering, 29*(3-4), 291-315.

DHI. (2008). MIKE 21 Hydrodynamic Scientifict Documentation. Denmark: DHI Water and Environment.

DHI. (2014). MIKE 21 Mud Trnasport Scientifict Documentation. Denmark: DHI Water and Environment.

DID. (2006). Annual report, years 2005-2006. Malaysia: Department of Irrigation and Drainage of Malaysia.

Ding, Y., & Wang, S. S. Y. (2008). Development and Application of a Coastal and Estuarine Morphological Process Modeling System. *Journal of Coastal Research*, 127-140.

Dyer, K. R. (1986). *Coastal and Estuarine Sediment Dynamics*. Washington, DC. : John Wiley & Sons.

Edwards, A. (1999). Rehabilitation of coastal ecosystems. *Marine Pollution Bulletin, 37*(8), 371-372.

Eissa, S. S., & Lebleb, A. A. (2015). Numerical modeling of nearshore wave conditions at Al Huwaisat Island, KSA. *Aquatic Procedia, 4*, 79-86.

Fairley, I. (2009). *Beach morphodynamics behind a series of detached breakwaters in a mesotidal environment.* (Doctoral Dissertation), University of Plymouth,, Pearl.

Fairley, I., Davidson, M., & Kingston, K. (2009). The morpho-dynamics of a beach protected by detached breakwaters in a high energy tidal environment. *Journal of Coastal Research*(56), 607.

Fan, D., Guo, Y., Wang, P., & Shi, J. Z. (2006). Cross-shore variations in morphodynamic processes of an open-coast mudflat in the Changjiang Delta, China: with an emphasis on storm impacts. *Continental Shelf Research, 26*(4), 517-538.

FAO. (2007). New global mangrove estimate. http://www.fao.org/forestry/foris/webview/forestry2/index.jsp%3Fgeold=0%26langid.

Franz, G., Pinto, L., Ascione, I., Mateus, M., Fernandes, R., Leitao, P., & Neves, R. (2014). Modelling of cohesive sediment dynamics in tidal estuarine systems: Case study of Tagus estuary, Portugal. *Estuarine, Coastal and Shelf Science, 151*, 34-44.

Friedrichs, C. T., & Aubrey, D. G. (1996). Uniform bottom shear stress and equilibrium hyposometry of intertidal flats. *Mixing in Estuaries and Coastal Seas*, 405-429.

Friend, P. L., Lucas, C. H., & Rossington, S. K. (2005). Day–night variation of cohesive sediment stability. *Estuarine, Coastal and Shelf Science, 64*(2), 407-418.

Ghazali, N. H. M. (2006). Coastal erosion and reclamation in Malaysia. *Aquatic ecosystem health & management, 9*(2), 237-247.

Gibeaut, J. C., Hepner, T., Waldinger, R., Andrews, J., Gutierrez, R., Tremblay, T. A., . . . Xu, L. (2001). Changes in gulf shoreline position, Mustang, and North Padre Islands, Texas. *A report of the Texas Coastal Coordination Council pursuant to National Oceanic and Atmospheric Administration. Bureau of Economic Geology, The University of Texas, Austin Texas*, 30.

Goodfellow, B. W., & Stephenson, W. J. (2005). Beach morphodynamics in a strong-wind bay: a low-energy environment? *Marine Geology, 214*(1), 101-116.

Hansen, L. (2004). Deltaic infill of a deglaciated arctic fjord, east Greenland: sedimentary facies and sequence stratigraphy. *Journal of Sedimentary Research, 74*(3), 422-437.

Hapke, C., & Richmond, B. (2000). Monitoring beach morphology changes using small-format aerial photography and digital softcopy photogrammetry. *Environmental Geosciences, 7*(1), 32-37.

Hashim, R., Fitri, A., & Motamedi, S. H., A M (2013). Modeling of coastal hydrodynamic associated with coastal structures: A review. *Malaysian Journal of Science, 32*, 149-154.

Hashim, R., Kamali, B., Tamin, N. M., & Zakaria, R. (2010). An integrated approach to coastal rehabilitation: mangrove restoration in Sungai Haji Dorani, Malaysia. *Estuarine, Coastal and Shelf Science, 86*(1), 118-124.

Holland, K. T., Vinzon, S. B., & Calliari, L. J. (2009). A field study of coastal dynamics on a muddy coast offshore of Cassino beach, Brazil. *Continental Shelf Research, 29*(3), 503-514.

Holthuijsen, L. H., Herman, A., & Booij, N. (2003). Phase-decoupled refraction–diffraction for spectral wave models. *Coastal Engineering, 49*(4), 291-305.

Huettel, M., Ziebis, W., Forster, S., (1996). Flow-induced uptake of particulate matter in permeable sediments. Limnol. *Oceanograph,* 41, 309 - 322.

Jain, M. (2007). *Wave attenuation and mud entrainment in shallow waters.* Thesis with Degree of Doctor of Philosophy in the Graduate School of the University of Florida, USA.

Jiang, F., & Mehta, A. J. (1995). Mudbanks of the southwest coast of India IV: Mud viscoelastic properties. *Journal of Coastal Research*, 918-926.

Jose, F., Kobashi, D., & Stone, G. W. (2007). Spectral wave transformation over an elongated sand shoal off south central Louisiana, USA. *Journal of Coastal Research (SI 50)*, 757-761.

Jose, F., & Stone, G. W. (2006). Forecast of nearshore wave parameters using MIKE-21 Spectral wave model.

JUPEM. (2013). Tidal Predictions. In M. Department of Survey and Mapping Malaysia (Ed.),

Kamali, B. (2011). *Design, construction and testing of L-Blok detached breakwater for coastal rehabilitation.* (Doctoral Dissertation), University of Malaya, Malaysia.

Kirby, R. (2002). *Distinguishing accretion from erosion-dominated muddy coasts. In: Healy, T., Wang, Y. and Healy, J. A. (eds.)* Paper presented at the Muddy Coasts of the World: Processes, Deposits and Functions. Elsevier Amsterdam, 61 - 81.

Komar, P. D. (1983). CRC handbook of coastal processes and erosion. *Boca Raton, Florida. CRC Press, 285–299.*

Komen, G. J., Cavaleri, L., Donelan, M., Hasselmann, K., Hasselmann, S., & Janssen, P. (1994). *Dynamics and modelling of ocean waves*: Cambridge University Press.

Krone, R. B. (1962). Flume studies of the transport of sediment in estuarial shoaling processes.

Lamberti, A., & Zanuttigh, B. (2005). An integrated approach to beach management in Lido di Dante, Italy. *Estuarine, Coastal and Shelf Science, 62*(3), 441-451.

Le Hir, P., Roberts, W., Cazaillet, O., Christie, M., Bassoullet, P., & Bacher, C. (2000). Characterization of intertidal flat hydrodynamics. *Continental Shelf Research, 20*(12), 1433-1459.

Lee, S.-C., & Mehta, A. J. (1997). Problems in characterizing dynamics of mud shore profiles. *Journal of Hydraulic Engineering, 123*(4), 351-361.

Lewis, R. R. (2005). Ecological engineering for successful management and restoration of mangrove forests. *Ecological Engineering, 24*(4), 403-418.

Liu, X. J., Gao, S., & Wang, Y. P. (2011). Modeling profile shape evolution for accreting tidal flats composed of mud and sand: A case study of the central Jiangsu coast, China. *Continental Shelf Research, 31*(16), 1750-1760.

Mahjoobi, J., Etemad-Shahidi, A., & Kazeminezhad, M. H. (2008). Hindcasting of wave parameters using different soft computing methods. *Applied Ocean Research, 30*(1), 28-36.

Maiti, S., & Bhattacharya, A. K. (2009). Shoreline change analysis and its application to prediction: a remote sensing and statistics based approach. *Marine Geology, 257*(1), 11-23.

Martinelli, L., Zanuttigh, B., & Lamberti, A. (2006). Hydrodynamic and morphodynamic response of isolated and multiple low crested structures: Experiments and simulations. *Coastal Engineering, 53*(4), 363-379.

Martosubroto, P., & Naamin, N. (1977). Relationship between tidal forests (mangroves) and commercial shrimp production in Indonesia. *Marine Research in Indonesia, 18*(8), 1-86.

Mehta, A. J., Hayter, E. J., Parker, W. R., Krone, R. B., & Teeter, A. M. (1989). Cohesive sediment transport. I: Process description. *Journal of Hydraulic Engineering, 115*(8), 1076-1093.

Merwade, V. M., Maidment, D. R., & Goff, J. A. (2006). Anisotropic considerations while interpolating river channel bathymetry. *Journal of Hydrology, 331*(3), 731-741.

Motamedi, S., Hashim, R., Zakaria, R., Song, K.-I., & Sofawi, B. (2014). Long-term assessment of an innovative mangrove rehabilitation project: case study on Carey Island, Malaysia. *The Scientific World Journal, 2014*.

Mourre, B., De Mey, P., Lyard, F., & Le Provost, C. (2004). Assimilation of sea level data over continental shelves: an ensemble method for the exploration of model errors due to uncertainties in bathymetry. *Dynamics of Atmospheres and Oceans, 38*(2), 93-121.

Munari, C., Corbau, C., Simeoni, U., & Mistri, M. (2011). Coastal defence through low crested breakwater structures: Jumping out of the frying pan into the fire? *Marine Pollution Bulletin, 62*(8), 1641-1651.

Nam, P. T., Larson, M., & Hanson, H. (2011a). Modeling morphological evolution in the vicinity of coastal structures. *Coastal Engineering Proceedings, 1*(32), 68.

Nam, P. T., Larson, M., & Hanson, H. (2011b). A numerical model of beach morphological evolution due to waves and currents in the vicinity of coastal structures. *Coastal Engineering, 58*(9), 863-876.

Nicholson, J., Broker, I., Roelvink, J. A., Price, D., Tanguy, J. M., & Moreno, L. (1997). Intercomparison of coastal area morphodynamic models. *Coastal Engineering, 31*(1), 97-123.

Nikmanesh, M. R. and Talebbeydokhti, N. (2013). Numerical simulation for predicting concentration profiles of cohesive sediments in surf zone. *Scientia Iranica, Transactions A*, 20: 454–465.

Overton, M., Petrina, C., & Fisher, J. (1996). *Determining shoreline position using historical photography and digital softcopy photogrammetry.* Paper presented at the ASPRS/ACSM Annual Convention And Expo. Technical Paper, 1: 512-513.

Özger, M., & Şen, Z. (2008). Return period and risk calculations for ocean wave energy applications. *Ocean Engineering, 35*(17), 1700-1706.

Pajak, M. J., & Leatherman, S. (2002). The high water line as shoreline indicator. *Journal of Coastal Research, 18*, 329-337.

Patra, S. K., Mohanty, P. K., Mishra, P., & Pradhan, U. K. (2015). Estimation and validation of offshore wave characteristics of Bay of Bengal cyclones (2008-2009). *Aquatic Procedia, 4*, 1522-1528.

Paw, J. N., & Chua, T.-E. (1991). *Assessment of the ecological and economic impact of mangrove conversion in Southeast Asia.* Paper presented at the ICLARM Conference Proceedings (Philippines). no. 22.

Rakha, K. A. (1998). A Quasi-3D phase-resolving hydrodynamic and sediment transport model. *Coastal Engineering, 34*(3), 277-311.

Rambabu, A. C., & Mani, J. S. (2005). Numerical prediction of performance of submerged breakwaters. *Ocean Engineering, 32*(10), 1235-1246.

Ranasinghe, R., Symonds, G., Black, K., & Holman, R. (2004). Morphodynamics of intermediate beaches: a video imaging and numerical modelling study. *Coastal Engineering, 51*(7), 629-655.

Roberts, W., Le Hir, P., & Whitehouse, R. J. S. (2000). Investigation using simple mathematical models of the effect of tidal currents and waves on the profile shape of intertidal mudflats. *Continental Shelf Research, 20*(10), 1079-1097.

Robertson, A. I., & Blaber, S. J. M. (1993). Plankton, epibenthos and fish communities. *Tropical Mangrove Ecosystems, 41*, 173-224.

Saied, U., & Tsanis, I. K. (2005). ICEM: Integrated coastal engineering model. *Journal of Coastal Research*, 1257-1268.

Saied, U., & Tsanis, I. K. (2008). A coastal area morphodynamics model. *Environmental Modelling & Software, 23*(1), 35-49.

Sasekumar, A., Chong, V. C., Leh, M. U., & D'cruz, R. (1992). Mangroves as a habitat for fish and prawns. *Hydrobiologia, 247*(1-3), 195-207.

Scheffer, F. (1999). *Rubble mound breakwaters for the new port of Ennore (India)- Evaluation of construction.* (MSc Thesis), TU Delft, Delft University of Technology.

Seif, A. K., Kuroiwa, M., Abualtayef, M., Mase, H., & Matsubara, Y. (2011). A hydrodynamic model of nearshore waves and wave-induced currents. *International Journal of Naval Architecture and Ocean Engineering, 3*(3), 216-224.

Shamji, V. R. (2011). *Studies on beach morphological changes using numerical models.* (Doctoral Dissertation), Cochin University of Science and Technology.

Shi, Z., & Chen, J. Y. (1996). Morphodynamics and sediment dynamics on intertidal mudflats in China (1961–1994). *Continental Shelf Research, 16*(15), 1909-1926.

Sierra, J. P., González-Marco, D., Mestres, M., Gironella, X., Oliveira, T. C. A., Cáceres, I., & Mösso, C. (2010). Numerical model for wave overtopping and transmission through permeable coastal structures. *Environmental Modelling & Software, 25*(12), 1897-1904.

Shore Protection Manual. (1984a). Shore protection manual: Introduction to Coastal Engineering *Department of the Army, Waterways Experiment Station, Washington, DC* (Vol. 1, Chapter 1)

Shore Protection Manual. (1984b). Shore protection manual: Mechanics of wave motion *Department of the Army, Waterways Experiment Station, Washington, DC* (Vol. 1, Chapter 2)

Sravanthi, N., Ramakrishnan, R., Rajawat, A. S., & Narayana, A. C. (2015). Application of Numerical Model in Suspended Sediment Transport Studies along the Central Kerala, West-coast of India. *Aquatic Procedia, 4*, 109-116.

Staples, D. J., Vance, D. J., & Heales, D. S. (1985). *Habitat requirements of juvenile penaeid prawns and their relationship to offshore fisheries.* Paper presented at the Second Australian national prawn seminar, CSIRO, Cleveland, 47, 53-54, .

Stockdonf, H. F., Sallenger Jr, A. H., List, J. H., & Holman, R. A. (2002). Estimation of shoreline position and change using airborne topographic lidar data. *Journal of Coastal Research, 18*, 502-513.

Sutherland, J., Peet, A. H., & Soulsby, R. L. (2004). Evaluating the performance of morphological models. *Coastal engineering, 51*(8), 917-939.

Taveira Pinto, F., & Valente Neves, A. C. (2004). Environmental aspects of using detached breakwaters for coastal protection purposes. *Management of Environmental Quality: An International Journal, 15*(1), 62-71.

Teeter, A. (1986). Vertical Transport In Fine-Grained Suspension And Newly-Deposited Sediment. *Estuarine Cohesive Sediment Dynamics*, 170-191.

Toorman, E. A. (2001). Cohesive sediment transport modeling: European perspective. In: McAnally, W. H. & Mehta A. J. (eds). *Coastal and Estuarine Fine Sediment Processes*, 1-18.

Van Rijn, L. C. (2011). Coastal erosion and control. *Ocean & Coastal Management, 54*(12), 867-887.

Wolters, G., Müller, G., Bruce, T., & Obhrai, C. (2005). *Large-scale experiments on wave downfall pressures.* Paper presented at the Proceedings of the Institution of Civil Engineers-Maritime Engineering, 158(4): 137-145.

Young, D. M. (2008). *A laboratory study on the effects of submerged vertical and semicircular breakwaters on near-field hydrodynamics and morphodynamics*: ProQuest.

Young, I. (1999). *Wind generated ocean waves* (Vol. 2): Elsevier.

Zanuttigh, B. (2007). Numerical modelling of the morphological response induced by low-crested structures in Lido di Dante, Italy. *Coastal Engineering, 54*(1), 31-47.

Zhou, Z. (2011). *Feasibility study of a coupled numerical model for longshore sediment transport and beach response.* (MSc Thesis), TU Delft, Delft University of Technology.

Zyserman, J. A., & Johnson, H. K. (2002). Modelling morphological processes in the vicinity of shore-parallel breakwaters. *Coastal Engineering, 45*(3), 261-284.

Zyserman, J. A., Johnson, H. K., Zanuttigh, B., & Martinelli, L. (2005). Analysis of far-field erosion induced by low-crested rubble-mound structures. *Coastal Engineering, 52*(10), 977-994.

LIST OF PUBLICATIONS AND PAPERS PRESENTED

JOURNAL PUBLICATIONS:

1) PUBLISHED

Fitri, A. Hashim, R., and Motamedi, S. Estimation and Validation of Nearshore Current Characteristics at the Carey Island Coast. P*ertanika Journal of Science and Technology*. 25(3) July 2017 (***Scopus** cited Publication*).

Hashim, R., Roy, C., Shamshirband, S., Motamedi, S., **Fitri, A**., Petković, D., & Song, K. I. (2016). Estimation of Wind-Driven Coastal Waves Near a Mangrove Forest Using Adaptive Neuro-Fuzzy Inference System. *Water Resources Management*, 1-14. *(**Q1 ISI-cited publication**)*

Fitri, A., Hashim, R., Song, K. I., & Motamedi, S. (2016). Evaluation of Morphodynamic Changes in the Vicinity of Low-Crested Breakwater on Cohesive Shore of Carey Island, Malaysia. *Coastal Engineering Journal*, Volume 57: Issue 04. (***Q1 ISI-cited Publication**).*

Hashim, R., **Fitri**, **A**., Motamedi, S., Hashim, A.M. (2013). Modelling of Coastal Hydrodynamic Associated with Coastal Structures: A Reviews. *Malaysian Journal of Science*. Vol. 32, pp: 149-154. (***Scopus-cited Publication**)*

2) UNDER REVIEW

Fitri, A., Hashim, R., Song, K. I., & Motamedi, S. (2016). Modeling of Suspended Sediment Transport in the Vicinity of a Detached Low-Crested Breakwater. *International Journal of Sediment Research*